Stability of closed granular filters under wave loading

T.A.C.A. Luijten

Delft University of Technology

TU Delft

Stability of closed granular filters under wave loading

by

T.A.C.A. Luijten

In partial fulfilment of the requirements of the degree of

Master of Science

in Civil Engineering

at the Delft University of Technology.

To be presented publicly on Thursday April 13, 2022 at 3:30 PM (CEST)

Student number: 4373375

Thesis committee:	Dr. ir. B. (Bas) Hofland,	TU Delft, Chairman thesis committee
	Ing. C. (Coen) Kuiper,	TU Delft, Witteveen+Bos, Daily supervisor
	Prof. dr. ir. M.R.A. (Marcel) van Gent,	TU Delft, Deltares

Preface

This report was written in partial fulfilment for the completion of the degree of Master of Science in Civil Engineering at the Delft University of Technology. This thesis was commissioned by the Delft University of Technology and was partly conducted in their Hydraulic Engineering Laboratory.

The completion of this thesis would not have been possible without the support of the following people. First of all, I would like to thank the members of my graduation committee, Bas Hofland, Coen Kuiper and Marcel van Gent. All three members provided valuable insights and feedback during the meetings with the committee, as well as during individual meetings.

Furthermore, I would like to thank Su Kalloe. Su performed part of her PhD research in the wave flume at the Hydraulic Engineering Laboratory before me and allowed me to follow along for a few days. This provided insights into the operation of the wave flume and its software, which was very helpful during the preparations for my physical model tests.

Finally, I would like to thank Chantal Willems, Pieter van der Gaag, Arno Doorn, Arie van der Vlies and Frank Kalkman. Their advice and guidance during the construction of the physical model and during the execution of the experiments was crucial for the fluent course of the lab work.

T.A.C.A. Luijten
Delft, April 2022

Summary

In many hydraulic structures, filters are used to prevent erosion and to relieve excess pore water pressure. One of the main filter types is a granular filter, which consists of a granular top 'filter' layer and a bottom 'base' layer. A granular filter can be geometrically open or geometrically closed. This research focuses on geometrically closed filters only. In the case of a geometrically closed filter, the geometry of the granular materials used for the filter and base layers is such that the base layer material is unable to pass through the pores of the filter layer material. In some cases, the filter structure is placed on a slope, for instance in the case of a bank protection or a breakwater. In these cases, the armour layer can be seen as the 'filter layer' and the under-layer can be seen as the 'base layer'.

A geometrically closed filter needs to fulfil different functions, these functions are described by filter rules that need to be adhered to. These rules are called the 'interface stability criterion', which describes the maximum ratio between the grain size of the armour layer material and the grain size of the under-layer material, the 'internal stability criterion', which describes the maximum allowable grading width of the armour layer material, and the 'permeability criterion', which relates the permeability of the armour layer to the permeability of the under-layer. Out of these criteria, the interface stability criterion, which is the criterion that this research focuses on, is the most important.

Starting in the 1930's, many research projects have been performed to quantify these filter functions. However, for the vast majority of these research projects the filter construction was loaded by uniform flow, either in the parallel or perpendicular direction. This means that, while for filters under flow loading multiple design options and diagrams are available, the knowledge on design rules for sloped, closed filters under wave loading remained limited. Because of this, for sloped, closed granular filters under wave loading, only a very strict interface stability criterion is proposed in the current design manuals. However, in practice this criterion is often ignored and the interface stability criteria for closed granular filters under flow loading are applied, even though these had not been verified for sloped, closed filters under wave loading, in which case the load on the filter structure is oscillatory and can be higher than under flow loading.

Therefore, the main objective of this research is to increase the knowledge on the interface stability of closed, sloped granular filters under wave loading and subsequently finding the interface stability limit. To achieve this, two sub-objectives were formulated. The first sub-objective of this research is to verify the use of the interface stability criteria for closed granular filters under flow loading for sloped, closed granular filters under wave loading. The second sub-objective of this research is to approximate from what size ratio between the armour layer and under-layer material a sloped granular filter structure under wave loading can be classified as 'geometrically closed'. This size ratio is described as the ratio between the 15% of the smallest stones of the armour layer material by mass and the 85% of the smallest stones of the under-layer material by mass, noted as $D_{15,a}/D_{85,u}$.

These objectives were achieved in two phases. First, small scale physical model tests were performed in a wave flume. A model, consisting of a slope of 1:2 and an impermeable core, was constructed. On top of the impermeable core, an under-layer and subsequently an armour layer were constructed. In total, five different test series were performed. For each test series the same armour layer material was used, while different under-layer materials were used. The five under-layer materials consisted of five different ratios of different gravel sizes, ranging from 1-3 mm to 16-22 mm. This means that for each test series, the value of $D_{15,a}/D_{85,u}$ was different. Next to this ratio, the uniformity coefficient of the under-layer material $C_{u,u}$, defined as $D_{60,u}/D_{10,u}$, was also varied. For each test series, the filter structure was exposed to six different wave conditions, ranging from $\frac{H_s}{\Delta * D_{n50,a}}$ values of 1.35 to 2.43. This means a total of 30 test runs were performed.

Next, it was determined which of the 5 different under-layer materials resulted in a geometrically closed filter construction. This was done by analyzing the test results, consisting of wave data, profiles of the armour layer before and after every test, photographs of the armour layers and post-test uncovered under-layers before and after every test, as well as video footage captured during every test. For the purpose of this research, a filter structure was classified as geometrically closed under the following conditions: For all tests performed using a certain combination of under-layer and armour layer material, no wash-out of under-layer material through the armour layer was observed during any test, no under-layer grains were found inside the armour layer when deconstructing the armour layer after any test and the damage sustained by the armour layer falls into the category 'start of damage' (S = 2-3) or 'no damage' (S < 2). Next to the results of this research, the results of two previous research projects regarding sloped, closed granular filters under wave loading by Thompson & Shuttler (1975) and van Gent & Wolters (2016. English: van Gent, Jacobsen, and Wolters, 2017) were also analyzed. In total, for 11 different filter structures, all with different combinations of values of $D_{15,a}/D_{85,u}$ and $C_{u,u}$, it was determined if they were geometrically closed or not.

Four commonly used interface stability criteria, namely the original criterion proposed by Terzaghi (1939), the criterion prescribed by the Cistin/Ziems diagram (1974), the criterion prescribed by the Giroud (2003) diagram and the criterion for filter structures with an armour layer thickness of $2 * D_{n50,a}$ prescribed by The Rock Manual errata (CIRIA, CUR, CETMEF, 2017), were applied to the experimental results by Thompson & Shuttler (1975) and van Gent & Wolters (2016), as well as to the results from this research. It was concluded that none of these four criteria are sufficiently safe for sloped, closed granular filters under wave loading.

Therefore, a new interface stability criterion relating $D_{15,a}$ and $D_{85,u}$ was proposed:

$$\frac{D_{15,a}}{D_{85,u}} < 2.5 \tag{1}$$

For all tests considered in this report, applying this interface stability criterion correctly determines whether the filter structure was geometrically closed or not. Therefore, it was concluded that the interface stability criterion proposed in equation 1 is sufficiently safe for sloped, closed granular filters under wave loading, provided that the filter structure falls within the parameter ranges used for the tests considered in this report. The most important parameters here are the slope angle (1:2 or more gentle), the value of $D_{15,a}/D_{85,u}$ (1.60 to 8.56), the values of $C_{u,u}$ (1.78 to 4.56) and $C_{u,a}$ (1.24 to 1.80), as well as the thickness of the armour layer ($\geq 2 * D_{n50,a}$).

The interface stability criterion proposed in equation 1 is more strict than the criteria for closed granular filters under flow loading proposed by Terzaghi (1939) ($D_{15,a}/D_{85,u} < 5.0$) and the latest design guidance in The Rock Manual (CIRIA, CUR, CETMEF, 2017) ($D_{15,a}/D_{85,u} < 3.3$), which are commonly used for sloped, closed filters under wave loading. However, the proposed interface stability criterion is still significantly more lenient than the current interface stability criterion for sloped, closed granular filters under wave attack, as prescribed in the curent design guidance like Coastal Engineering Manual and Rock Manual ($D_{50,a}/D_{50,u} < 2.2$ to 2.5, which is roughly equivalent to $D_{15,a}/D_{85,u} < 1.0$ to 1.3).

While the criterion proposed in equation 1 was valid for all values of $C_{u,u}$ considered in this report, it was clear that the value of $C_{u,u}$ does play a role in the interface stability criterion of sloped, closed granular filters under wave loading, possibly leading to higher allowed values of $D_{15,a}/D_{85,u}$ for certain values of $C_{u,u}$. However, with the amount of data points available in this research, no definite conclusions regarding the influence of $C_{u,u}$ could be made. Therefore, it was recommended to perform more tests with previously untested combinations of $D_{15,a}/D_{85,u}$ and $C_{u,u}$, to gain more insight into the full stability envelope of sloped, closed granular filters under wave loading.

Contents

List of symbols

Symbol	Definition	Unit
C_u	Coefficient of uniformity. The ratio of the sieve size through which 60% (by weight) of the material passes to the sieve size that allows 10% of the material to pass.	[-]
d	Layer thickness	[m]
D_n	Nominal grain diameter	[m]
$D_{x,a}$	Grain diameter of which x% (by mass) of the armour layer material has a smaller diameter	[m]
$D_{x,u}$	Grain diameter of which x% (by mass) of the under-layer material has a smaller diameter	[m]
F_1	Mass fraction of the granular material which is smaller than a certain diameter D	[-]
F_2	Mass fraction of the granular material which is smaller than 4*D	[-]
Fr	Froude number	[-]
g	Gravitational acceleration	[m/s^2]
h	Water depth	[m]
H	Wave height	[m]
H_s	Significant wave height	[m]
H_{m0}	Significant wave height as estimated from the wave spectrum	[m]
i	Hydraulic gradient	[-]
i_c	Critical hydraulic gradient in filter	[-]
L	Characteristic length	[m]
M_x	Grain mass of which x% (by mass) of the material has a lower mass	[kg]
$M_{50,a}$	Median particle mass of the armour layer material	[kg]
$M_{50,u}$	Median particle mass of the under-layer material	[kg]
Re	Reynolds number	[-]
Re_D	Reynolds number inside the armour layer	[-]
S	Damage level	[-]
s_{om}	Fictitious wave steepness based on the mean wave period	[-]
s_{op}	Wave steepness based on the peak wave period	[-]
T_p	Peak period of the wave spectrum	[s]
u	Particle velocity	[m/s]
We	Weber number	[-]
Δ	relative density	[-]
ν_k	Kinematic viscosity of water	[m^2/s]
ξ_{cr}	Critical value of the breaker parameter	[-]
ξ_m	Breaker parameter related to the mean wave period	[-]
ξ_{op}	Breaker parameter related to offshore peak wave period	[-]
ρ_s	Density of rock	[kg/m^3]
ρ_w	Density of water	[kg/m^3]
σ	surface tension	[N/m]

1 Introduction

1.1. Background information

In many hydraulic structures, filters are used to protect the bed or part of the structure against scour or erosion. In many cases, granular filters are applied, which consist of a granular material, usually rock, and can consist of one or multiple layers, depending on the size difference of the bottom layer and top layer material. There are two types of granular filters, namely geometrically open and geometrically closed filters.

In a geometrically closed filter the geometry of the filter and the base material is such that the base material is prevented from moving through the filter, thus preventing erosion by flow- or wave-generated forces. In a geometrically open filter the geometry of the filter and the base material is such that the base material could be eroded through the filter. Still, a geometrically open filter can be hydraulically closed if the design of the filter is such that the hydraulic gradient in the filter construction is lower than the critical hydraulic gradient for this to happen. However, a geometrically open filter can also be hydraulically open, which means that transport of the base material can occur. For such filters the amount of transport should be limited to an acceptable level. This thesis deals with geometrically closed filters only.

Often, these closed granular filters are used on a slope, for instance in the case of breakwaters and bank protections. In this case there is often an under-layer between the core of the breakwater, or the bank material to be protected, and the protective armour layer. In this case, the under-layer can be seen as the base layer and the armour layer can be seen as the filter layer. Subsequently, when moving down one layer, the breakwater core or (often sandy) bank material can be seen as the base layer and the under-layer can be seen as the filter layer.

Several design approaches consist for closed granular filters, dating back to the 1930's. Experiments have led to filter rules that can be used for the first design of a filter construction. These filter rules are usually split into an *interface stability criterion*, a *permeability criterion* and an *internal stability criterion* (Schiereck & Verhagen, 2012), with the first criterion being the most important. These rules describe the allowed ratios of the sizes of the base layer to filter layer material size, as well as the allowed grading widths, in order for the geometrically closed filter to fulfil its purpose.

1.2. Problem statement

In these experiments, the geometrically closed filter constructions tested were always subject to a (uniform) flow, either in the direction parallel or perpendicular to the filter. In design practice, these design formula derived in flow conditions are usually also applied for wave situations. However, a sloped filter construction under wave load experiences conditions different from a non-sloped filter under flow loading. For instance, under wave conditions the load on the filter construction is cyclic, with a possibility of very high peak loads during wave impact. Also, due to a sloped design, gravitational forces act at an angle instead of perpendicular to the filter, reducing its strength. Finally, extensive wave loading

can cause damage to the armour layer, decreasing its thickness. This leads to an increased hydraulic loading on the base layer. All of this could mean that in practice, different design formula should be applied to the former.

Only three extensive research programs have been performed on sloped, closed granular filters under wave loading, providing a limited number of suggested design criteria. Therefore there are still knowledge gaps in this area, one of which being that previous tests were performed on a limited amount of slope angles.

Filling in these knowledge gaps will lead to a clearer insight into the use of the current design formula for sloped, geometrically closed filter constructions under wave loading and could even lead to the proposition of entirely new design criteria.

1.3. Research questions

The aim of this research is to expand the knowledge on the stability of geometrically closed granular filters under wave loading on a slope. By performing small scale physical model tests and analysing the results, while simultaneously analyzing the results of previously conducted research, it will be attempted to find the stability boundary. The research question is as follows:

”What is the interface stability limit of a geometrically closed granular filter under wave loading on a slope?”

The sub-questions are as follows:

- ”To what extent are existing interface stability criteria for closed granular filters under flow loads (e.g. Terzaghi (1939), Cistin/Ziems (1974), Giroud (2003)) valid for sloped, closed granular filter layers on slopes under wave loading?”
- ”To what extent is the stricter interface stability criterion for closed granular filters prescribed in The Rock Manual errata (CIRIA, CUR, CETMEF, 2017) valid for sloped, closed granular filter layers on slopes under wave loading?”
- ”From what size ratio between the armour layer and the under-layer material can a sloped granular filter structure be classified as ’geometrically closed’?”

1.4. Scope and Research method

To collect the necessary data to be able to answer the research questions, small scale physical model tests were performed. These were performed in the wave flume of the TU Delft Hydraulic Engineering Laboratory. The scope of this research is limited to a three-layer sloped system, consisting of an impermeable core, an under-layer and an armour layer, the former of which consists of a wooden support structure and the two latter consist of rubble stone. Since the aim of the physical model is to portray realistic conditions, the wave loading consists of a random wave field.

The data collected during the experiments, consisting of laser measurements, pictures, wave data and video data, were then analyzed and the relevant data was analyzed using correlation techniques. Finally, this analysis will be combined with conclusions drawn from earlier reports describing tests performed on sloped, closed granular filters under wave loading to draw the final conclusions regarding the research questions.

1.5. Outline of the report

Chapter 2 gives a theoretical background for this research. First, the use of filters in hydraulic engineering is discussed and nomenclature is defined. Then, a historic overview of the design criteria for closed granular filters is reviewed and the criteria most commonly used today are discussed. Finally, three major research projects regarding closed filters under wave loading are discussed.

In chapter 3 the physical model setup is explained. Next to the model itself, the material properties and wave conditions in the wave flume are shown, together with the test program. Finally, scale effects in the flume are discussed.

In chapter 4 the results of the model tests are presented. In chapter 5 the data from the model tests is analyzed, together with the data from historic model tests.

In chapter 6 the results of the data analysis are discussed. Finally, in chapter 7 the conclusions and recommendations are given.

2

Literature review

2.1. Rock grading curves and the associated definitions

The most commonly used material in bed, bank and shore protection is natural rock. This natural rock is extracted from rock quarries using mechanical and blasting equipment. The output of a rock quarry consists of stones and rocks spanning a large range of sizes, which means no single quantity can be used to describe the size of the rocky material. However, the size or mass distribution of the material can still be shown in a single figure, called the grading curve. The grading curve shows the relationship between the diameter and the cumulative mass fraction of the material. An example of a grading curve can be seen in figure 2.1. More information of the obtainment of the grading curve can be found in appendix A.

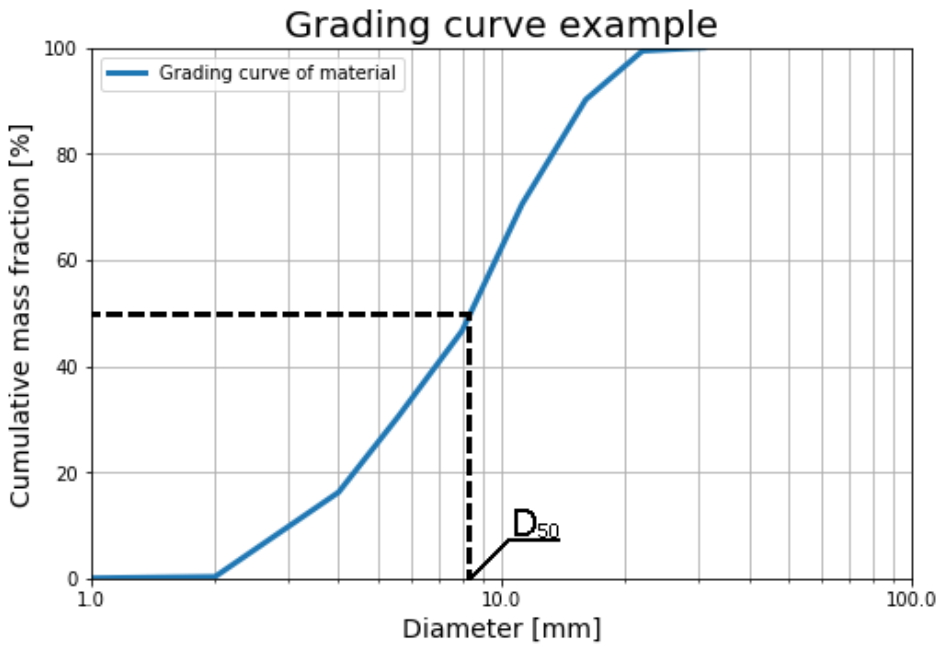

Figure 2.1: An example of a grading curve

When referring to the size distribution of a material, a number of quantities are used. The size D_x of a material is defined as the size where x% (by mass) of the material has a smaller diameter. This diameter is found by starting with x on the vertical axis of the grading curve diagram and then finding the corresponding value for D_x on the horizontal axis of the diagram. An example, showing D_{50}, is shown in figure 2.1. D_{50} is also referred to as the mean grain diameter of the material.

Another commonly used quantity is the coefficient of uniformity of the material, C_u. This coefficient can be used to describe the width of the grading curve. The value of C_u is obtained as follows (CIRIA, CUR, CETMEF, 2007):

$$C_u = \frac{D_{60}}{D_{10}} \tag{2.1}$$

Another way to describe the width of the grading curve is the ratio between D_{85} and D_{15}. In The Rock Manual (CIRIA, CUR, CETMEF, 2007), the following definitions of the width of the grading curve are given:

Table 2.1: Quarry rock grading widths as defined in The Rock Manual (CIRIA, CUR, CETMEF, 2007)

Grading width	D85/D15	M85/M15
Narrow or *single sized* grading	<1.5	1.7-2.7
Wide grading	1.5-2.5	2.7-16
Very wide or *quarry run* grading	2.5-5.0+	16-125+

As can be seen in table 2.1, the ratio between M_{85} and M_{15} can also be used to describe the width of a grading curve. When the individual stones of the material are large, the grading curve is determined by weighing individual rocks rather than sieving the material, or a sample of the material. In this case the quantity M_x can be used, which is defined as the grain mass where x% (by mass) of the material has a smaller mass.

However, in design practice it is not practical to use M_x, since many design formulae use the diameter of the rock, rather than the mass. When assuming that each rock is a perfect cube, the mass of the rock is related to the size of the rock with the following relation (Schiereck and Verhagen, 2012):

$$D_{n,50} = \sqrt[3]{\frac{W_{50}}{\rho_s}} \tag{2.2}$$

Where ρ_s is the density of the rock. It must be noted that equation 2.2 yields the *nominal diameter* of the rock, not the actual diameter. Since quarry rocks are not perfect cubes, a shape factor is used to relate the nominal diameter to the actual diameter of the rock (Schiereck and Verhagen, 2012):

$$D_{n,50} = F_s * D_{50} \tag{2.3}$$

Where F_s is the shape factor. The value of F_s can vary, but is usually assumed to be 0.84. This value was determined experimentally by Laan (1981). Laan's original report was lost, but this value was later verified by Verhagen and Jansen (2014). For the remainder of this report, a value of 0.84 will therefore be used for the shape factor.

2.2. Filters in hydraulic engineering

In the field of hydraulic structures, filters are often used. CUR report 161 (1993) defines two main functions of filters, namely:

- The prevention of erosion;
- The drainage of excess water pressure.

In a given hydraulic structure, filters fulfil either one or both of these functions. The prevention of erosion refers to the washing out of the layer under the filter layer, called the base layer, due to flow or wave forces. The two filter types used most commonly are geotextile filters and granular filters, of which the latter can be divided into two types: Geometrically open granular filters and geometrically closed granular filters.

2.2.1. Geometrically closed granular filters

Like the name suggests, a geometrically closed filter means that the geometry of the filter layer prevents the base layer from washing out. This means that the voids of the filter material are physically smaller than the grains of the base material. This principle is shown in figure 2.2 (Schiereck & Verhagen, 2012). For spheres of equal diameter, this happens when the diameter of the base layer material is larger than roughly 0.15 times the diameter of the filter layer material. In reality however, the materials of which the base and filter layers consist of are never uniform and spherical (unless they are man-made) but consist of natural granular material like rock or sand which follows a certain grading curve. Therefore, research has been done to determine the filter rules for closed granular filters. This is discussed in section 2.3.

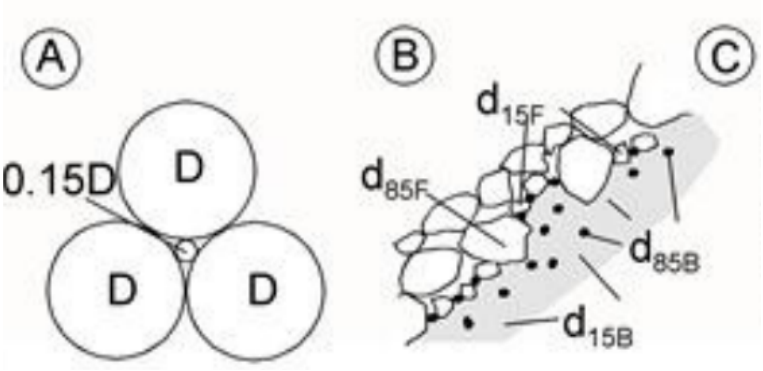

Figure 2.2: Principle of a geometrically closed filter (Schiereck & Verhagen, 2012)

2.2.2. Geometrically open granular filters

When using a geometrically open filter, the grain size of the filter layer material is much larger than the grain size of the base layer material. This means that the base layer material could be transported through the filter layer. However, as long as the hydraulic gradient i inside the filter remains below the critical gradient i_c, the filter is still stable. This concept is shown in figure 2.3 (Schiereck & Verhagen, 2012).

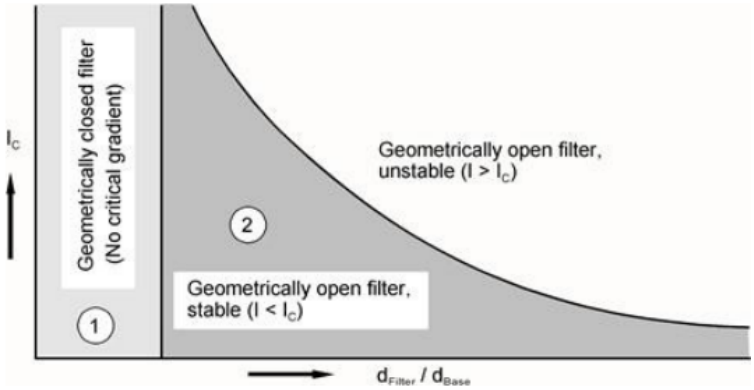

Figure 2.3: Influence of the filter material to base layer material size on the critical gradient of the filter (Schiereck & Verhagen, 2012)

Since geometrically open granular filters fall outside the scope of this research, the rest of this literature review will concern only closed granular filters. For more detailed information on open filters, one is referred to CUR report 161 (1993) (Dutch) and the book ”Introduction to bed, bank and shore protection” by Schiereck and Verhagen (2012).

2.2.3. Definition: filter layer vs filter criteria

In many literature, the term ’filter layer’ is used to describe the top layer in a two-layer system, while the term ’base layer’ is used to describe the bottom layer. However, sometimes, especially for sloped

structures like breakwaters or bank protections, these layers are referred to as the 'top layer' or 'armour layer' for the top layer and the 'under-layer' for the bottom layer. Therefore, a two-layer system can be referred to as consisting of a base layer and a filter layer, but also as consisting of an under-layer and a top layer. This is shown in figure 2.4.

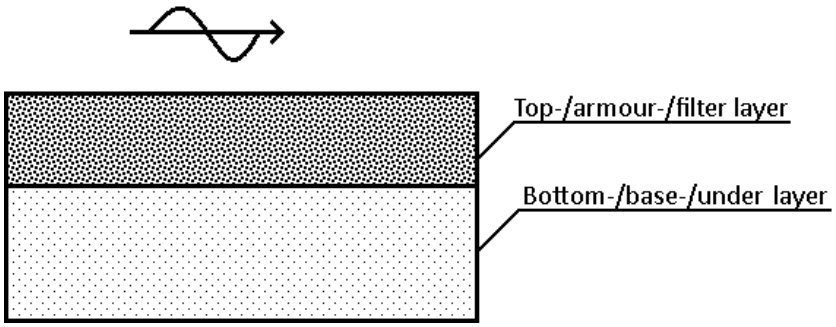

Figure 2.4: Nomenclature of the different layers in a two-layer system

For a system with three layers or more, the top layer is usually referred to as 'top layer' or 'armour layer', the bottom layer is usually referred to as 'base layer' and all layers in between are referred to as 'filter layer(s)'. This is shown in figure 2.5.

Whether a granular filter system has two, three or more layers, all different layers have to meet the filter *criteria*, even though there may not be a filter *layer* present between the top and base layers. These filter criteria will be discussed in section 2.3.

As discussed in section 1.4, the scope of this report contains three-layer systems only. To keep notation in this report consistent, from this point, the top layer will always be referred to as the 'armour layer' and the layer under the armour layer will always be referred to as the 'under-layer', with the corresponding indices 'a' and 'u' respectively. For instance, if the mean nominal grain size diameter of the top layer is referred to, it will be noted as $D_{n50,a}$

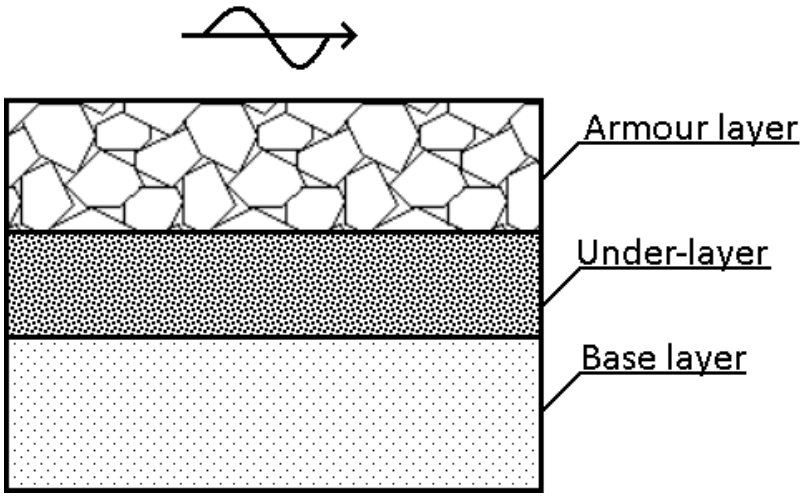

Figure 2.5: Nomenclature of the different layers in a three (or more)-layer system

2.3. Design criteria for closed granular filters

In order for a granular filter to fulfil its function, it is important that the filter is stable. This means that no material from the under-layer may be transported out of the layer above (Verheij, Hoffmans, Dorst, & Vandesande, 2012). CUR report 161 (CUR, 1993) describes three criteria that have to be met for the stability of closed granular filters, namely:

- The interface stability criterion;
- The internal stability criterion;
- The permeability criterion.

The interface stability criterion describes the ratio between the grain size of the under-layer material and the grain size of the armour layer material. As discussed before, for a geometrically closed filter no under-layer material may be transported out of the armour layer, regardless of the hydraulic gradient present. However, no criteria are set for transport of the under-layer material *through* the armour layer, meaning transport parallel to the slope of the filter construction, through the armour layer itself, but not reaching the interface between the armour layer and the water.

The internal stability criterion relates to the grading curve of the armour material. If the grading of the armour material is too wide, the finer particles of the armour layer material can pass through the larger voids of the armour layer itself, resulting in internal erosion. Next to the width of the grading curve, the shape of the grading curve is of importance as well. (CUR, 1993).

The permeability criterion relates the permeability of the armour layer to the permeability of the under-layer. If the permeability of the armour layer is too small compared to the permeability of the under-layer, a pressure build-up can occur within the filter construction, which can lead to lifting or sliding of the armour layer (Schiereck & Verhagen, 2012).

Section 2.3.1 will give a brief historic overview of the determination of the three criteria for closed granular filters discussed above, with an overview of the design criteria used most commonly today under loading by flow and waves in sections 2.3.2 and 2.3.3 respectively.

2.3.1. Historic overview

Terzaghi (1922-1939)

Because of his patent for weighted filters in 1922, Terzaghi is credited for the development of filters in hydraulic engineering, as well as for suggesting the first filter criteria later, in the 1930's (Montalvo-Bartolomei & Robbins, 2015). In 1939, Terzaghi first published a recommendation for the filter criteria. The criteria were formulated based on tests performed to design a filter for a rock-fill dam in Algeria. Only stationary flow in the direction parallel to the filter was considered. It was found that the filter would fulfil its purpose if the following relations between the size of the armour layer material and the under-layer material are true:

$$\frac{D_{15,a}}{D_{85,u}} < 4 \; to \; 5 \tag{2.4}$$

$$\frac{D_{15,a}}{D_{15,u}} > 4 \tag{2.5}$$

The relations shown in equations 2.4 and 2.5 can be seen as the first criteria recommended for the interface stability and the permeability respectively. Since Terzaghi's research included seepage under a rock-fill dam, no filter criteria for cyclic flow were recommended. In the book "Soil Mechanics in Engineering Practice", by Terzaghi and Peck (1948), the interface stability and permeability criteria shown in equations 2.4 and 2.5 respectively get recommended once again, but no further theoretical substantiation is given.

Bertram (1940)

In his research, Bertram (1940) studied granular filters, consisting of a uniformly graded material ($C_{u,u} = 1.0$), under loading by perpendicular flow with a constant hydraulic gradient. Because Bertram only had limited time available for his experiments, hydraulic gradients much larger than occur in reality were used (Douglas, 1968). The hydraulic gradient used in his experiments ranged from 6 to 20. In his experiments, Bertram (1940) used materials such that values as high as $D_{15,a}D_{85,u}$ were tested. Based on the results of the experiments the following two interface stability criteria for geometrically closed filters were recommended:

$$\frac{D_{15,a}}{D_{85,u}} < 6 \tag{2.6}$$

$$\frac{D_{15,a}}{D_{15,u}} < 9 \tag{2.7}$$

It must be noted that the criteria shown in equations 2.6 and 2.7 are only valid for armour- and under-layers consisting of a uniformly graded material. Also, the criteria are only valid for filters with a packing density of 50 to 70 percent. Furthermore, Bertram did not perform any tests under cyclic loading. However, tests were performed with flow in both directions separately. The conclusion was that the direction of the flow had no influence on the test results.

U.S. Army Corps of Engineers (1941-1953)
In 1941, the U.S. Army Corps of Engineers performed experiments to "determine the minimum grain size of filter materials required to prevent (...) infiltration of fines into the filter material." (U.S. Army Corps of Engineers, 1941). This is equivalent to determining an interface stability criterion for geometrically closed filters. The interface stability requirement recommended by Terzaghi (see equation 2.4) was used as a starting point and the ratio of $D_{15,a}$ to $D_{85,u}$ was varied from there. All tests were performed under loading by perpendicular flow with a hydraulic gradient of 1 to 2. Based on the results of the experiments, the following interface stability criterion was formulated:

$$\frac{D_{15,a}}{D_{85,u}} < 5 \tag{2.8}$$

In 1948, more experiments were performed by the Corps. The main purpose of the experiments was to "Check the designs of various proposed filters for Enid and Grenada Dams" (U.S. Army Corps of Engineers, 1948), but another objective was to validate the stability criterion for closed granular filters found in the 1941 experiments (see equation 2.8). Again, all tests were performed under loading by perpendicular flow, in both the upward and downward direction. It was concluded that the internal stability criterion found in 1941 was indeed valid. However, two additional criteria, which describe the shape of the grading curve of the armour material compared to the shape of the grading curve of the under-layer material were recommended. These are as follows:

$$\frac{D_{15,a}}{D_{15,u}} < 20 \tag{2.9}$$

$$\frac{D_{50,a}}{D_{50,u}} < 25 \tag{2.10}$$

The Corps concluded that the additional interface stability criteria shown in equations 2.9 and 2.10 are not necessary for a stable design, but desirable. Next to the validation of the interface stability criterion, the permeability criterion recommended by Terzaghi in 1939 (see equation 2.5) was validated as well.

Cistin (1968), Ziems (1968), Busch & Luckner (1974)
In 1968, Cistin proposed design criteria for the interface stability of filters under flow loading, based on physical experiments. In the same year, further tests were added by Ziems (1968). Between Cistin and Ziems, many tests were performed. (Heibaum, 2004). Hydraulic gradients of up to $i = 9$ were tested with coefficients of uniformity ranging from $C_u = 1$ to $C_u = 20$, for both the armour layer and under-layer materials. Grain sizes of the armour layer ranged from $D_a = 4mm$ up to $D_a = 100mm$ while grain sizes for the under-layer ranged from $D_u = 0.1mm$ to $D_u = 30mm$. Later, the tests results by Cistin (1968) and Ziems (1968) were published by Busch & Luckner (1974). They summarized the recommendations by Cistin and Ziems in a single design chart, which can be seen in figure 2.6. In this diagram, U_I refers to $C_{u,u}$, U_{II} refers to $C_{u,a}$, $d_{50,I}$ refers to $D_{50,u}$ and $d_{50,II}$ refers to $D_{50,a}$. The term A_{50} is simply a scaling factor, where $D_{50,a} = A_{50} * D_{50,u}$. According to the Cistin/Ziems design approach, the design is safe when this factor does not exceed a certain value, which is determined by both $C_{u,u}$ and $C_{u,a}$. This design chart incorporates a factor of safety of 1.5 (Heibaum, 2004).

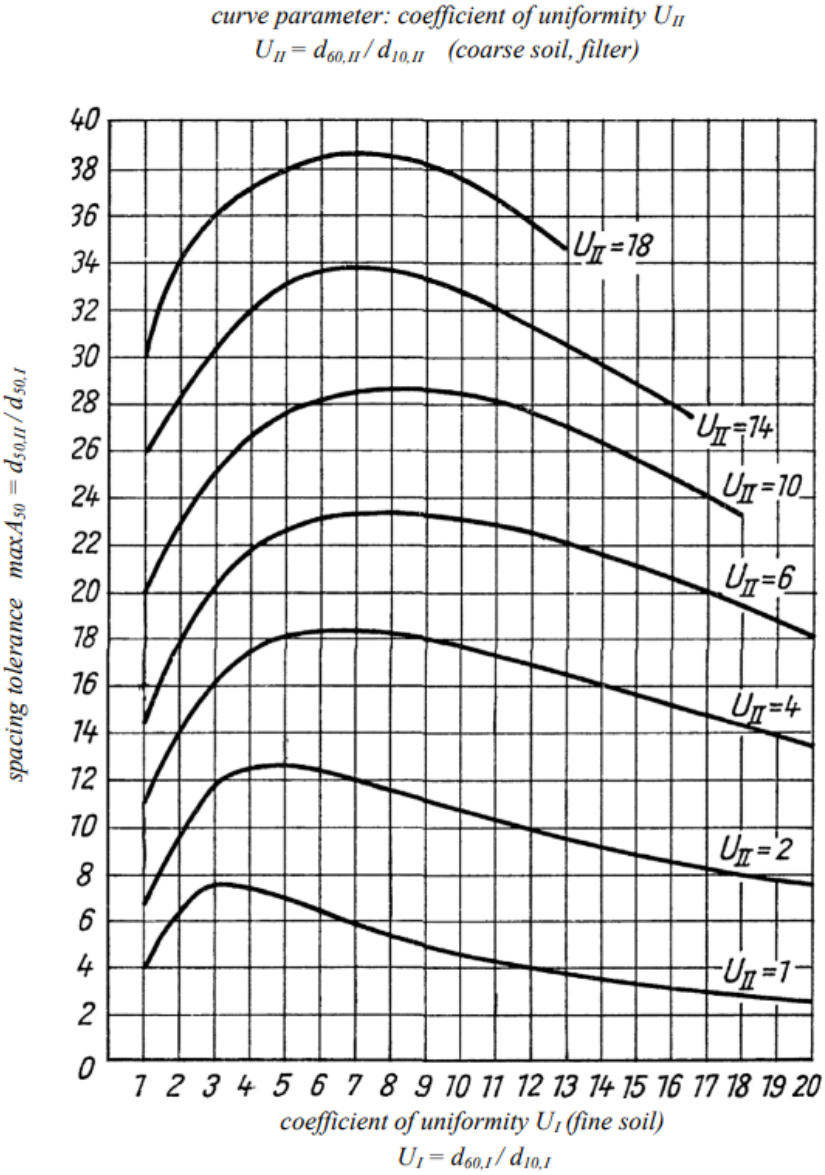

Figure 2.6: Filter design chart according to Cistin/Ziems (1968)

It must be noted that, while the test results from Cistin (1968) and Ziems (1968) are valid for a wide range of size ratios between the top and under-layers, as well as a wide range of C_u values, the Cistin/Ziems diagram has not yet been validated under wave loading. Also, while Busch & Luckner (1974) advised that caution should be exercised when considering larger rock sizes, in practice the Cistin/Ziems approach has been shown to be applicable to material up to $d_{50,a} = 250mm$ (Heibaum, 2004).

Kenney & Lau (1985)

In 1985, Kenney and Lau performed research on the internal stability of granular filters. They defined the parameters F_1 and F_2, where F_1 is the mass fraction of the granular material which is smaller than a certain diameter D and F_2 is the mass fraction of the granular material which is smaller than 4 times the same diameter D. A graphical representation of these values can be seen in figure 2.7 (CUR, 1993). For the internal stability of a closed granular filter, with vertical flow in the downward direction, the following criterion was found (Kenney & Lau, 1985):

$$(\frac{F_2 - F_1}{F_1})_{min} > 2.3 \tag{2.11}$$

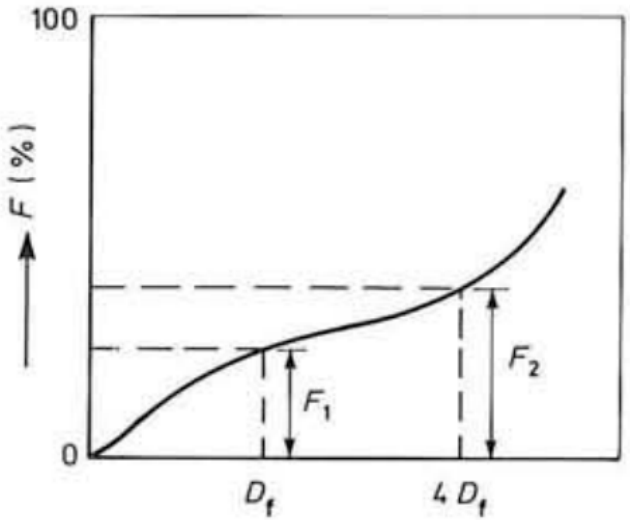

Figure 2.7: Graphical representation of the mass fractions F_1 and F_2 (CUR, 1993)

Giroud (2003)
In 2003, Giroud developed and proposed a new interface stability criterion for closed granular filters under flow conditions. This time, the basis for the proposed criterion were not the results of physical model tests. Giroud (2003) based the criterion on the retention criterion for geotextile filters (Giroud, 2006). The result of this derivation can be shown in the Giroud diagram, shown in figure 2.8. Similarly to the Cistin/Ziems approach, the maximum ratio between the size of the armour layer and under-layer materials, in this case $D_{15,a}/D_{85,u}$, is dependent on $C_{u,u}$. However, according to this approach, there is no dependence on $C_{u,a}$.

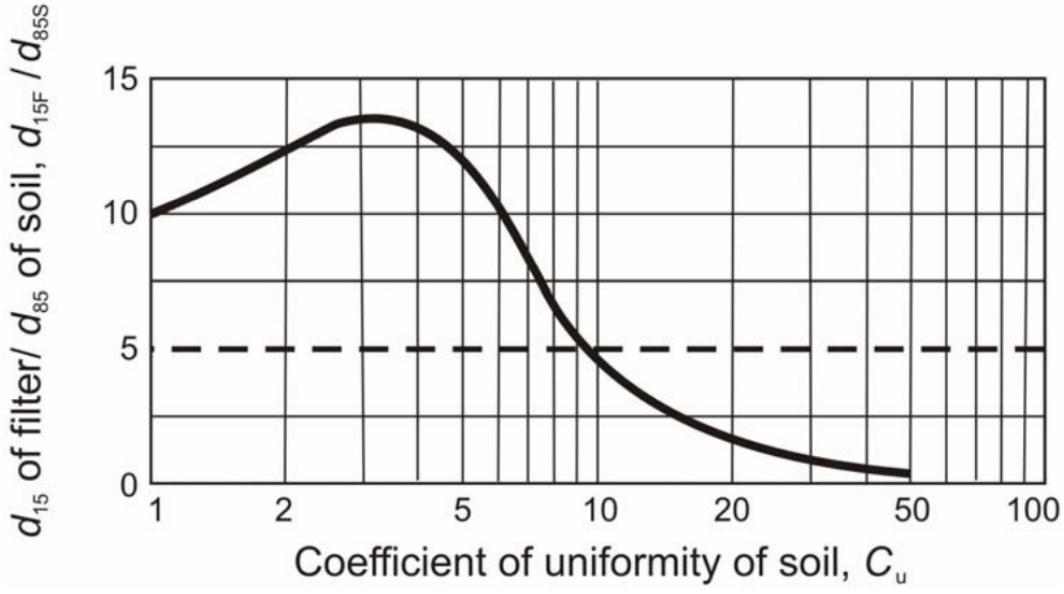

Figure 2.8: Retention criterion for granular filters derived from the retention criterion for geotextile filters (Giroud, 2003)

Inside the diagram, the classical interface stability criterion by Terzaghi (1939) is shown as a dashed line. Similarly to the Cistin/Ziems approach, the Giroud approach has not yet been validated for sloped, closed granular filters under wave loading.

2.3.2. Currently used design criteria for closed granular filters under flow loading

The current design rules for closed granular filters under non-cyclic flow are, among other literature, presented in The Rock Manual (CIRIA, CUR, CETMEF, 2007). The *interface stability criterion* described in The Rock Manual is based on the various research discussed in section 2.3.1. For thick armour layers ($h = 5 * D_{50,a}$), the interface stability criterion is defined as:

$$\frac{D_{15,a}}{D_{85,u}} < 5 \tag{2.12}$$

For more conventional armour layer thicknesses ($h = 2 * D_{50,a}$) a stricter interface stability criterion is prescribed in The Rock Manual errata list of December 5th, 2017 (CIRIA, CUR, CETMEF, 2017):

$$\frac{D_{15,a}}{D_{85,u}} < 3.3 \tag{2.13}$$

The interface stability criteria shown in equations 2.12 and 2.13 can also be written as a ratio between the *mean* diameters of the armour layer and under-layer materials. This criterion is prescribed in CUR 161 (CUR, 1993):

$$\frac{D_{50,a}}{D_{50,u}} < 6 \; to \; 10 \tag{2.14}$$

Next to these simpler interface stability criteria, in The Rock Manual errata list (CIRIA, CUR, CETMEF, 2017) it is advised to use the Cistin/Ziems design diagram. While in the USA and Western Europe the simpler design criteria as prescribed by equations 2.12 through 2.14 are often used for filter design under flow conditions, in Eastern Europe diagrams like the Cistin/Ziems diagram and the Giroud diagram are more popular (Heibaum, 2004).

The *Permeability criterion* for closed granular filters under flow conditions prescribed in The Rock Manual is:

$$\frac{D_{15,a}}{D_{15,u}} > 1 \tag{2.15}$$

Note: This criterion is only valid for cases where a non-uniformly graded material is used for the filter construction, as is often the case for hydraulic structures. For other types of filters, for example drinking water wells, drainage pipes etc, the following permeability criterion is prescribed:

$$\frac{D_{15,a}}{D_{15,u}} > 4 \; to \; 5 \tag{2.16}$$

The *Internal stability criterion* prescribed in The Rock Manual is based on the criterion found by Kenney & Lau (1985, see also section 2.3.1) and describes the desired shape of the grading curve of the armour layer material:

$$\begin{aligned} \frac{D_{10}}{D_5} &< 3 \\ \frac{D_{20}}{D_{10}} &< 3 \\ \frac{D_{30}}{D_{15}} &< 3 \\ \frac{D_{40}}{D_{20}} &< 3 \end{aligned} \tag{2.17}$$

Another commonly used internal stability criterion is based formulation by Pilarczyk (1998). This criterion is more general and only prescribes an upper limit for the uniformity coefficient:

$$\frac{D_{60}}{D_{10}} < 10 \tag{2.18}$$

2.3.3. Currently used design criteria for closed granular filters under wave loading

For loading by waves, The Rock Manual only prescribes an *interface stability criterion* for granular structures, which is described by the ratio of the mean particle mass of the under- and armour layer. The criterion is as follows (CIRIA, CUR, CETMEF, 2007):

$$\frac{M_{50,u}}{M_{50,a}} = \frac{1}{15}\ to\ \frac{1}{10} \tag{2.19}$$

Which leads to the following criterion for the ratio of the median *nominal* diameters of the armour and under-layer (CIRIA, CUR, CETMEF, 2007):

$$\frac{D_{n50,a}}{D_{n50,u}} = 2.2\ to\ 2.5 \tag{2.20}$$

The criteria shown in equations 2.19 and 2.20 are based on recommendations from the Shore Protection Manual (1984), which subsequently are based on experiments by Carver (1980) (See also 2.4.2).

2.3.4. Comparison of the interface stability criteria for loading by flow and waves

From the above it is evident that much more knowledge is available on the interface stability criteria for closed granular filters under flow loading than on the same criteria for (sloped) filters under wave loading. This is confirmed by the errata list of The Rock Manual (CIRIA, CUR, CETMEF, 2017, see equation 2.13), where it is stated that "Design recommendations for the interface stability of (sloped) granular structures subject to waves are neither widely known, nor broadly applied."

Historically, three large studies on sloped, closed granular filter structures under wave loading were performed, by Thompson & Shuttler (1975), Carver (1980) and van Gent & Wolters (2016). These three research projects will be discussed more extensively in section 2.4. While the study by Carver (1980) has led to the current interface stability criteria prescribed in The Rock Manual (2.19 & 2.20), the proposed criteria by Thompson & Shuttler (1975) have never been included in official guidelines, though they are briefly mentioned in The Rock manual errata list of 2017 (CIRIA, CUR, CETMEF, 2017). The recommendations by van Gent & Wolters (2016) were included in a design guideline by SBRCURnet (2017). However, it is not yet evident that these novel guidelines are used extensively in practice, possibly because they are very recent.

In practice this means that only the rather strict interface stability criteria presented in equations 2.19 and 2.20 are verified for the use of closed filters under wave loading. However, in practice the original criterion by Terzaghi (see equation 2.4) is often applied for closed filters under wave loading on a slope, though this criterion has not yet been verified for this situation.

2.4. Previous research on closed filters under wave loading

As mentioned in the previous section, three previous studies on sloped, closed granular filter structures were performed. In this section, these will be discussed in more detail. Thompson and Shuttler (1975) suggested filter criteria for closed filters under wave loading. Carver (1980) studied the effect of the size of the first under-layer material on the armour layer of a breakwater trunk section under wave loading. Van Gent and Wolters (2016) performed physical model tests to develop a new guideline for under-layers under a sloped rock armour layer under wave loading.

2.4.1. Thompson & Shuttler (1975)

Thompson and Shuttler (1975) performed physical model tests with different ratios of the under-layer to armour layer material size under wave loading. All tests were performed on a slope of 1:3 on top of an impermeable core. These tests were performed as preliminary tests for the main test program. Three

different gradings were used for the under-layer in this preliminary test program, while the armour layer material was constant for all tests. The properties of the three different under-layer gradings are shown in table 2.2. The layer thickness of the armour layer was $2 * D_{50,a}$ and the thickness of the under-layer was $0.5 * D_{50,u}$, which equates to 60 mm and 15 mm respectively, for all tests in the preliminary test program.

Table 2.2: Three different under-layer gradings tested by Thompson & Shuttler (1975)

Material name	$D_{50,a}$ [mm]	$D_{50,u}$ [mm]	$D_{50,a}/D_{50,u}$ [-]	$D_{15,a}/D_{85,u}$ [-]	$D_{85,a}/D_{15,a}$ [-]	$D_{85,u}/D_{15,u}$ [-]	$C_{u,a}$ [-]	$C_{u,u}$ [-]
5/30	30	2.2	13.6	5.0	2.3	3.3	1.8	2.4
2	30	3.2	9.5	3.2	2.3	4.0	1.8	2.7
4/30	30	6.6	4.5	2.0	2.3	2.3	1.8	1.8

It was found that, out of the three gradings used for the under-layer, only the 4/30 grading was sufficient, meaning that no washout of the under-layer or early failure of the armour layer occurred. Based on the results of these tests, Thompson and Shuttler (1975) proposed the following set of interface stability criteria for a geometrically closed filter under wave loading:

$$\begin{aligned} \frac{D_{15,a}}{D_{85,u}} &\leq 4 \\ \frac{D_{50,a}}{D_{50,u}} &\leq 7 \\ \frac{D_{15,a}}{D_{15,u}} &\leq 7 \end{aligned} \tag{2.21}$$

Out of the 32 tests that Thompson and Shuttler (1975) performed, the criteria shown in equation 2.21 correctly predicted whether or not the filter construction was stable 26 times. In the other 6 tests, the filter construction was still stable, even with values of $D_{50,a}/D_{50,u}$ and $D_{15,a}/D_{15,u}$ much higher than 7. In these tests, "the riprap grading curve had a long tail of fines which was not reflected in the above ratios" (Thompson & Shuttler, 1975). This implies that the criteria shown above could be relaxed if the armour layer consists of a widely graded material, as the finer armour layer material could block the armour layer pores.

2.4.2. Carver (1980)

Carver (1980) performed physical model tests with different ratios of the under-layer to armour layer material size with a varying slope and wave conditions. Tests were performed on slopes of both 1:3 and 1:1.5. The physical model used consisted of a permeable core, two under-layers and an armour layer. Three different gradings were used for the first under-layer material, while the armour layer material was constant for all tests. All three gradings were tested on both slopes. The properties of the three different under-layer gradings are shown in table 2.3

Table 2.3: Three different under-layer gradings tested by Carver (1980)

Material name	$W_{50,a}$ [kg]	$D_{n50,a}$ [mm]	$W_{50,u}$ [kg]	$D_{n50,u}$ [mm]	$D_{50,a}/D_{50,u}$ [-]
Wr/5	0.249	45	0.050	27	1.7
Wr/10	0.249	45	0.025	21	2.1
Wr/20	0.249	45	0.012	17	2.7

The values for $D_{n50,a}$ and $D_{n50,u}$ were obtained from the values of $M_{50,a}$ and $M_{50,u}$ using equation 2.22 (Schiereck & Verhagen, 2012). Carver (1980) used granite with a density of 2675 kg/m^3 for the armour layer and limestone with a density of 2643 kg/m^3 for the under-layer.

$$D_{n50} = (\frac{M_{50}}{\rho_s})^{1/3} \tag{2.22}$$

Carver (1980) found that no extra damage to the armour layer occurred, for both the 1:3 slope and the 1:1.5 slope and for all three under-layer materials. Therefore, Carver concluded that, for a breakwater trunk section loaded by non-breaking waves at 90 degrees, "Variations in first-under-layer stone weights (Wr) from Wr/5 to Wr/20 do not have a significant effect on armor stability"

However, this does not mean that a mean mass ratio of $M_{50,u} = M_{50,a}/20$, which in this case is equal to a mean diameter ratio of $M_{50,u} = M_{50,a}/2.7$ is the upper stability limit for a geometrically closed filter under wave loading. This is because no under-layer material smaller than this was tested.

Unlike in Thompson's and Shuttler's, in Carver's research multiple slopes were tested, namely 1:1.5 and 1:3. However, Carver only provided the M_{50} values for the materials used for the under- and amour layer, without providing information about the grading widths.

2.4.3. Van Gent & Wolters (2016)

Van Gent and Wolters (2016) performed extensive physical model tests with different ratios of the under-layer to armour layer material size under various wave conditions on a 1:3 slope with an impermeable core. The thickness of the under-layer was also varied. In total, 8 series of tests were performed, of which the properties can be found in table 2.4

Table 2.4: Material properties of the 8 testing series by van Gent & Wolters (2016)

Series name	$D_{50,a}$ [mm]	$D_{50,u}$ [mm]	$D_{50,a}/D_{50,u}$ [-]	$D_{15,a}/D_{85,u}$ [-]	$D_{15,a}/D_{15,u}$ [-]	$C_{u,a}$ [-]	$C_{u,u}$ [-]	d_a [mm]	d_u [mm]
1	75	17	4.4	2.7	6.0	1.3	2.0	126	32
2	75	11	7.0	2.5	15.2	1.3	3.7	126	32
3	75	17	4.6	1.6	9.7	1.3	3.5	126	32
4	75	11	7.2	4.2	9.5	1.3	1.8	126	32
5	75	11	7.2	4.2	9.5	1.3	1.8	126	32
6	75	11	7.0	2.5	15.2	1.3	3.7	126	110
7	75	8	9.8	3.0	15.6	1.3	2.9	126	110
8	75	11	7.0	2.5	15.2	1.3	3.7	126	110

Series 1, 2, 3, 4, 6 and 7 consisted of 6 consecutive tests with varying wave conditions, each consisting of 1000 waves. Series 5 and 8 consisted of a single, long duration test of 10000 waves, but with profile measurements after 1000, 3000 and 10000 waves. The model was only reconstructed after each test series, not after every individual test, at which point the under-layer could be inspected. To determine the damage levels of the armour layer in between individual tests, a mechanical profiler was used. The damage S was defined as the total erosion area of the armour layer from 0.25 m below the mean water level to 0.25 m above the mean water level, divided by $D^2_{n50,a}$.

The following observations were reported by van Gent and Wolters (2016):

- For $D_{n50,a}/D_{50,u} = 2.0$, or $D_{50,a}/D_{50,u} = 2.4$, no movement or washout of the under-layer material was observed.
- For $D_{n50,a}/D_{50,u} = 3.7$, or $D_{50,a}/D_{50,u} = 4.4$, no increase in damage of the armour layer was observed, for both $S_a < 2.5$ and $S_a > 2.5$. Movement of the under-layer material was observed, as well as washout of the under-layer material. However, the latter was only observed for $S_a > 2.5$ and the amount of washout was limited.
- For $D_{n50,a}/D_{50,u} = 6.0$, or $D_{50,a}/D_{50,u} = 7.1$, no increase in damage of the armour layer was observed for $S_a < 2.5$, but an increase was observed for $S_f > 2.5$. More movement of the under-layer material was observed, as well as much washout of the under-layer material. The latter was only observed for $S_a > 2.5$.
- For $D_{n50,a}/D_{50,u} = 8.2$, or $D_{50,a}/D_{50,u} = 9.8$, no increase in damage of the armour layer was observed for $S_a < 2.5$, but an increase was observed for $S_a > 2.5$. In addition, significant movement

of the under-layer material was observed, as well as much washout of the under-layer material, for both $S_a < 2.5$ and $S_a > 2.5$

The observations described above led to the creation of 5 classes for sloped, geometrically closed granular filter constructions under wave loading, for different ratios of $D_{n50,a}$ to $D_{50,u}$ (van Gent & Wolters, 2016):

Table 2.5: Armour layer classes suggested by van Gent and Wolters (2016)

Class	Phenomenological criterion	Requirements for armour layer
I	Movement of under-layer material inadmissible.	$D_{n50,a}/D_{50,u}$ <2.1 ($D_{50,a}/D_{50,u}$ <2.5)
II	Movement of under-layer material admissible but washout of under-layer material inadmissible.	$D_{n50,a}/D_{50,u}$ <3.7 ($D_{50,a}/D_{50,u}$ <4.4) and S_f <2.5
III	Movement of under-layer material admissible and some washout of under-layer material admissible.	$D_{n50,a}/D_{50,u}$ <3.7 ($D_{50,a}/D_{50,u}$ <4.4)
IV	Much movement of under-layer material admissible but washout of under-layer material not admissible.	$D_{n50,a}/D_{50,u}$ <6.0 ($D_{50,a}/D_{50,u}$ <7.1) and S_f <2.5
V	Much movement of under-layer material admissible, some washout of under-layer material admissible and extra damage to armour layer admissible.	$D_{n50,a}/D_{50,u}$ <6.0 ($D_{50,a}/D_{50,u}$ <7.1)

As mentioned before, the model was only reconstructed after each full test series. This means the damage of the under-layer could only be fully assessed at the end of each series of tests, by removing the armour layer. In 6 of the 8 test series, considerable damage (S = 8.2 to S = 21.6) had already occurred to the armour layer. Therefore it was difficult to assess if damage to the under-layer occurred due to washout of the under-layer through the armour layer, or because a hole in the armour layer had formed due to damage.

Also, van Gent and Wolters (2016) performed tests on the same slope as Thompson & Shuttler, namely 1:3. Therefore, van Gent and Wolters recommend to test other slopes as well.

2.4.4. Comparison with Cistin/Ziems and Giroud diagrams

To easily compare the earlier studies described in this section with each other and to establish a baseline for the test program of this thesis, the test programs of the earlier studies can be plotted in the Cistin/Ziems (1974) and Giroud (2003) diagrams. In chapter 5, these diagrams can be used to analyze the validity of these diagrams for sloped, closed granular filters under wave conditions.

Only the test programs of Thompson & Shuttler (1975) and van Gent & Wolters (2016) can be plotted in this way. Since Carver (1980) only provided the median grain masses and no further information on the grading curves of the materials used, the C_u values needed to plot his test program in the diagrams cannot be resolved. The position of the test programs of Thompson & Shuttler and van Gent & Wolters in the Cistin/Ziems diagram can be seen in figure 2.9. The position of the same test programs in the Giroud diagram can be seen in figure 2.10.

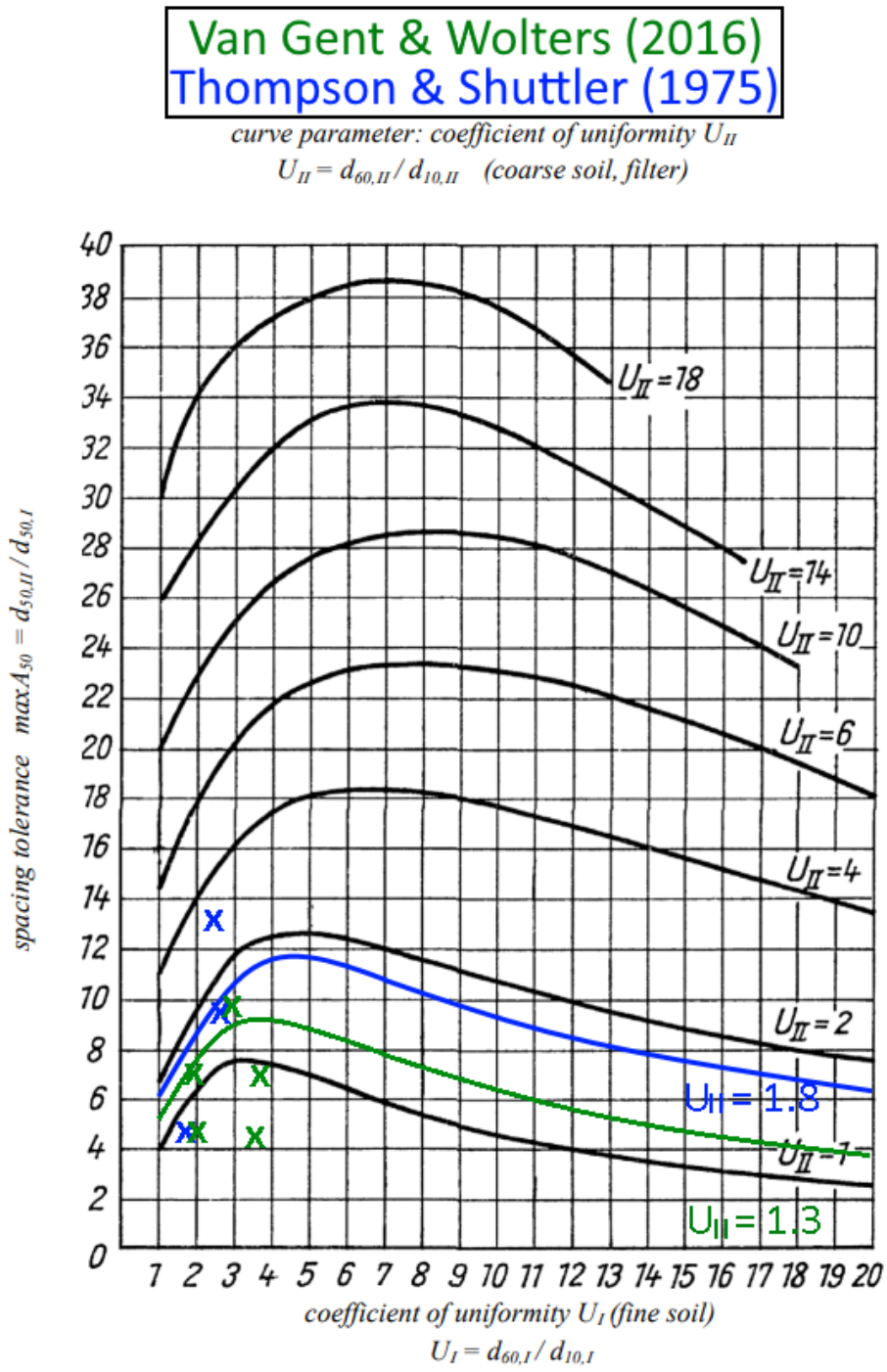

Figure 2.9: Cistin/Ziems diagram with the test programs of Thompson & Shuttler (1975) and van Gent & Wolters (2016)

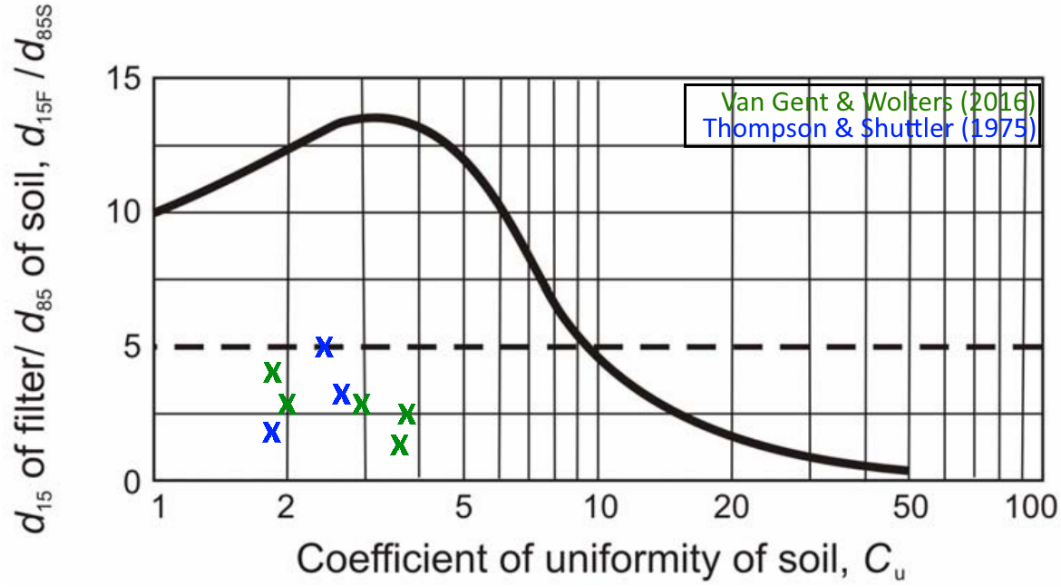

Figure 2.10: Giroud diagram with the test programs of Thompson & Shuttler (1975) and van Gent & Wolters (2016)

2.5. Chapter summary and conclusions

Starting in the 1930's, many research projects have been performed with the intent to establish rules, which can be used to design granular, geometrically closed filter constructions for hydraulic structures. However, for the vast majority of these research projects, the filter construction was loaded by uniform flow, either in the parallel or perpendicular direction. This means that, while for filters under flow loading multiple design options and diagrams are available, the knowledge on design rules for sloped, closed filters under wave loading remained limited.

Three extensive research projects have been performed where sloped, geometrically closed filter constructions were tested under wave loading. Thompson and Shuttler (1975) tested three different ratios of the armour layer to under-layer material size under wave loading. Carver (1980) also used three different ratios of the armour layer to under-layer material size. The most extensive research project regarding closed filters under wave loading was performed by van Gent and Wolters (2016).

As can be seen in sections 2.3.2 through 2.3.4, there are some clear knowledge gaps regarding geometrically closed filters under wave loading. These knowledge gaps mean that stricter filter rules are prescribed by design guidelines such as The Rock Manual (CIRIA, CUR, CETMEF, 2007) for closed granular filters under wave loading, compared to closed filters under flow loading. However, in practice, often the design criteria for closed filters under flow loading, for instance the original criterion by Terzaghi (1939), are used for the design of closed filters under wave loading, while these have not yet been experimentally verified for this use case.

3

Physical model and test program

In this chapter the physical model setup is introduced and explained. The model tests are carried out in the wave flume of the Hydraulic Engineering Laboratory at Delft University of Technology. Next to the model itself, the material properties and wave conditions in the wave flume are shown, together with the test program. Finally, scale effects in the flume are discussed.

3.1. Model description

A technical drawing of the model can be seen in figure 3.2. A full-sized drawing can be found in appendix B. The wave flume has a length of 39 m, height of 1 m and a width of 0.8 m. The model consists of a wooden slope of 1:2. This slope simulates an impermeable core. A slope of 1:2 was chosen to supplement earlier experiments described in section 2.4, which have been performed on different slopes of 1:1.5 and 1:3. On top of this 'core', first the granular under-layer is placed and then the armour layer. The wooden material used for the model is concrete plywood. Unlike normal plywood or OSB, this material experiences little to no expansion when in contact with moisture, making it a suitable material for a wave flume model.

However, the face of concrete plywood is very smooth, giving it a low coefficient of friction compared to normal plywood or OSB. This causes the under-layer to slide very easily down the wooden slope, which is not realistic. Therefore, gravel (1/3 mm) is glued to the wooden slope with epoxy glue. To further counteract the sliding of the rocky slope a toe structure, in the form of a vertical wooden piece, is attached to the bottom of the slope. Another function of this impermeable toe is to support the armour layer. An image of the base model, before the placement of the under-layer and armour layer, can be seen in figure 3.1

Figure 3.1: Model setup, before the placement of the under-layer and armour layer

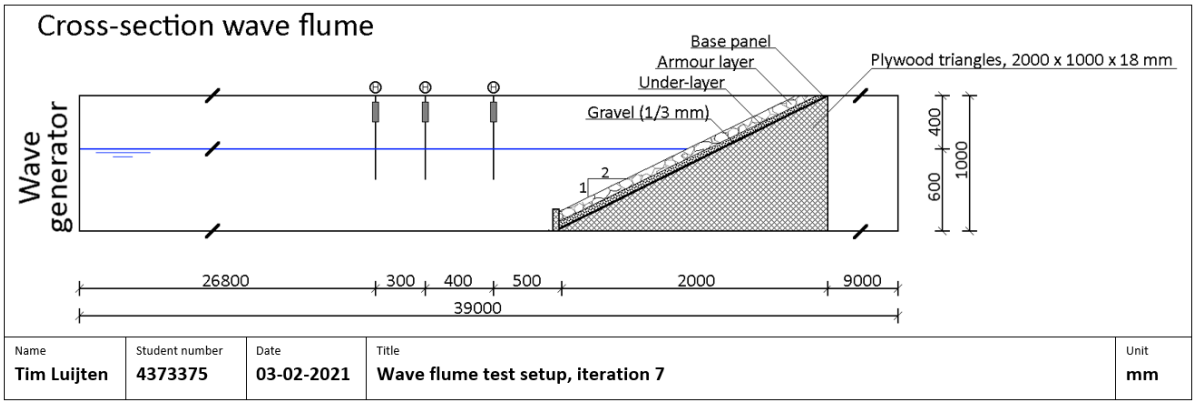

Figure 3.2: Wave flume setup, technical drawing

3.2. Instrumentation

This section discusses the instrumentation used before, during an after the experiments. During the tests, video recordings are made and the wave height is measured. Before and after every test, the profile of the armour layer is measured using a laser setup. All measurements are done using DASYLab software and post-processing is done using Python and Matlab.

3.2.1. Wave generator

The wave generator is located at the front side of the wave flume and consists of a wave paddle which is driven by a computer. The wet-back, piston type paddle is capable of generating both regular and irregular wave fields. The software driving the wave paddle is equipped with active reflection compensation, which means that the wave paddle automatically compensates for the incoming wave reflections.

3.2.2. Wave gauges

As can be seen in figure 3.2, one set of three, resistant type wave gauges is placed right in front of the model, along the longitudinal symmetry axis of the wave flume. Thus it is possible to measure the wave conditions at the location of the model. Part of the the incoming wave energy will be reflected back to the wave paddle, where it will be damped out by the active reflection compensation. By placing three wave gauges in a row, the signal from the wave gauges can be decomposed into an incoming and a reflected signal. This is done in the post-processing stage using the method described by Zelt and Skjelbreia (1992). Using three wave gauges, this method is identical to the method described by Mansard and Funke (1980). The wave gauges is are calibrated every morning before tests are taking place.

3.2.3. Laser and distance wheel

A laser is used to measure the profile of the armour layer before and after every test. This laser is mounted to a cart, which can ride freely on rails which are mounted on top of the wave flume. This can be seen in figure 3.3. The cart ensures that the laser remains at a constant height above the model during all measurements. The laser is mounted in such a way that it can be moved in the transverse direction of the flume. To attempt to achieve a high accuracy in this direction, so measurements can be made along the same transect multiple times, a measuring tape is attached to the top of the cart. The desired accuracy in the transverse direction is ±0.5 mm. The laser used is an OptoNCDT 1700-750. This laser is a class II, 1 mW laser and has a measuring range of 200-950 mm and an accuracy of 50 µm.

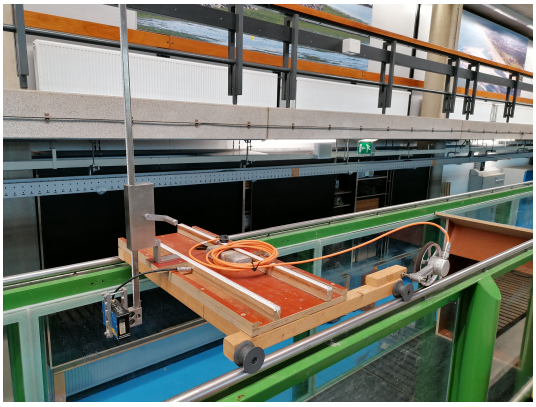

Figure 3.3: Laser cart

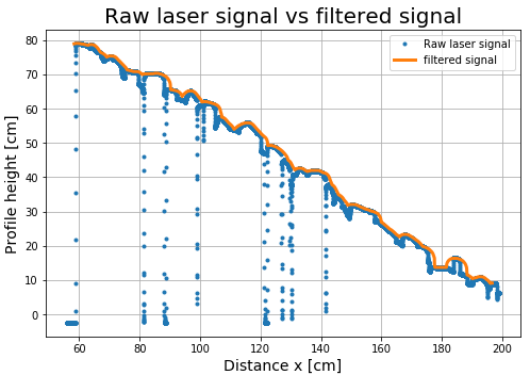

Figure 3.4: An example of an unfiltered and a filtered laser signal

Accompanying the laser is a distance measuring wheel. This wheel can be seen extending in front of the laser cart in figure 3.3. During a laser measurement, this wheel rolls along the aforementioned rails and measures the distance from the start of the measurement. A marking is applied on the rails to attempt to start each measurement at the same point in the longitudinal direction. The desired accuracy in the transverse direction is ±0.5 mm. The wheel has a rubber ring around it to prevent slip on the steel rails. The extra diameter caused by the addition of the rubber wheel is accounted for in the measurement software.

Laser measurements of the armour layer are performed before and after every test. Each measurement consists of 8 profiles, leading to a spacing of 0.89 m inside the 0.8 m wide wave flume. During each run with the laser cart, a measurement is taken every 0.1 mm. The output voltage is converted to a distance measurement using a calibration formula. The laser is calibrated every day before tests are taking place. An example of a single profile measurement can be seen in figure 3.4. The signal is then filtered by simulating a mechanical profilometer with a semicircle measuring foot with a diameter of $0.5 * D_{n50,a}$, as prescribed by CUR (2000). An example of this can be seen in figure 3.4. To attain the final profile of the armour layer, the average of the 8 individual, filtered profiles is taken.

The average slope profiles are then used to calculated the damage sustained by the armour layer after every test. The damage level is defined as:

$$S = \frac{A}{{D_{n50,a}}^2} \tag{3.1}$$

Where A is the erosion area between MWL + $2 * H_s$ and MWL - $2 * H_s$.

3.2.4. (film)camera setup

Before and after each experiment, photos of the slope are taken from above. Both the armour layer and the under-layer are photographed. The camera is mounted to the same cart that is used for the laser measurements, which is placed at the same location along the rails of the wave flume, indicated by a marking. This ensures the photo frame is the same for both before and after the experiment, which makes comparing the photos much easier.

Video recordings are made during each experiment. The video camera is placed next to the wave flume, facing the transparent side of the flume. To minimize reflections interfering with the video recordings, a temporary tarp is built around the video camera. Inside the tarp a LED panel is placed. To ensure the frame and the lighting are the same for every video recording, markings are made on the floor where the tripod legs for both the camera and the LED panel need to be placed.

Figure 3.5: Camera tarp

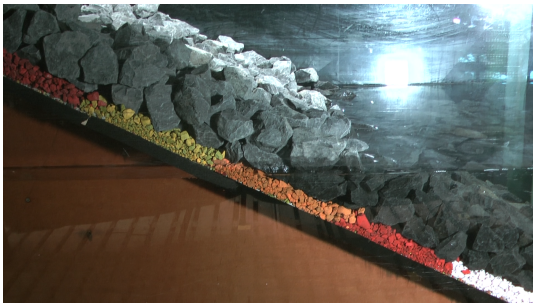

Figure 3.6: Camera shot through the transparent side panel of the wave flume

3.3. Material properties

The focus of this research is the ratio of the size of the armour layer material to the size of the under-layer material. To accomplish this, it is chosen to use the same armour layer material for every test series, but to vary the under-layer material. Also important is the effect of the coefficient of uniformity of the under-layer material. Therefore, for some test series, this coefficient needs to be varied, while the ratio $D_{50,a}/D_{50,u}$ remains constant.

3.3.1. Armour layer material

For the armour layer material, basalt rubble stone is used. By using a stone type with a higher density for the armour layer, the hydraulic load on the under-layer can be increased without causing extra damage to the armour layer, which is desirable in this case (see section 3.4). The grading curve is obtained by taking a random sample from the big bag of stones and weighing the stones individually. The density of the armour layer material is obtained using Archimedes' principle. For a more detailed description and for more background information the reader is referred to appendix A. The armour layer material is classified as a narrow grading, with $D_{85,a}/D_{15,a} = 1.31$. The grading curve of the armour layer is most similar to the EN 13383 coarse grading 45/125, with $D_{15,a} = 48.6mm$ However, this grading curve is narrower, leading to lower values of $D_{50,a}$ and $D_{85,a}$ compared to the standard coarse grading 45/125. An overview of the armour layer material properties is found in table 3.1 and figure 3.7.

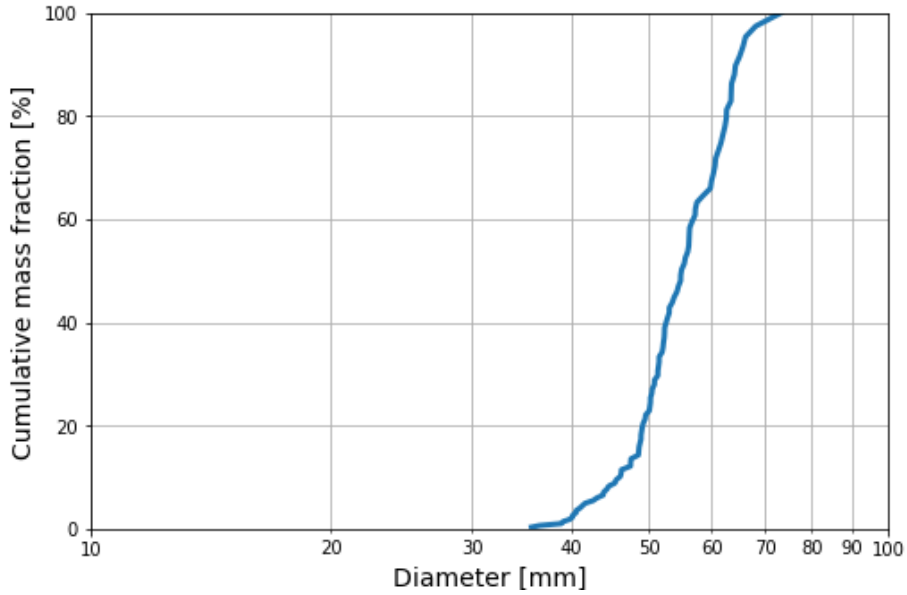

Figure 3.7: Grading curve of the armour layer material

Table 3.1: Overview of armour layer material properties

Material	D_{10} [mm]	D_{15} [mm]	D_{50} [mm]	D_{n50} [mm]	D_{60} [mm]	D_{85} [mm]	C_u [-]	ρ_s [kg/m^3]
Armour layer	46.0	48.6	55.0	46.2	57.2	63.5	1.24	2984

3.3.2. Under-layer material

In total, five differently graded granular materials are used for the under-layer. For the reasoning behind the chosen grading curves for the five materials, the reader is referred to section 3.4. The materials used consist of a mix of different sizes of gravel. The different sizes used are ”Nederlandse steenslag 1-3mm”, ”Japanese split 2-4mm”, ”Japanese split 4-8mm”, ”Japanese split 8-11mm”, ”Japanese split 11-16mm” and ”Japanese split 16-22mm”. First the grading curves of the individual stone types are obtained. This is again accomplished by taking a random sample from the big bag of stones and weighing the stones individually. Next, the individual stone types are mixed with pre-calculated ratios to obtain the desired grading curve for the under-layer material. Finally, the resulting mixes are sieved using different sieve sizes to obtain the final grading curve per mix and to verify if the final grading curves correspond to the pre-calculated curves. For a more detailed description of the process and for more background information the reader is referred to appendix A. An overview of the material properties of the five mixes is found in table 3.2 and figure 3.8.

Material	D_{10} [mm]	D_{15} [mm]	D_{50} [mm]	D_{n50} [mm]	D_{60} [mm]	d_{85} [mm]	C_u [-]	rho [kg/m^3]
Mix 1	4.6	5.7	11.6	9.7	13.5	19.1	2.94	2627
Mix 2	2.4	2.8	6.2	5.2	7.4	10.9	3.09	2618
Mix 3	2.1	2.3	3.6	3.0	4.1	5.7	1.96	2614
Mix 4	3.1	3.8	8.4	7.0	9.3	14.9	3.03	2621
Mix 5	2.5	2.9	8.7	7.3	11.5	17.7	4.57	2621

Table 3.2: Overview of under-layer material properties

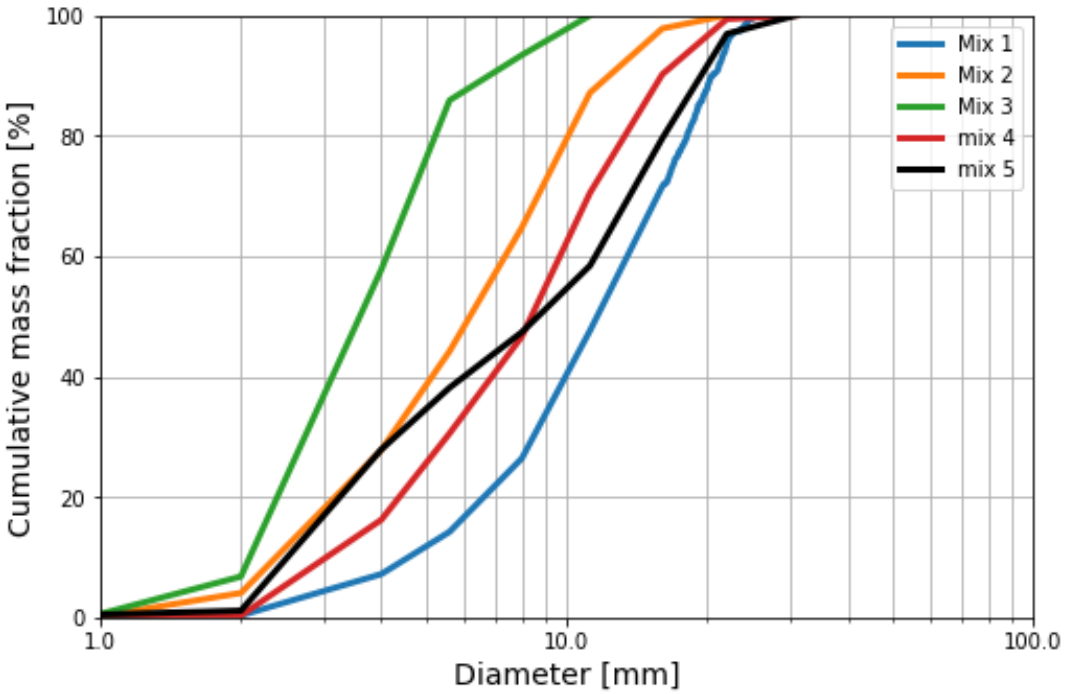

Figure 3.8: Grading curve of the different under-layer mixes

The under-layer mixes are painted to enable easier determination of under-layer material transport.

Around the waterline, The under-layer is installed in 5 colour bands with a uniform width of 15 cm, because it can be expected that material transport in this region is most likely. Lower down on the slope one larger colour band of 30 cm is installed, followed by the lowest, uncoloured band of stones where no transport of under-layer material at all is expected. Given that photographs are taken of the under-layer after each test sub-series, these different colour bands can be used to more accurately observe the movement of the under-layer stones. Many examples of this can be seen in chapter 4.

3.4. Test program

The test program consists of five test series. Each test series uses its respective under-layer mix (Mix 1 for test series 1, mix 2 for test series 2, etc.), while the armour layer material is constant. In each test series, three different wave heights are used, as well as two different wave steepnesses, resulting in six tests per test series. Because two different wave steepnesses are used, each test series TSx can be further subdivided into test sub-series TSx.1 and TSx.2. A total of 30 tests were performed.

The following parameters are constant throughout the whole test program:

- Diameter of the armour layer stones ($D_{50,a}$)
- Thickness of the armour layer ($2 * D_{n50,a}$)
- Width of the armour layer material grading curve ($C_{u,a} = 1.24$)
- Thickness of the under-layer ($0.5 * D_{n50,a}$)
- Water level ($h = 0.6m$)
- Number of waves ($N = 1000$)

The following parameters are varied throughout the test program:

- Ratio of the size of the armour layer material to the size of the under-layer material ($D_{15,a}/D_{85,u}$)
- Grading width of the under-layer material ($C_{u,u}$)
- Wave height (H_s)
- Wave steepness (s_{op})

Since the main goal of this research is to expand the knowledge on the stability of closed granular filters under wave loading, the values of $D_{15,a}/D_{85,u}$ and $C_{u,u}$ (and by extension $D_{50,a}/D_{50,u}$) are largely determined by the values used in previous research programs. On one hand, it is desirable to test values that are close to those used in earlier research, since a different slope, which has not been used in these earlier test programs, is used this time. On the other hand, it is also desirable to test values that have not been tested before to add to the variety of test results which can be used for the analysis. The values of $D_{15,a}/D_{85,u}$ and $C_{u,u}$ were chosen to meet both of these criteria. However, due to the randomness of rubble stone, the grading curves of the under-layer mixes cannot be made to the exact specification of the theoretical, pre-calculated grading curves. Therefore, a distinction is made between the desired values for $D_{15,a}/D_{85,u}$ and $C_{u,u}$, and the realized values. An overview of the desired and realized values is shown in table 3.3.

Table 3.3: Desired and realized values of $D_{15,a}/D_{85,u}$ and $C_{u,u}$ for all under-layer mixes

Mix name	Desired $D_{15,a}/D_{85,u}$	Realized $D_{15,a}/D_{85,u}$	Desired $C_{u,u}$	Realized $C_{u,u}$
1	2.00	2.55	3.00	2.94
2	4.00	4.48	3.00	3.10
3	8.00	8.56	2.00	1.96
4	3.00	3.27	3.00	3.04
5	3.00	2.75	4.50	4.56

For mix 1 and 2, the uniformity coefficient of the under-layer material is kept constant while the size was varied. For mix 3, the ratio $D_{15,a}/D_{85,u}$ is increased to a value as high as possible with the six different stone types available. However, this results in a decrease of the uniformity coefficient. For mix 4, a middle ground is chosen between mixes 1 and 2, while keeping the uniformity coefficient as close as

those two mixes as possible. For mix 5, the uniformity coefficient is increased to a value as high as possible with the six stone types available, while keeping the ratio $D_{15,a}/D_{85,u}$ as close as possible to earlier mixes, namely 4.5.

In figure 3.9, the Giroud diagram with the realized values is shown, as well as the values used by Thompson & Shuttler (1975) and van Gent & Wolters (2016). The large dashed line is the Terzaghi (1939) criterion ($D_{15,a}/D_{85,u} < 5$). The dash-dot line is the ratio given by Thompson & Shuttler ($D_{15,a}/D_{85,u} < 4$). The small dashed line is the criterion given by The Rock Manual errata list (CIRIA, CUR, CETMEF, 2017, see also section 2.3.2) for under-layer thicknesses of $2 * D_{50}$ ($D_{15,a}/D_{85,u} < 3.3$). As can be seen in the figure, this research explores the boundaries of the diagram slightly more than previous research. As well as testing a larger $D_{15,a}/D_{85,u}$ ratio, higher yet than Terzaghi recommend, a wider grading curve for the under-layer is also tested. At the same time, values close to those used by Thompson & Shuttler and van Gent & Wolters are tested as well. Hereby, the criteria set in the paragraph before table 3.3 are met.

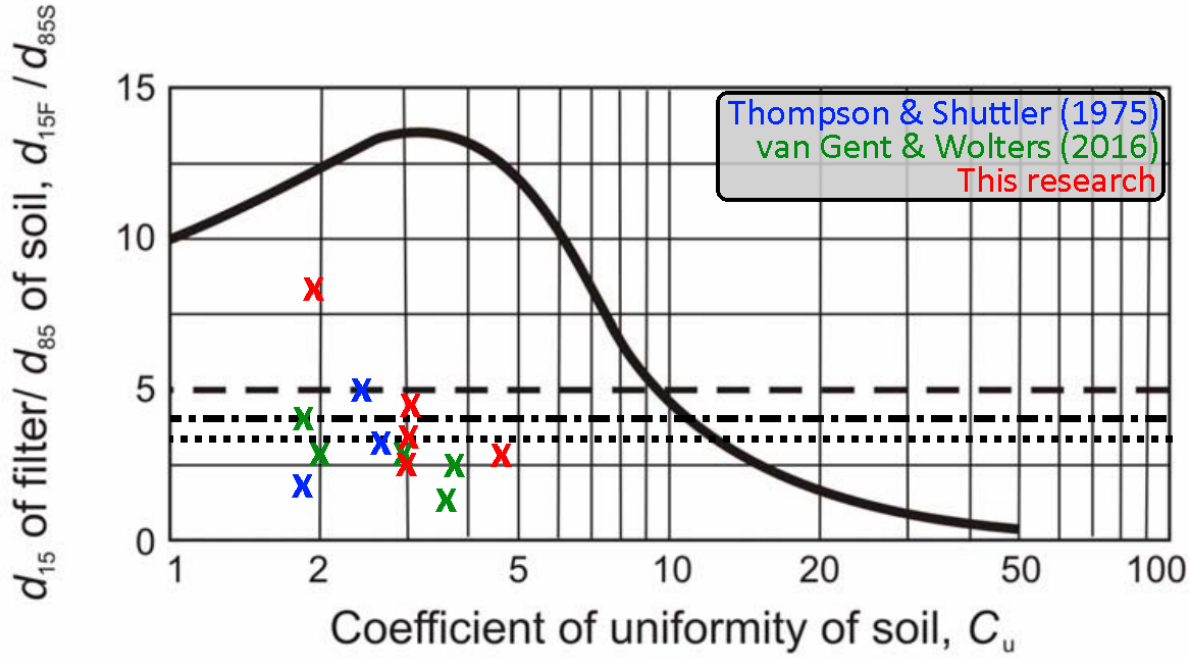

Figure 3.9: Giroud diagram with the test programs of Thompson & Shuttler (1975), van Gent & Wolters (2016) and this research plotted

In figure 3.10, the Cistin/Ziems diagram with the realized values is shown, as well as the values used by Thompson & Shuttler (1975) and van Gent & Wolters (2016). As can be seen in the figure, the Cistin/Ziems diagram is more strict than the Giroud diagram. According to the latter, full retention of the under-layer is expected during the tests, while according to the former, during two of the five test series, washout of the under-layer material through the armour layer is expected.

For the wave conditions, it is chosen to use both shorter ($s_{op} = 0.04$) and longer ($s_{op} = 0.02$) waves. This results in Iribarren numbers of $\xi_{op} = 2.5$ and $\xi_{op} = 3.5$ respectively. This way the most common breaker types occurring at bank protections and breakwaters, namely plunging, collapsing and surging breakers, are considered. The main focus of the tests is the stability of the filter construction without damage to the armour layer. In that case, the hydraulic load on the under-layer is as high as possible while simultaneously not exposing it due to damage to the armour layer. This is desirable, as it would otherwise not be possible to differentiate between under-layer damage due to washout (because the filter construction is not geometrically closed) and damage caused by direct wave attack due to the exposure of the under-layer. Therefore the wave heights have been chosen such that, given the size and density of the armour layer material, the armour layer is designed for a start of damage criterion (S = 2-3 (CIRIA, CUR, CETMEF, 2007)). This has been done using the van der Meer formulae.

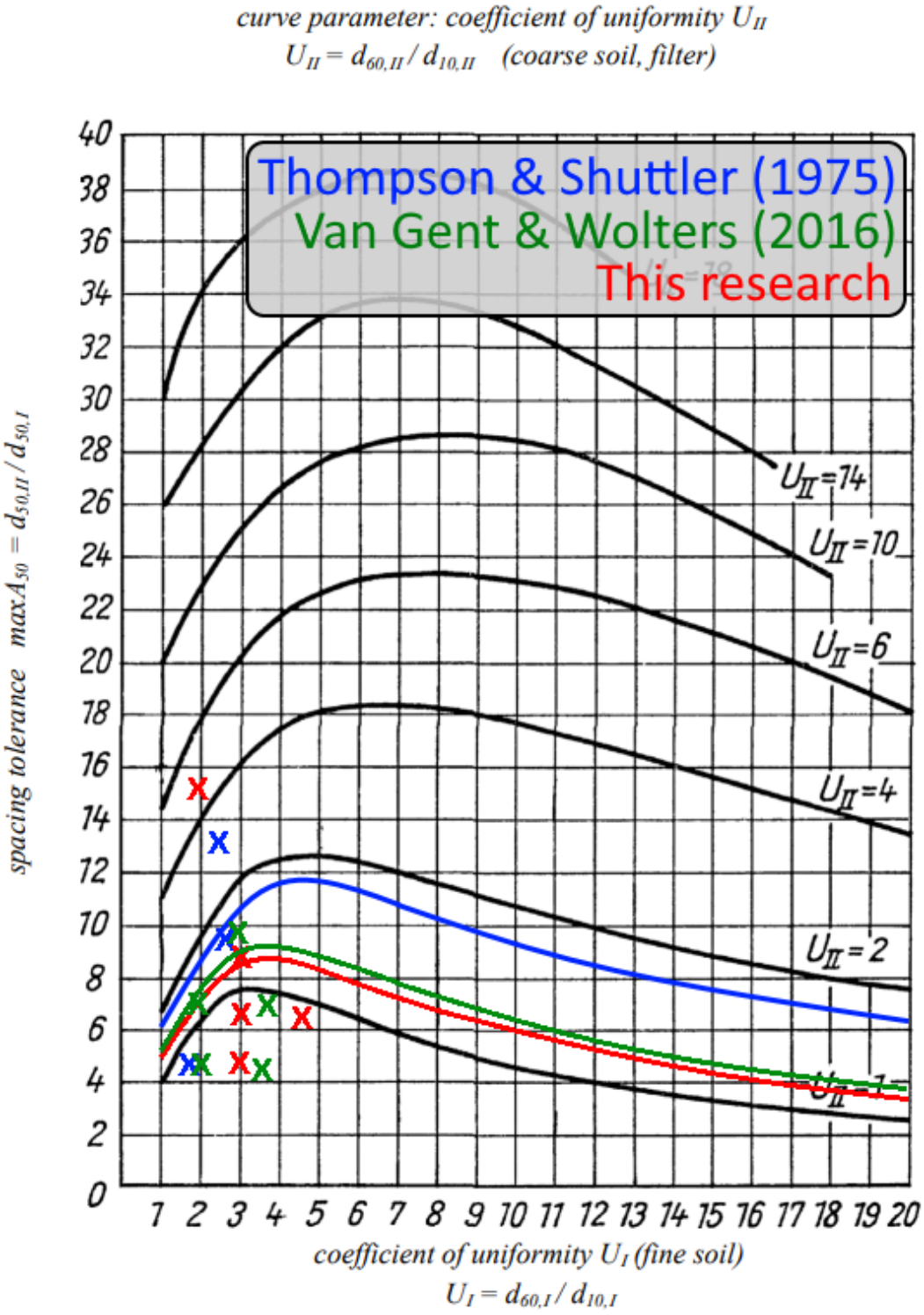

Figure 3.10: Cistin/Ziems with the test programs of Thompson & Shuttler (1975), van Gent & Wolters (2016) and this research plotted

A summary of the full test program can be found in table 3.4. The nomenclature of the tests is as follows: *Test series*.*Test subseries*.*Test number*. The values used in table 3.4 for the stone sizes and wave conditions are the realized values. For a full overview of the hydraulic conditions, the reader is referred to appendix C.

Table 3.4: Test program with measured stone sizes and wave conditions

Test	Test parameters					Loading parameters				
	$D_{50,a}$ [mm]	$D_{50,u}$ [mm]	$\frac{D_{15,a}}{D_{85,u}}$ [-]	$\frac{D_{50,a}}{D_{50,u}}$ [-]	$C_{u,u}$ [-]	h [m]	H_{m0} [m]	T_p [s]	s_{op} [-]	ξ_{op} [-]
1.1.1	55	11.60	2.55	4.74	2.94	0.6	0.089	1.26	0.034	2.71
1.1.2	55	11.60	2.55	4.74	2.94	0.6	0.115	1.44	0.034	2.72
1.1.3	55	11.60	2.55	4.74	2.94	0.6	0.142	1.57	0.035	2.67
1.2.1	55	11.60	2.55	4.74	2.94	0.6	0.074	1.52	0.019	3.58
1.2.2	55	11.60	2.55	4.74	2.94	0.6	0.105	1.84	0.019	3.64
1.2.3	55	11.60	2.55	4.74	2.94	0.6	0.130	2.00	0.020	3.56
2.1.1	55	6.19	4.48	8.89	3.10	0.6	0.090	1.28	0.033	2.73
2.1.2	55	6.19	4.48	8.89	3.10	0.6	0.114	1.43	0.034	2.71
2.1.3	55	6.19	4.48	8.89	3.10	0.6	0.141	1.57	0.035	2.68
2.2.1	55	6.19	4.48	8.89	3.10	0.6	0.078	1.58	0.019	3.63
2.2.2	55	6.19	4.48	8.89	3.10	0.6	0.104	1.89	0.018	3.76
2.2.3	55	6.19	4.48	8.89	3.10	0.6	0.134	2.06	0.019	3.61
3.1.1	55	3.61	8.56	15.24	1.96	0.6	0.090	1.27	0.034	2.71
3.1.2	55	3.61	8.56	15.24	1.96	0.6	0.116	1.41	0.036	2.65
3.1.3	55	3.61	8.56	15.24	1.96	0.6	0.142	1.53	0.037	2.60
3.2.1	55	3.61	8.56	15.24	1.96	0.6	0.078	1.56	0.020	3.58
3.2.2	55	3.61	8.56	15.24	1.96	0.6	0.105	1.84	0.019	3.64
3.2.3	55	3.61	8.56	15.24	1.96	0.6	0.136	2.06	0.020	3.58
4.1.1	55	8.39	3.27	6.56	3.04	0.6	0.091	1.24	0.036	2.63
4.1.2	55	8.39	3.27	6.56	3.04	0.6	0.116	1.42	0.035	2.67
4.1.3	55	8.39	3.27	6.56	3.04	0.6	0.139	1.61	0.033	2.77
4.2.1	55	8.39	3.27	6.56	3.04	0.6	0.078	1.58	0.019	3.63
4.2.2	55	8.39	3.27	6.56	3.04	0.6	0.103	1.79	0.020	3.58
4.2.3	55	8.39	3.27	6.56	3.04	0.6	0.134	2.06	0.019	3.61
5.1.1	55	8.67	2.75	6.34	4.56	0.6	0.091	1.26	0.035	2.68
5.1.2	55	8.67	2.75	6.34	4.56	0.6	0.117	1.43	0.035	2.68
5.1.3	55	8.67	2.75	6.34	4.56	0.6	0.141	1.63	0.032	2.78
5.2.1	55	8.67	2.75	6.34	4.56	0.6	0.078	1.62	0.018	3.72
5.2.2	55	8.67	2.75	6.34	4.56	0.6	0.103	1.84	0.019	3.67
5.2.3	55	8.67	2.75	6.34	4.56	0.6	0.133	2.05	0.019	3.60

3.5. Model scaling

Physical models are a widely used tool in the field of hydraulic engineering. Often, a scale model of the full scale design is used for experiments. The model is scaled in such a way that all important hydraulic and structural conditions are similar to the full scale design. This is called similitude. The most important parameters for which similitude needs to be achieved for wave models are the Froude number Fr, the Reynolds number Re and the Weber number We (Kirkegaard et al., 2011). These parameters are defined as:

$$Fr = \frac{u}{\sqrt{g * L}} \tag{3.2}$$

$$Re = \frac{u * L}{\nu_k} \tag{3.3}$$

$$We = \frac{\rho_w * u^2 * L}{\sigma} \tag{3.4}$$

In which u is the particle velocity, g is the gravitational acceleration, L is the characteristic length, ν_k is the kinematic viscosity of water, ρ_w is the density of water and σ is the surface tension. Le Méhauté (1976) found that if the model is not too small ($\lambda > 2\ cm$, $T > 0.35\ s$ and $h > 0.02\ m$), the surface

tension is negligible and thus the Weber similitude can be neglected. As can be seen in table 3.4, this is the case for all tests in this test program.

In this research, no full scale design is considered, but the model represents a more general case for bank protections, or breakwaters with impermeable cores. As such, there is no full-scale design that the Froude and Reynolds numbers need to be similar to. However, this does not mean that all similitude can be neglected. In order for this general physical model to be valid at larger scales, turbulent flow conditions need to exist throughout the armour layer (Kirkegaard et al., 2011). According to Dai & Kamel (1969), this is the case if $Re > 30000$. For flow conditions in the armour layer, equation 3.3 can be written as (Kirkegaard et al., 2011):

$$Re_D = \frac{\sqrt{g * H_{m0} * D_{n50,a}}}{\nu_k} \tag{3.5}$$

Since g, $D_{n50,a}$ and ν_k are constants, namely 9.81 m/s^2, 0.0462 m and 10^{-6} respectively, the minimum value of Re_D can be found by minimizing H_{m0}. In table 3.4 it can be seen that the lowest value of H_{m0} during the tests was 0.074 m. When substituting all values into equation 3.5, it is found that $Re_D = 1.83{*}10^5$. This is higher than the value of 30000 as prescribed by Dai & Kamel (1969). Therefore, it can be assumed that no scaling effects took place during the tests.

4

Results

In this chapter the results of the model tests are presented. In section 4.1 a summary of the test results is given. In section 4.2 the results of the tests are elaborated in more detail, supported by observations, photographs and plots.

4.1. Overview of the results

An overview of the model test results is shown in table 4.1. The damage level S of the armour layer was calculated as described in section 3.2.3. The damage level was determined using the cumulative damage per test sub-series. After every sub-series, the armour layer was removed, the under-layer was repaired and the armour layer was reconstructed. In section 4.2 the results are discussed in more detail. For the realized wave conditions during the tests, the reader is referred to table 3.4

Table 4.1: Small overview of test results

		Armour layer	Under-layer		
	Test	**S (SWL +/- 2*H_s)**	**Displacement of under-layer stones (>$D_{50,a}$)**	**Intrusion of under-layer stones into armour layer**	**Washout of under-layer material**
Test series 1 $D_{15,a}/D_{85,u} = 2.55$ $D_{50,a}/D_{50,u} = 4.74$ $C_{u,u} = 2.94$	**1.1.1**	0.6	No	No	No
	1.1.2	0.8	No	No	No
	1.1.3	2.4	No	No	No
	1.2.1	0.9	No	No	No
	1.2.2	1.5	No	No	No
	1.2.3	2.3	No	No	No
Test series 2 $D_{15,a}/D_{85,u} = 4.48$ $D_{50,a}/D_{50,u} = 8.89$ $C_{u,u} = 3.10$	**2.1.1**	0.7	No	No	No
	2.1.2	0.9	Yes	No	No
	2.1.3	1.2	Yes	Yes	No
	2.2.1	0.6	No	No	No
	2.2.2	0.8	Yes	No	No
	2.2.3	2.0	Yes	Yes	No
Test series 3 $D_{15,a}/D_{85,u} = 8.56$ $D_{50,a}/D_{50,u} = 15.24$ $C_{u,u} = 1.96$	**3.1.1**	0.9	Yes	Yes	No
	3.1.2	1.8	Yes	Yes	Yes
	3.1.3	3.1	Yes	Yes	Yes
	3.2.1	1.1	Yes	Yes	No
	3.2.2	1.9	Yes	Yes	Yes
	3.2.3	4.3	Yes	Yes	Yes
Test series 4 $D_{15,a}/D_{85,u} = 3.27$ $D_{50,a}/D_{50,u} = 6.56$ $C_{u,u} = 3.04$	**4.1.1**	0.6	No	No	No
	4.1.2	1.1	No	No	No
	4.1.3	2.8	No	No	No
	4.2.1	0.8	No	No	No
	4.2.2	1.3	No	No	No
	4.2.3	2.4	No	No	No
Test series 5 $D_{15,a}/D_{85,u} = 2.75$ $D_{50,a}/D_{50,u} = 6.34$ $C_{u,u} = 4.56$	**5.1.1**	0.4	No	No	No
	5.1.2	1.2	No	No	No
	5.1.3	2.1	No	No	No
	5.2.1	0.4	No	No	No
	5.2.2	1.5	No	No	No
	5.2.3	2.9	Yes	Yes	No

4.2. Individual test series results

In this section the results of the individual test (sub-)series are shown. Images of the armour- and under-layers before and after the test sub-series are shown, as well as plots of the average profiles of the armour layers before and after every sub-series, so before tests x.x.1 and after tests x.x.3. For the average profiles of the armour layers after every test (including the x.x.1 and x.x.2 tests), the reader is referred to appendix C. Unfortunately, the images of the armour layer before and after sub-series TS1.1, before sub-series TS2.1, and before and after sub-series TS3.1 were corrupted.

Observations made during the tests are also noted. In these observations, a distinction is made in the amount of movement of the under-layer material. When the term *rocking* is used, it refers to the movement type where individual stones move back and forth, but only by less than one stone-diameter and in a cyclic manner, such that ultimately the position of the stones themselves remains the same. When the term *displacement* is used, it refers to an actual change in position of the stones themselves.

4.2.1. Test series 1

For test series 1, the under-layer material with the largest size relative to the armour layer material was used. Here, the ratio $D_{50,a}/D_{50,u}$ is already larger than the present conservative design guidance in The Rock manual (CIRIA, CUR, CETMEF, 2007; see also section 2.3.3). Photos of the under-layer before and after sub-series TS1.1 can be seen in figures 4.1 and 4.2 respectively. The measured profile before and after sub-series TS1.1 can be seen in figure 4.3. The damage of the armour layer after test 1.1.3 was S = 2.4. Therefore, the 'start of damage' (S = 2-3 (CIRIA, CUR, CETMEF, 2007)) criterion is satisfied.

Figure 4.1: Under-layer before sub-series TS1.1

Figure 4.2: Under-layer after sub-series TS1.1

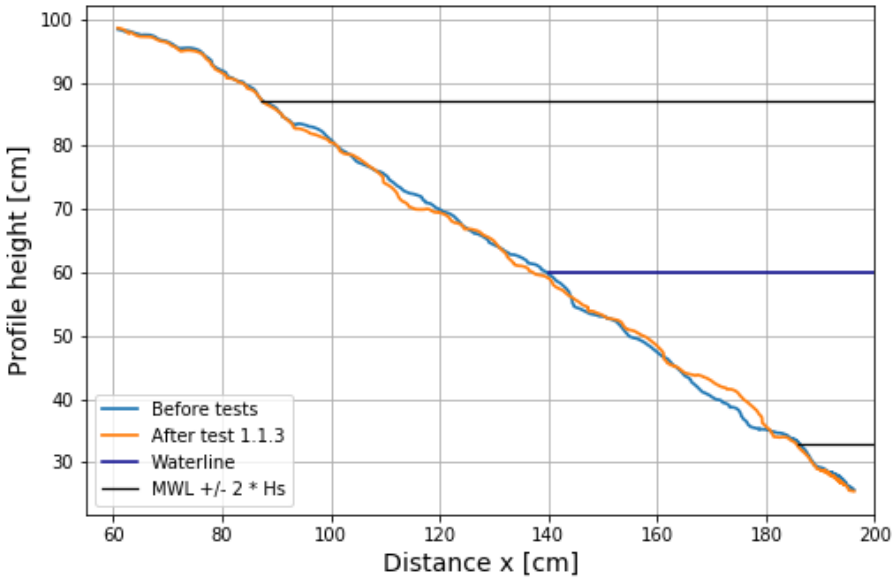

Figure 4.3: Average armour layer profile before and after test sub-series TS1.1

Photos of the under-layer before and after sub-series TS1.2 can be seen in figures 4.4 and 4.5 respectively. Photos of the armour layer before and after sub-series TS1.2 can be seen in figures 4.6 and 4.7 respectively. The measured profile before and after sub-series TS1.2 can be seen in figure 4.8.

The damage of the armour layer after test 1.2.3 was S = 2.3. Therefore, the 'start of damage' (S = 2-3 (CIRIA, CUR, CETMEF, 2007)) criterion is satisfied.

Figure 4.4: Under-layer before sub-series TS1.2

Figure 4.5: Under-layer after sub-series TS1.2

Figure 4.6: Armour layer before sub-series TS1.2

Figure 4.7: Armour layer after sub-series TS1.2

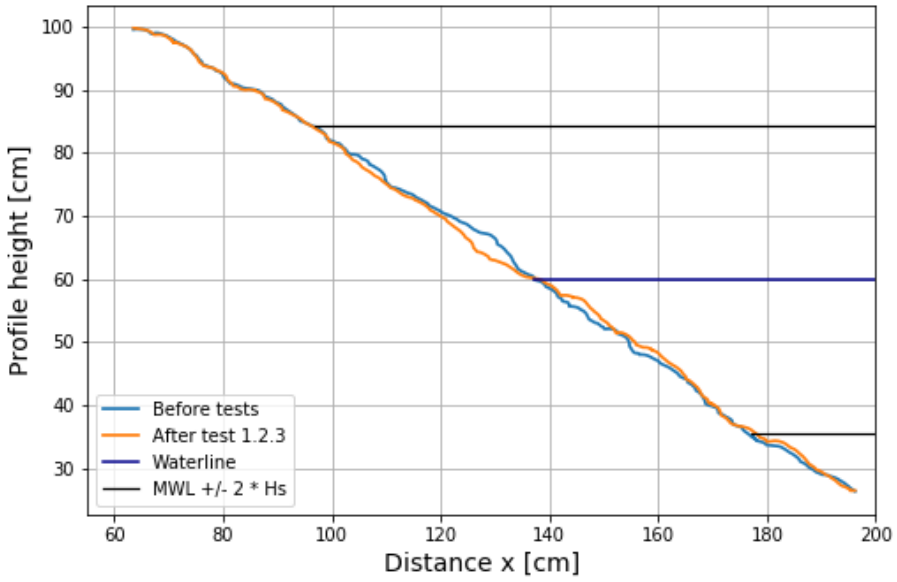

Figure 4.8: Average armour layer profile before and after test sub-series TS1.2

The following observations were made during and after test series 1:

- A very small amount of rocking of the under-layer material was observed near the glass sidewall. Rocking was only observed during the larger waves of the test.
- For both sub-series TS1.1 and TS1.2, no displacement of under-layer stones of more than $D_{50,a}$ was observed near the glass, nor was it observed after dismantling the armour layer.
- No washout of under-layer stones through the armour layer was observed during the test.
- No under-layer stones were found inside the armour layer while disassembling the armour layer for both sub-series TS1.1 and TS1.2.

4.2.2. Test series 2

For test series 2, the under-layer material with a ratio of $D_{15,a}/D_{85,b} = 4.48$ was used. This ratio coincides with Terzaghi's original interface stability requirement of $D_{15,a}/D_{85,b} = 4\ to\ 5$. Photos of the under-layer before and after sub-series TS2.1 can be seen in figures 4.9 and 4.10 respectively. The measured profile before and after sub-series TS2.1 can be seen in figure 4.11. The damage of the armour layer after test 2.1.3 was S = 1.2. According to The Rock Manual (CIRIA, CUR, CETMEF, 2007), this value classifies as 'no damage'. This is less than 'start of damage' (S = 2-3), which is the ideal damage level, as the hydraulic load on the under-layer could have been increased without causing damage to the armour layer. However, the objective is to keep the under-layer from being exposed due to armour layer damage (see also section 3.4), which was achieved in this case.

Figure 4.9: Under-layer before sub-series TS2.1

Figure 4.10: Under-layer after sub-series TS2.1

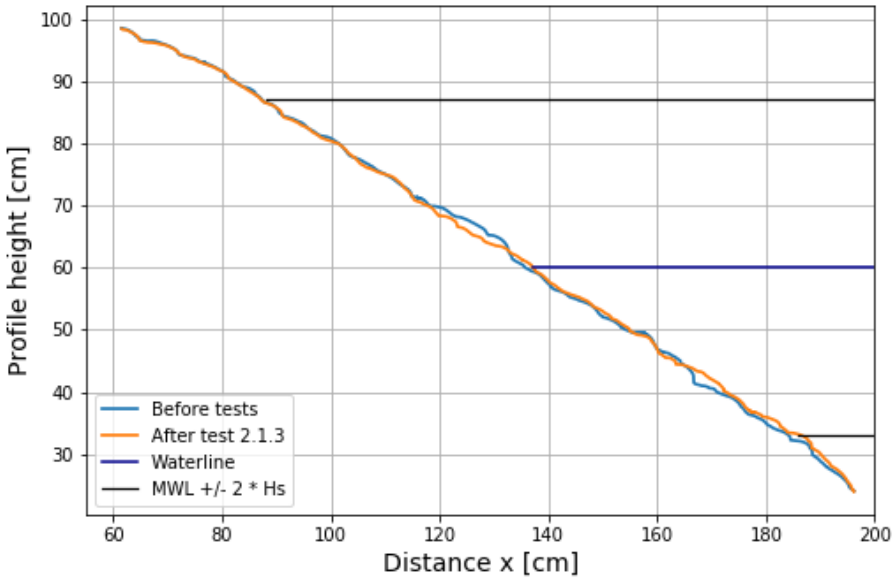

Figure 4.11: Average armour layer profile before and after test sub-series TS2.1

Photos of the under-layer before and after sub-series TS2.2 can be seen in figures 4.12 and 4.13 respectively. Photos of the armour layer before and after sub-series TS2.2 can be seen in figures 4.14 and 4.15 respectively. The measured profile before and after sub-series TS2.2 can be seen in figure 4.16. The damage of the armour layer after test 1.2.3 was S = 2.0. Therefore, the 'start of damage' (S = 2-3 (CIRIA, CUR, CETMEF, 2007)) criterion is satisfied.

Figure 4.12: Under-layer before sub-series TS2.2

Figure 4.13: Under-layer after sub-series TS2.2

Figure 4.14: Armour layer before sub-series TS2.2

Figure 4.15: Armour layer after sub-series TS2.2

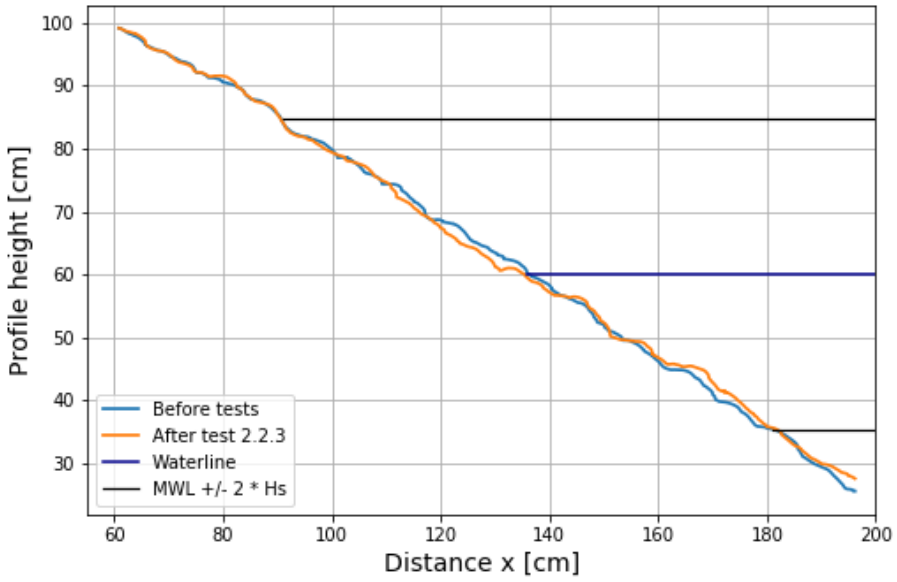

Figure 4.16: Average armour layer profile before and after test sub-series TS2.2

The following observations were made during and after test series 2:

- Continuous rocking of the under-layer material was observed near the glass sidewall, even during the smaller waves of the tests.
- Displacement of under-layer stones of more than $D_{50,a}$ was observed near the glass, but only during the larger waves of the tests.
- Significant displacement of under-layer stones of more than $D_{50,a}$ was observed after dismantling the armour layer for both sub-series TS2.1 and TS2.2.
- After dismantling the armour layer after sub-series TS2.1, two erosion holes were found inside the under-layer, both of which went all the way through to the impermeable core. The rightmost erosion hole was situated 3 cm below the waterline (vertically) and the leftmost erosion hole was situated 10 cm below the water line (vertically). After dismantling the armour layer after sub-series 2.2, an erosion hole was found on the right side of the under-layer, next to the right glass wall of the wave flume. Vertically, the erosion hole reached from 2 cm below the waterline to 10 cm above the waterline. Again, the erosion reached all the way through the under-layer to the impermeable core.
- No full washout of under-layer stones through the armour layer was observed during the test. However, after both sub-series TS2.1 and TS2.2, under-layer stones could be seen without removing any armour layer stones, indicating that under-layer stones had migrated upward into the armour layer, without completely washing out. Confirming this, some under-layer stones were found inside the armour layer while disassembling the armour layer for both sub-series TS2.1 and TS2.2.

4.2.3. Test series 3

For test series 3, the under-layer material with the smallest size was used. According to the Giroud diagram, it is expected that the under-layer stones are retained. However, according to the Cistin/Ziems diaggram it is expected that the under-layer stones are not retained and washout will occur. Photos of the under-layer before and after sub-series TS3.1 can be seen in figures 4.17 and 4.18 respectively. Photos of the armour layer before and after sub-series TS3.1 can be seen in figures 4.19 and 4.20 respectively. The measured profile before and after sub-series TS3.1 can be seen in figure 4.21. The damage of the armour layer after test 3.1.3 was S = 3.1. Therefore, the 'start of damage' (S = 2-3 (CIRIA, CUR, CETMEF, 2007)) criterion not satisfied. However, during the tests in sub-series TS3.1, no significant increase in the erosion of armour layer stones was observed, compared to earlier tests. Therefore it was hypothesized that the increase in armour layer damage was caused by subsidence

of the armour layer due to washout of the under-layer, as significant washout of the under-layer was observed during sub-series TS3.1. This will be further analyzed in section 5.2.2.

Figure 4.17: Under-layer before sub-series TS3.1

Figure 4.18: Under-layer after sub-series TS3.1

Figure 4.19: Armour layer before sub-series TS3.1

Figure 4.20: Armour layer after sub-series TS3.1

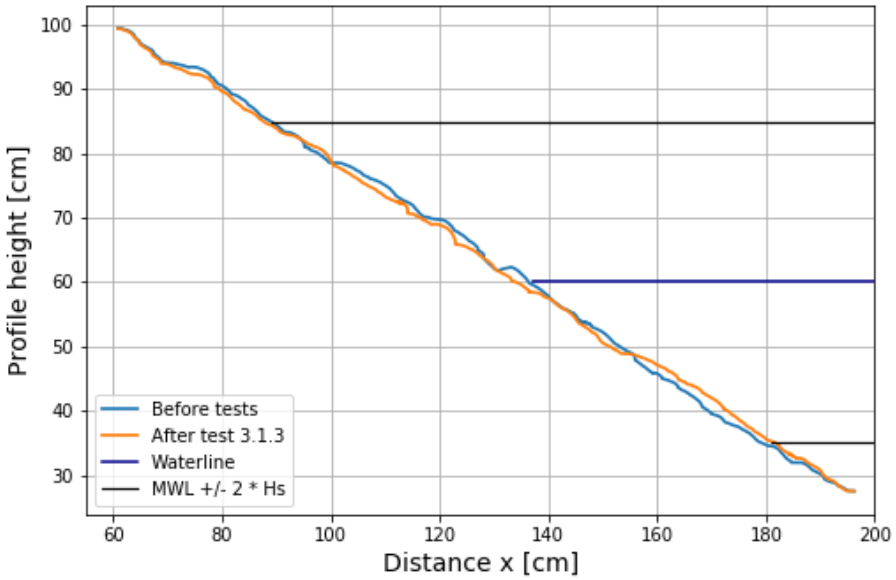

Figure 4.21: Average armour layer profile before and after test sub-series TS3.1

Photos of the under-layer before and after sub-series TS3.2 can be seen in figures 4.22 and 4.23 respectively. The measured profile before and after sub-series TS3.2 can be seen in figure 4.24. The damage of the armour layer after test 3.2.3 was S = 4.3. Therefore, the 'start of damage' (S = 2-3 (CIRIA, CUR, CETMEF, 2007)) criterion not satisfied. Similarly to sub-series TS3.1, it was hypothesized that the increase in armour layer damage was caused by subsidence of the armour layer due to washout of the under-layer, rather than extra erosion of the armour layer. Again, this will be analyzed in section 5.2.2.

Figure 4.22: Under-layer before sub-series TS3.2

Figure 4.23: Under-layer after sub-series TS3.2

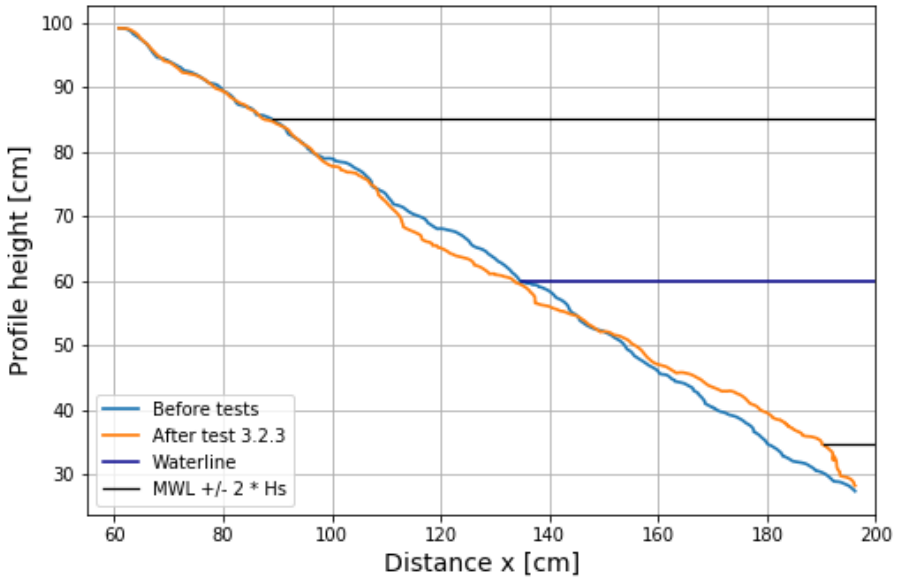

Figure 4.24: Average armour layer profile before and after test sub-series TS3.2

The following observations were made during and after test series 3:

- Continuous rocking of the under-layer material was observed near the glass sidewall, even during the smaller waves of the tests.
- Displacement of under-layer stones of more than $D_{50,a}$ was observed near the glass, even during the smaller waves of the tests.
- Significant displacement of under-layer stones of more than $D_{50,a}$ was observed after dismantling the armour layer for both sub-series TS3.1 and TS3.2.
- After dismantling the armour layer after sub-series TS3.1, a large hole was found inside the under-layer, which went all the way through to the impermeable core. The erosion hole extended from the glass right side of the wave flume to the middle of the flume. After dismantling the armour layer after sub-series 3.2, total destruction of the under-layer was found across the entire width of the under-layer, extending from 8 cm below the waterline to 8 cm above the waterline vertically.
- Significant washout of under-layer stones through the armour layer was observed during the test for both sub-series 3.1 and 3.2. After both sub-series, many under-layer stones could be rested on top of the armour layer without removing any armour layer stones, indicating that many under-layer stones washed out.
- Many under-layer stones were found inside the armour layer while disassembling the armour layer for both sub-series TS3.1 and TS3.2.

4.2.4. Test series 4

For test series 4, the ratio of the under-layer material size to the armour layer material size was in between that of test series 1 and 2. Photos of the under-layer before and after sub-series TS4.1 can be seen in figures 4.25 and 4.26 respectively. Photos of the armour layer before and after sub-series TS4.1 can be seen in figures 4.27 and 4.28 respectively. The measured profile before and after sub-series TS4.1 can be seen in figure 4.29. The damage of the armour layer after test 4.1.3 was S = 2.8. Therefore, the 'start of damage' (S = 2-3 (CIRIA, CUR, CETMEF, 2007)) criterion is satisfied.

Figure 4.25: Under-layer before sub-series TS4.1

Figure 4.26: Under-layer after sub-series TS4.1

Figure 4.27: Armour layer before sub-series TS4.1

Figure 4.28: Armour layer after sub-series TS4.1

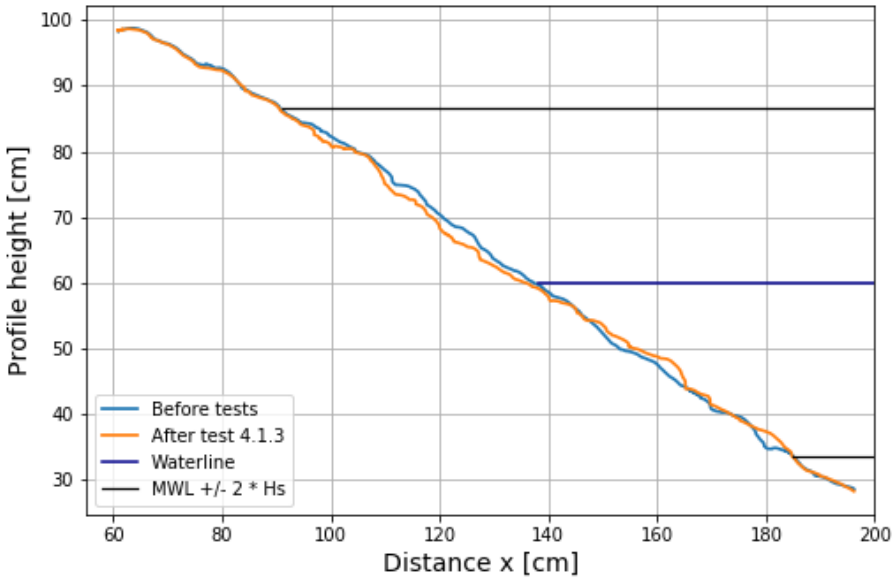

Figure 4.29: Average armour layer profile before and after test sub-series TS4.1

Photos of the under-layer before and after sub-series TS4.2 can be seen in figures 4.30 and 4.31 respectively. Photos of the armour layer before and after sub-series TS4.2 can be seen in figures 4.32 and 4.33 respectively. The measured profile before and after sub-series TS4.2 can be seen in figure 4.34. The damage of the armour layer after test 4.2.3 was S = 2.4. Therefore, the 'start of damage' (S = 2-3 (CIRIA, CUR, CETMEF, 2007)) criterion is satisfied.

Figure 4.30: Under-layer before sub-series TS4.2

Figure 4.31: Under-layer after sub-series TS4.2

Figure 4.32: Armour layer before sub-series TS4.2

Figure 4.33: Armour layer after sub-series TS4.2

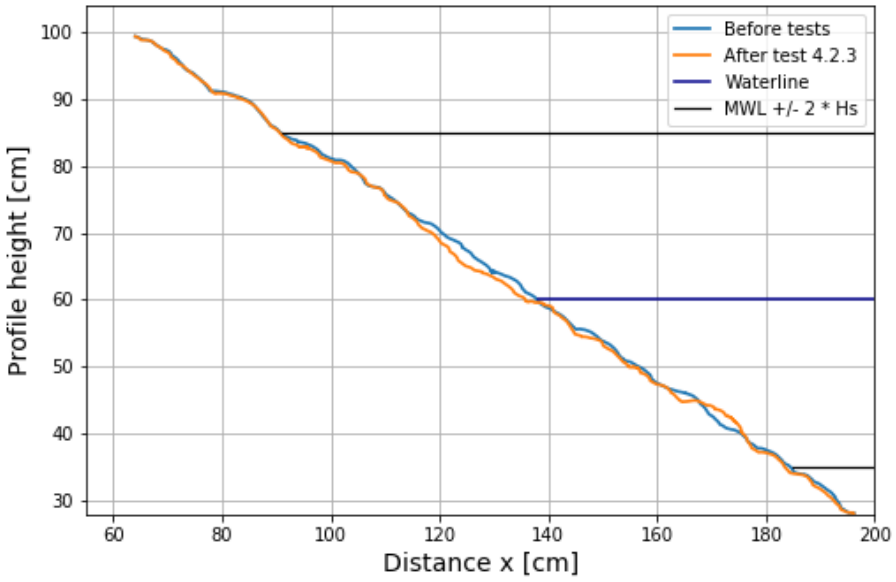

Figure 4.34: Average armour layer profile before and after test sub-series TS4.2

The following observations were made during and after test series 4:

- A very small amount of rocking of the under-layer material was observed near the glass sidewall. Rocking was only observed during the highest waves of the tests.
- For both sub-series TS4.1 and TS4.2, no displacement of under-layer stones of more than $D_{50,a}$ was observed near the glass, nor was it observed after dismantling the armour layer.
- No washout of under-layer stones through the armour layer was observed during the test.
- No under-layer stones were found inside the armour layer while disassembling the armour layer for both sub-series TS4.1 and TS4.2.

4.2.5. Test series 5

For test series 5, the ratio of the under-layer material size to the armour layer material size was close to that of test series 4 ($D_{50,a}/D_{50,u}$ = 6.34 and 6.56 respectively). However, for test series 5, the uniformity coefficient was significantly higher ($C_{u,u}$ = 4.56 and 3.04 respectively). Photos of the under-layer before and after sub-series TS5.1 can be seen in figures 4.35 and 4.36 respectively. Photos of the armour layer before and after sub-series TS5.1 can be seen in figures 4.37 and 4.38 respectively. The measured profile before and after sub-series TS5.1 can be seen in figure 4.39. The damage of the armour layer after test 5.1.3 was S = 2.1. Therefore, the 'start of damage' (S = 2-3 (CIRIA, CUR, CETMEF, 2007)) criterion is satisfied.

Figure 4.35: Under-layer before sub-series TS5.1

Figure 4.36: Under-layer after sub-series TS5.1

Figure 4.37: Armour layer before sub-series TS5.1

Figure 4.38: Armour layer after sub-series TS5.1

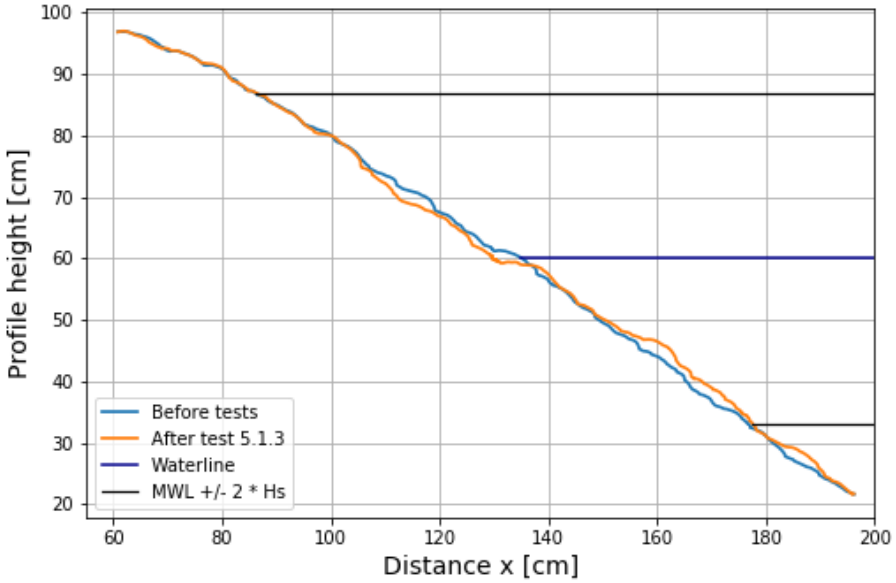

Figure 4.39: Average armour layer profile before and after test sub-series TS5.1

Photos of the under-layer before and after sub-series TS5.2 can be seen in figures 4.40 and 4.41 respectively. Photos of the armour layer before and after sub-series TS5.2 can be seen in figures 4.42 and 4.43 respectively. The measured profile before and after sub-series TS5.2 can be seen in figure 4.44. The measured profile before and after sub-series TS5.1 can be seen in figure 4.39. The damage of the armour layer after test 5.2.3 was S = 2.9. Therefore, the 'start of damage' (S = 2-3 (CIRIA, CUR, CETMEF, 2007)) criterion is satisfied.

Figure 4.40: Under-layer before sub-series TS5.2

Figure 4.41: Under-layer after sub-series TS5.2

Figure 4.42: Armour layer before sub-series TS5.2

Figure 4.43: Armour layer after sub-series TS5.2

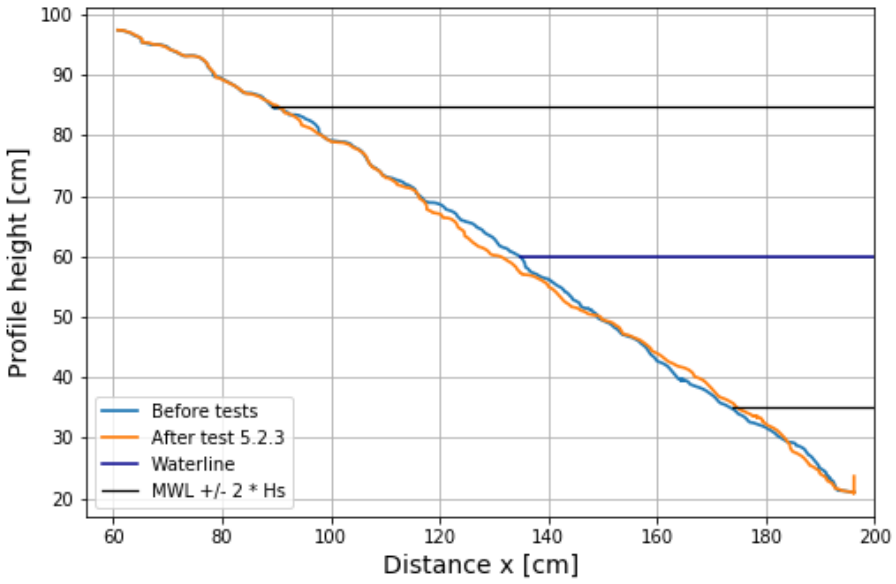

Figure 4.44: Average armour layer profile before and after test sub-series TS5.2

The following observations were made during and after test series 5:

- A very small amount of rocking of the under-layer material was observed near the glass sidewall. Rocking was only observed during the highest waves of the tests.
- No displacement of under-layer stones of more than $D_{50,a}$ was observed near the glass.
- After dismantling the armour layer for both sub-series TS5.1 and TS5.2, it was observed that some under-layer stones were displaced more than $D_{50,a}$.
- No washout of under-layer stones through the armour layer was observed during the test.
- No under-layer stones were found inside the armour layer while disassembling the armour layer for both sub-series TS5.1 and TS5.2.

5

Analysis

In this chapter the results are analyzed. First, a clear definition of 'geometrically closed' is proposed. Next, the mobility of the armour layer is analyzed. Combining the results from sections 5.1 and 5.2, it is determined which of the under-layer mixes used resulted in a geometrically closed filter structure. After this has been determined, the results of the tests performed in this research are combined with the results from earlier research projects to analyze the validity of several commonly used interface stability criteria for flow loading for sloped granular filters under wave loading. Finally, it is attempted to find the interface stability boundary for closed granular filters under wave loading.

5.1. Interpretation of 'geometrically closed'

Before analyzing the results, a clear definition of 'geometrically closed' is required. In a classical sense, a filter is geometrically closed if "the size of the grains is chosen such that thee grains cannot move in the filter" (Schiereck & Verhagen, 2012). This criterion in itself is relatively simple to validate. However, when the under-layer is being obscured from view by the armour layer, as is the case for bank protections and breakwater, it can be rather difficult to determine if grains from the under-layer move inside the armour layer. In this case, there are multiple methods to determine if the filter structure is geometrically closed or not.

First, it is possible that under-layer material visually gets extracted from the armour layer into the water above. In this case, it is easily determined if the filter structure is geometrically closed or not. After all, in order for this to happen, grains from the under-layer moved through the entire armour layer, as this is the only way that the grains could be moved to this position. Thus, the grains of the under-layer were able to move through the voids of the armour layer, meaning that the filter structure is not geometrically closed.

It is also possible that under-layer material passes the interface between the under-layer and the armour layer, but is not fully extracted from the armour layer. In this case, it cannot be visually determined during the test if the filter structure is geometrically closed or not. By definition, the filter structure is not geometrically closed in this case, because grains from the under-layer were moved from the under-layer into the armour layer, meaning that the grains were able to move through the voids of the armour layer. However, this can only be observed during the deconstruction of the armour layer after the test, as grains from the under-layer can be found inside the armour layer.

Complicating the matter is the fact that, during the test, limited damage to the armour layer is permitted, as is described in section 3.4. In the case that under-layer material has been displaced by a significant distance or has been washed out, but the armour layer has also eroded such that a hole in the armour layer was formed, it is very difficult to determine if the filter structure was geometrically closed or not. After all, the displacement or washing-out of the under-layer material could have been caused by a direct wave attack on the under-layer caused by an erosion hole in the armour layer.

Taking all of the above into consideration, it was determined that for the purpose of this research, a filter structure is geometrically closed if and only if:

For all performed tests using a certain combination of under-layer and armour layer material:

1. No wash-out of under-layer material through the armour layer was observed during any test;

and

2. No under-layer grains were found inside the armour layer when deconstructing the armour layer after any test;

and

3. At the end of the test, the damage sustained by the armour layer falls into the category 'start of damage' (S = 2-3) or 'no damage' (S < 2).

This means that, if the armour layer damage was larger than S > 3, it is impossible to conclude if the filter structure was geometrically closed. However, on the basis of observations made during the test, it *can* still be concluded if the filter structure was *definitely not* geometrically closed. An example: If, after a test, the armour layer damage was S = 5, but at the beginning of the test it was observed that under-layer material was already being washed out, before any erosion to the armour layer had occurred, it can be assumed that the filter structure was not geometrically closed.

It must be noted that in the case where under-layer material is briefly transported into the armour layer, but then falls back onto the under-layer, the filter structure would be qualified as 'closed' according to the above criteria, while in fact it is not. However, for the purpose of this research this is considered as acceptable, since it would be impossible to determine if any filter structure is closed when taking this into consideration.

5.2. Analysis of armour layer mobility

5.2.1. Comparison with van der Meer (1988)

In figure 5.1, the measured damage levels of the armour layer are plotted against the stability number $(H_s/(\Delta * D_{n50,a}))$ times the square root of ξ_m. As well as these points, the trend-line of the van der Meer (1988) is plotted as a continuous gray line. The 5% and 95% values of the van der Meer formula are plotted as dashed lines. For these lines, the 5% and 95% values for c_{pl} were determined using the mean value and standard deviation as documented in The Rock Manual (CIRIA, CUR, CETMEF, 2007). The van der Meer formula for plunging waves was used, as the value of ξ_m was below the critical value ξ_{cr} for all tests.

It must be noted that the van der Meer (1988) formula was not developed for situations where the armour layer damage is very low. This is shown in figure 5.1 by the fact that, for the lowest values of $(H_s/(\Delta * D_{n50,a})) * \xi_m^{0.5}$ (tests x.x.1) nearly all the measured points are outside of the 5% to 95% confidence interval of the van der Meer formula. For the medium values of $(H_s/(\Delta * D_{n50,a})) * \xi_m^{0.5}$ (tests x.x.2), only the points of test series 3 fall outside of the 5% to 95% confidence interval of the van der Meer formula. For the highest values of $(H_s/(\Delta * D_{n50,a})) * \xi_m^{0.5}$, which correspond to the final test of each sub-series (tests x.x.3), all of the points fall within the confidence interval. Therefore it can be concluded that the measured values for the final armour layer damage with damage values above S = 2 are within the 5% to 95% confidence bands of the van der Meer (1988) formula.

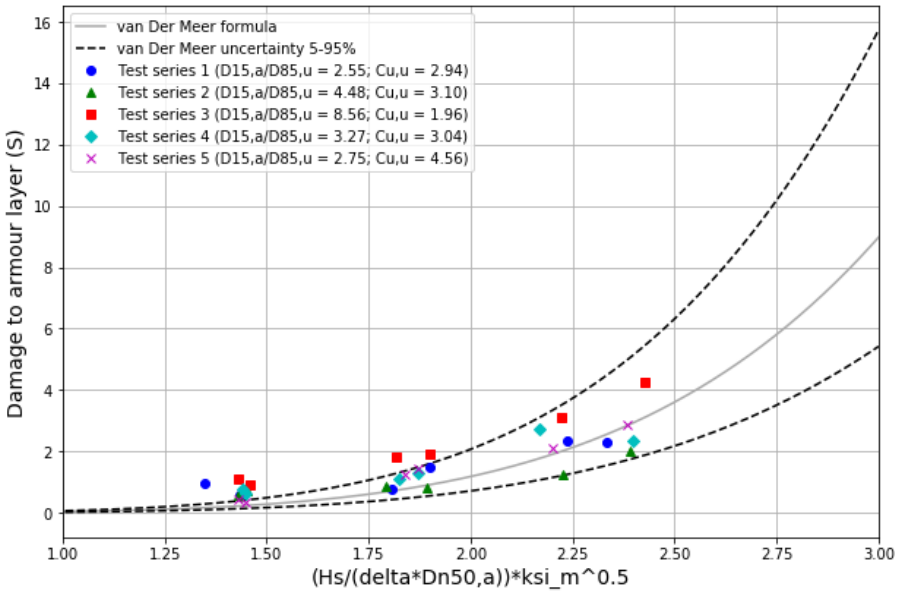

Figure 5.1: Armour layer damage per test series plotted against the stability number times the square root of ξ_m. Solid line: trend van der Meer (1988) formula. Dashed line: 5% and 95% values of van der Meer (1988) formula. Poins of various shapes and colours: values from this research.

5.2.2. Analysis of extra armour layer damage

As discussed in section 4.2, the measured damage levels of the armour layer for test series 3 did not meet the criteria of 'start of damage'. The measured armour layer damage after sub-series TS3.1 was S = 3.1 and the measured damage after sub-series TS3.2 was S = 4.3. It was hypothesized that the increase in measured damage was not caused by a significant amount of armour layer erosion, but by subsidence of the armour layer, caused by extensive wash-out of under-layer material.

Figure 5.2: Armour layer before sub-series TS3.1

Figure 5.3: Armour layer after sub-series TS3.1

When comparing figure 5.2 to 5.3 it can be seen that the armour layer was indeed largely undamaged. Though, a large amount of under-layer material is visible in figure 5.3, which is usually a sign of damage to the armour layer. However, in this case the visible under-layer material is material that was washed out completely. This is indicated in figure 5.4. As can be seen in the figure, there was a significant decrease in under-layer thickness after sub-series TS3.1 in the area indicated by the dark blue lines. In half of this area, the under-layer was completely eroded until the impermeable core of the structure. This means that, at the end of sub-series TS3.1, the armour layer had subsided and was situated directly on top of the impermeable core.

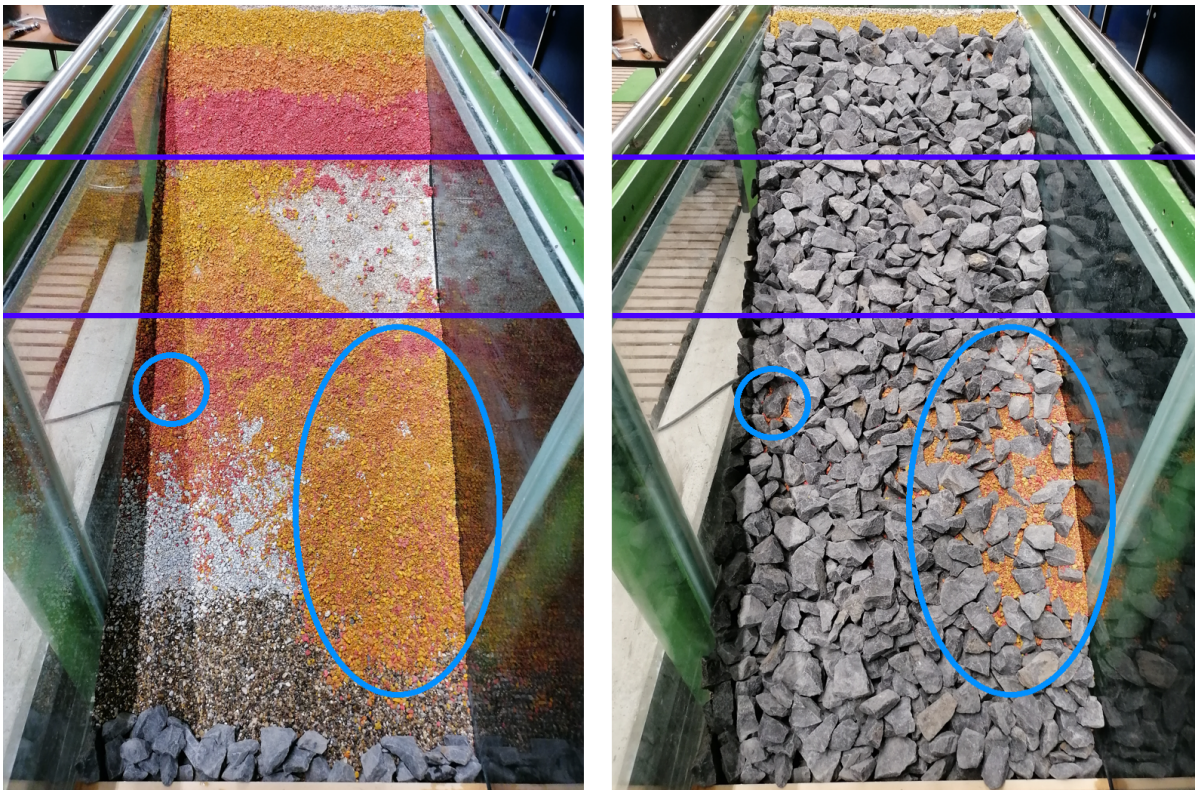

Figure 5.4: Comparison of under-layer and armour layer after sub-series TS3.1.

A similar damage pattern was observed after dismantling the armour layer after sub-series TS3.2, as can be seen in figure 5.6. As was the case after test series TS3.1, after sub-series TS3.2 part of the armour layer located in the area marked by the dark blue lines had subsided and was resting directly on top of the impermeable core. Contrary to sub-series TS3.1, during sub-series TS3.2 most of the erosion to the under-layer took place near the left side wall of the wave flume, where the video camera setup was located. When reviewing the video file from tests 3.2.1 through 3.2.3 the subsidence of the armour layer due to washout of the under-layer was clearly observed, further confirming the hypothesis. This can be seen in figure 5.5. Unfortunately, the images of the armour layer after sub-series TS3.2 were corrupted. However, from visual inspection after sub-series 3.2 it was concluded that no extra damage was sustained by the armour layer during sub-series TS3.2, compared to earlier test series.

During tests 3.1.2 and 3.1.3, as well as tests 3.2.2 and 3.2.3 it was observed that under-layer material was being washed out at the start of the tests. Since the damage level of the armour layer is the cumulative damage per sub-series, the armour layer damage at the end of tests x.x.1 is the same as the damage at the start of tests x.x.2. The same holds for tests x.x.2 and x.x.3 respectively. In figure 5.1 it can be seen that at the armour layer damage at the end of tests 3.1.1, 3.1.2, 3.2.1 and 3.2.2 (the four leftmost red squares) was still below S = 3. Therefore, the same is true for the beginning of tests 3.1.2, 3.1.3, 3.2.2 and 3.2.3.

In conclusion, during both sub-series TS3.1 and TS3.2, it was observed that under-layer material was

being washed out, while the damage to the armour layer still qualified as 'start of damage'. Combined with the fact that the extra measured damage to the armour layer after these sub-series was caused by subsidence of the armour layer rather than extra armour layer erosion, and when using the criteria established in section 5.1, it can be concluded that the filter structure was not geometrically closed for test series 3.

Figure 5.5: Side view of the filter structure. Left: Before test 3.2.1; Right: After test 3.2.3

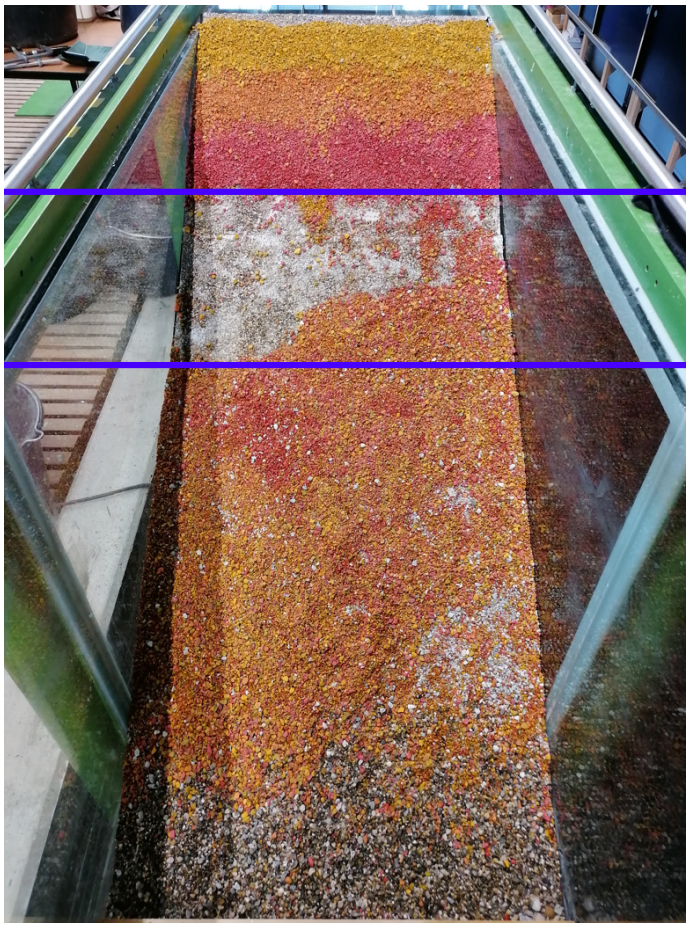

Figure 5.6: Under-layer damage after test series TS3.2.

5.3. Determination of geometrically closed under-layer mixes

In table 5.1, the observations made during the tests, as well as a qualitative description of the measured armour layer damages, are summarized. For a full description of the observations made and for a quantification of the measured values the reader is referred to chapter 4. In table 5.1, if during or after

any of the tests where a certain under-layer material mix was used a certain observation was made or the threshold value of the armour layer damage was exceeded, 'yes' was entered in the corresponding cell.

Table 5.1: Determination if the under-layer mixes used led to geometrically closed filters.

Under-layer mix	Observations		Measurements	Conclusion
	Intrusion of under-layer stones into armour layer	Washout of under-layer material	Armour layer damage S >3	Geometrically closed
Mix 1 $D_{15,a}/D_{85,u} = 2.55$ $D_{50,a}/D_{50,u} = 4.74$ $C_{u,u} = 2.94$	No	No	No	Yes
Mix 2 $D_{15,a}/D_{85,u} = 4.48$ $D_{50,a}/D_{50,u} = 8.89$ $C_{u,u} = 3.10$	Yes	No	No	No
Mix 3 $D_{15,a}/D_{85,u} = 8.56$ $D_{50,a}/D_{50,u} = 15.24$ $C_{u,u} = 1.96$	Yes	Yes	Yes	No
Mix 4 $D_{15,a}/D_{85,u} = 3.27$ $D_{50,a}/D_{50,u} = 6.56$ $C_{u,u} = 3.04$	No	No	No	Yes
Mix 5 $D_{15,a}/D_{85,u} = 2.75$ $D_{50,a}/D_{50,u} = 6.34$ $C_{u,u} = 4.56$	Yes	No	No	No

Combining table 5.1 with the criteria defined in section 5.1, and taking into consideration section 5.2.2, it is concluded that the use of under-layer mixes 1 and 4 resulted in a geometrically closed filter structure, while the use of under-layer mixes 2, 3 and 5 did not result in a geometrically closed filter structure.

5.4. Validity of the original Terzaghi (1939) criterion under wave loading

In the previous section it was determined which of the five under-layer mixes led to geometrically closed filter structures and which ones did not. In this section, as well as the next three sections, this knowledge is combined with knowledge from previously conducted experiments by Thompson & Shuttler (1975) and van Gent & Wolters (2016) to validate frequently used interface stability criteria for geometrically closed granular filters loaded by flow for sloped, geometrically closed filters under wave loading.

Recalling from section 2.3.1, according to Terzaghi (1939), a closed, granular filter under flow loading must adhere to the following interface stability criterion: $D_{15,a}/D_{85,u} < 5$. In table 5.2 it can be seen that, when applying this criterion to the five under-layer mixes used in this research, mixes 1, 2, 4 and 5 lead to a geometrically closed filter while mix 3 does not. However, as was previously determined, only under-layer mixes 1 and 4 led to geometrically closed filters. Therefore, the interface stability criterion proposed by Terzaghi did not correctly predict the stability in this case.

Table 5.2: Applying the Terzaghi interface stability criterion to the under-layer mixes used for this research.

Mix name	$\frac{D_{15,a}}{D_{85,u}}$ [-]	$\frac{D_{50,a}}{D_{50,u}}$ [-]	$C_{u,u}$ [-]	Meets Terzaghi requirement	Geometrically closed
1	2.55	4.74	2.94	Yes	Yes
2	4.48	8.89	3.10	Yes	No
3	8.56	15.24	1.96	No	No
4	3.27	6.56	3.04	Yes	Yes
5	2.75	6.34	4.56	Yes	No

In table 5.3 the Terzaghi interface stability criterion is applied to the under-layer materials used by Thompson & Shuttler (1975). In the table, it can be seen that, when applying this criterion to the three under-layer materials used by Thompson & Shuttler, mixes TS 2 and TS3 lead to a geometrically closed filter while TS 1 does not. Thompson & Shuttler found that, out of the three materials used for the under-layer, only TS 3 was sufficient, meaning that no wash-out of under-layer material or early failure of the armour layer occurred. Therefore, the interface stability criterion proposed by Terzaghi did not correctly predict the stability this case.

Table 5.3: Applying the Terzaghi interface stability criterion to the under-layer mixes used by Thompson & Shuttler (1975).

Mix name	$\frac{D_{15,a}}{D_{85,u}}$ [-]	$\frac{D_{50,a}}{D_{50,u}}$ [-]	$C_{u,u}$ [-]	Meets Terzaghi requirement	Geometrically closed
TS 1	5.01	13.64	2.36	No	No
TS 2	3.17	9.68	2.68	Yes	No
TS 3	2.01	4.55	1.78	Yes	Yes

In table 5.4 the Terzaghi interface stability criterion is applied to the under-layer materials used by van gent & Wolters (2016). In the table, it can be seen that, when applying this criterion to the five under-layer materials used by van Gent & Wolters, all mixes lead to a geometrically closed filter. Van Gent & Wolters found that, for values up to $D_{n50,a}/D_{50,u} = 3.7$, or $D_{50,a}/D_{50,u} = 4.6$, no wash-out of under-layer material occurred if the damage of the armour layer was S < 2.5. Additionally, no increase in armour layer damage was reported for these values of $D_{50,a}/D_{50,u}$, compared to the strict, currently prescribed values for $D_{50,a}/D_{50,u}$ (See also section 2.3.3). Therefore, under-layer materials VGW 1 and VGW 3 were sufficient. For values of $9.8 > D_{50,a}/D_{50,u} > 4.6$, van Gent and Wolters reported that wash-out of under-layer material was observed. However, it is not clear if this was caused by damage to the armour layer, causing a direct wave attack on the under-layer, or by the geometry of the filter. This means it is unknown if the application of under-layer mixes VGW 2 and VGW 4 resulted in a geometrically closed filter. For $D_{50,a}/D_{50,u} = 9.8$, van Gent and Wolters reported that washout of under-layer material was observed, even when the damage value of the armour layer was S < 3. Therefore, under-layer material VGW 5 was not sufficient.

Table 5.4: Applying the Terzaghi interface stability criterion to the under-layer mixes used by van Gent & Wolters (2016).

Mix name	$\frac{D_{15,a}}{D_{85,u}}$ [-]	$\frac{D_{50,a}}{D_{50,u}}$ [-]	$C_{u,u}$ [-]	Meets Terzaghi requirement	Geometrically closed
VGW 1	2.7	4.4	2.0	Yes	Yes
VGW 2	2.5	7.0	3.7	Yes	Unknown
VGW 3	1.6	4.6	3.5	Yes	Yes
VGW 4	4.2	7.2	1.8	Yes	Unknown
VGW 5	3.0	9.8	2.9	Yes	No

In conclusion, the interface stability criterion proposed by Terzaghi (1939) ($D_{15,a}/D_{85,u} < 5$) did not correctly predict the stability in the case of sloped, granular filters under wave loading for this research, as well as for the research performed by Thompson & Shuttler (1975) and van Gent & Wolters (2016). All in all, it can be concluded that the interface stability criterion proposed by Terzaghi is not valid for sloped, closed granular filters under wave loading.

5.5. Validity of the Cistin/Ziems diagram (1974) under wave loading

Figure 5.7 shows the Cistin/Ziems diagram (1974) with the results of this research project, as well as the results of the tests of Thompson & Shuttler (1975) and van Gent & Wolters (2016). If the under-layer material used led to a geometrically closed filter structure, the data point is shown as a circle. If the under-layer material used did not lead to a geometrically closed filter structure, the data point is shown as a cross. These data points correspond to the rightmost columns of tables 5.2 through 5.4. Any unknown data points were omitted from the diagram.

As can be seen in the figure, the Cistin/Ziems diagram (1974) was valid for 4 out of 5 under-layer materials used for this research. However, for mix 5 ($D_{50,a}/D_{50,u}$ = 6.34, $C_{u,u}$ = 4.56), according to the diagram the resulting filter is geometrically closed, while this was not the case in practice.

As can be seen in the figure, the Cistin/Ziems diagram (1974) was valid for 2 out of 3 under-layer materials used by Thompson & Shuttler (1975). However, for TS 2 ($D_{50,a}/D_{50,u}$ = 9.68, $C_{u,u}$ = 2.68), according to the diagram the resulting filter is geometrically closed, while this was not the case in practice.

As can be seen in the figure, the Cistin/Ziems diagram (1974) was valid for all under-layer materials used by van Gent & Wolters (2016), of which it was determined if the resulting filter structure was geometrically closed.

In conclusion, the interface stability criterion according to the Cistin/Ziems diagram (1974) did not correctly predict the stability in the case of sloped, granular filters under wave loading for this research and for the research performed by Thompson & Shuttler (1975). For the research by van Gent & Wolters (2016), the diagram correctly predicted the stability of the filter structure. All in all, it can be concluded that the Cistin/Ziems diagram is not valid for sloped, closed granular filters under wave loading.

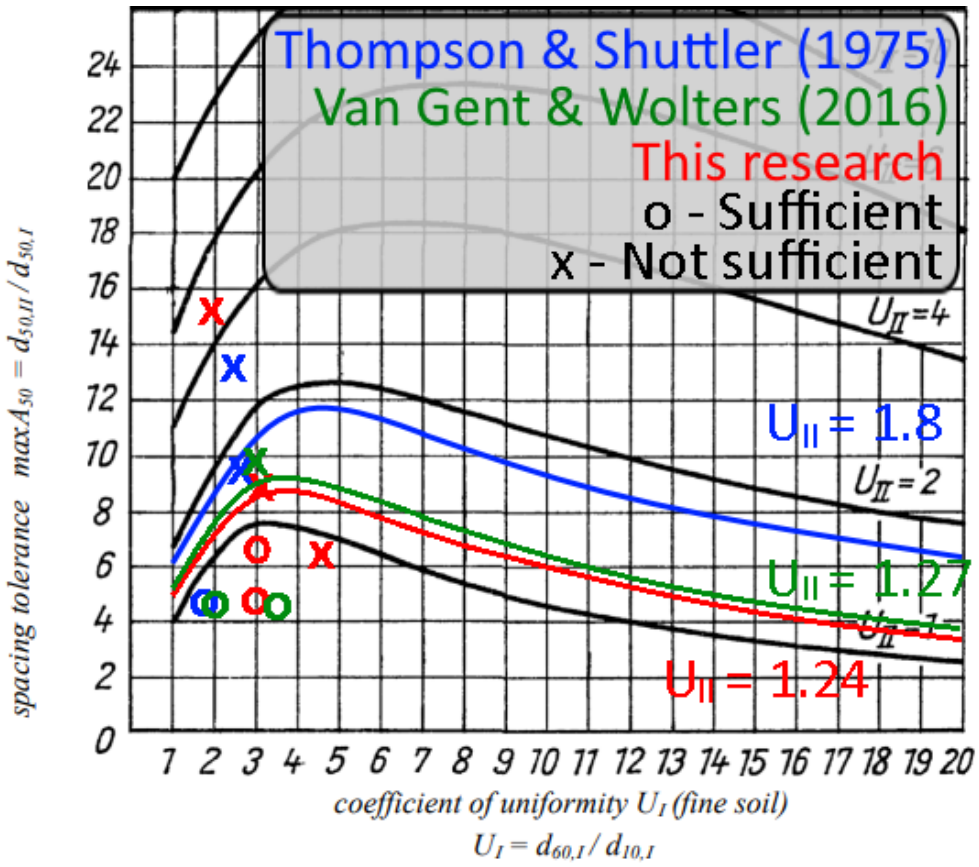

Figure 5.7: Cistin/Ziems diagram (1974) with data of this research program (red, U_{II} = 1.24), Thompson & Shuttler (1975) (blue, U_{II} = 1.8) and van Gent & Wolters (2016) (green, U_{II} = 1.27).

5.6. Validity of the Giroud diagram (2003) under wave loading

Figure 5.8 shows the Giroud (2003) diagram with the results of this research project, as well as the results of the tests of Thompson & Shuttler (1975) and van Gent & Wolters (2016). If the under-layer material used led to a geometrically closed filter structure, the data point is shown as a green cross. If the under-layer material used did not lead to a geometrically closed filter structure, the data point is shown as a red cross. Again, the data points correspond to the rightmost columns of tables 5.2 through 5.4.

As can be seen in figure 5.8, the interface stability criterion according to the Giroud 2003) diagram did not correctly predict the stability in the case of sloped, granular filters under wave loading. According to the diagram, all tested combinations of under-layer and armour layer materials lead to a geometrically closed filter structure. In reality, this was not the case for roughly half of the tested under-layers. The dash-dotted line in the figure shows a more representative stability boundary, based on the test results. However, this line is only a first estimate based on the 11 available data points. Therefore, it was only drawn where multiple data points were available. All in all, it can be concluded that the Giroud diagram is not valid for sloped, closed granular filters under wave loading.

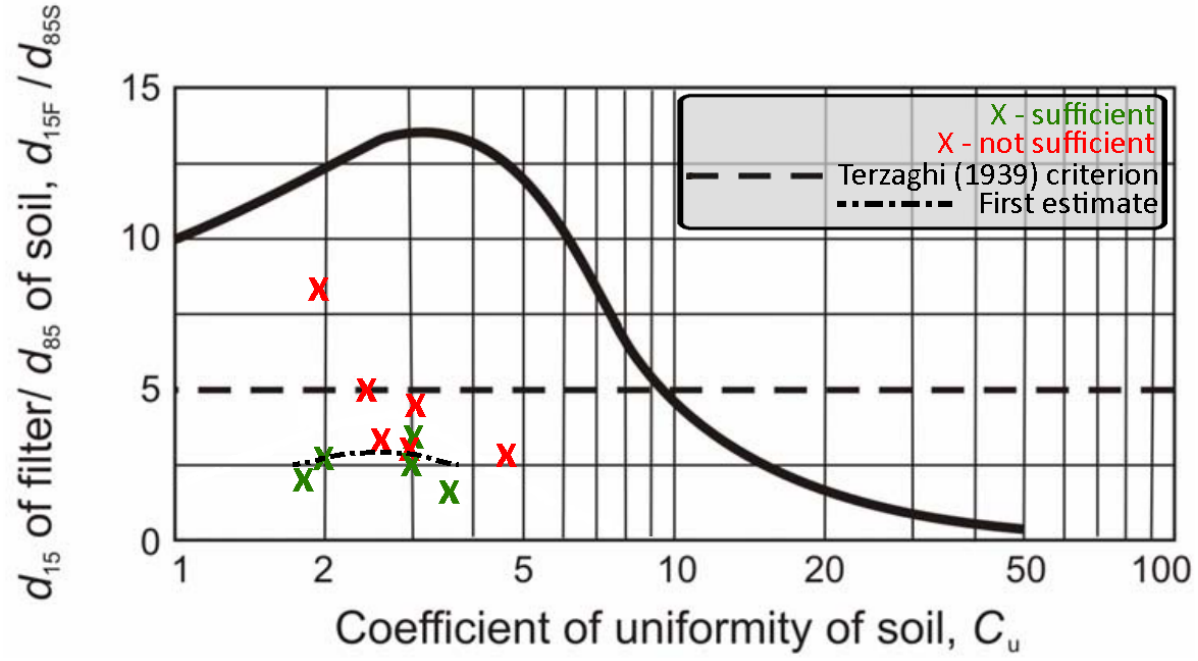

Figure 5.8: Giroud (2003) with data of this research program, Thompson & Shuttler (1975) and van Gent & Wolters (2016).

5.7. Validity of the Rock Manual flow loading stability criterion for wave loading

Recalling from section 2.3.2, according to The Rock Manual errata (CIRIA, CUR, CETMEF, 2017), a closed, granular filter under flow loading, with an armour layer thickness of $2 * D_{50,f}$ must adhere to the following interface stability criterion: $D_{15,a}/D_{85,u} < 3.3$. In table 5.5, this criterion is applied to the five under-layer mixes used in this research. In the table, it can be seen that, when applying this criterion to the five under-layer mixes used in this research, mixes 1, 4 and 5 lead to a geometrically closed filter while mix 2 and 3 do not. However, as was previously determined, only under-layer mixes 1 and 4 led to geometrically closed filters. Therefore, the interface stability criterion for closed filters under flow loading according to The Rock Manual errata did not correctly predict the stability for this research.

Table 5.5: Applying The Rock Manual errata interface stability criterion to the under-layer mixes used for this research.

Mix name	$\frac{D_{15,a}}{D_{85,u}}$ [-]	$\frac{D_{50,a}}{D_{50,u}}$ [-]	$C_{u,u}$ [-]	Meets Rock Manual errata requirement	Geometrically closed
1	2.55	4.74	2.94	Yes	Yes
2	4.48	8.89	3.10	No	No
3	8.56	15.24	1.96	No	No
4	3.27	6.56	3.04	Yes	Yes
5	2.75	6.34	4.56	Yes	No

In table 5.6 The Rock Manual errata interface stability criterion is applied to the under-layer materials used by Thompson & Shuttler (1975). In the table, it can be seen that, when applying this criterion to the three under-layer materials used by Thompson & Shuttler, mixes TS 2 and TS3 lead to a geometrically closed filter while TS 1 does not. However, as discussed in section 5.4, only TS 3 was sufficient. Therefore, the interface stability criterion for closed filters under flow loading according to The Rock Manual errata did not correctly predict the stability in this case.

Table 5.6: Applying The Rock Manual errata interface stability criterion to the under-layer mixes used by Thompson & Shuttler (1975).

Mix name	$\frac{D_{15,a}}{D_{85,u}}$ [-]	$\frac{D_{50,a}}{D_{50,u}}$ [-]	$C_{u,u}$ [-]	Meets Rock Manual errata requirement	Geometrically closed
TS 1	5.01	13.64	2.36	No	No
TS 2	3.17	9.68	2.68	Yes	No
TS 3	2.01	4.55	1.78	Yes	Yes

In table 5.7 The Rock Manual errata interface stability criterion is applied to the under-layer materials used by van Gent & Wolters (2016). In the table, it can be seen that, when applying this criterion to the five under-layer materials used by van Gent & Wolters, mixes VGW 1, VGW 2, VGW 3 and VGW 5 lead to a geometrically closed filter while VGW 4 does not. This is correct for mixes VGW 1 and VGW 3, but not for VGW 5. As discussed in section 5.4, for VGW 2 and VGW 4 it is unknown if the filter was geometrically closed or not. In conclusion, the interface stability criterion for closed filters under flow loading according to The Rock Manual errata did not correctly predict the stability in this case.

Table 5.7: Applying The Rock Manual errata interface stability criterion to the under-layer mixes used by van Gent & Wolters (2016).

Mix name	$\frac{D_{15,a}}{D_{85,u}}$ [-]	$\frac{D_{50,a}}{D_{50,u}}$ [-]	$C_{u,u}$ [-]	Meets Rock Manual errata requirement	Geometrically closed
VGW 1	2.7	4.4	2.0	Yes	Yes
VGW 2	2.5	7.0	3.7	Yes	Unknown
VGW 3	1.6	4.6	3.5	Yes	Yes
VGW 4	4.2	7.2	1.8	No	Unknown
VGW 5	3.0	9.8	2.9	Yes	No

In conclusion, the interface stability criterion for geometrically closed filters under flow loading ,according to The Rock Manual errata (2017) ($D_{15,a}/D_{85,u} < 3.3$), did not correctly predict the stability in the case of sloped, granular filters under wave loading for this research, as well as for the research performed by Thompson & Shuttler(1975) and van Gent & Wolters (2016). Therefore, it can be concluded that the interface stability criterion for closed filters under flow loading prescribed in The Rock Manual is not valid for sloped, closed granular filters under wave loading.

5.8. Approximating the interface stability limit

In sections 5.4 through 5.7 it is shown that the most commonly used interface stability criteria for closed granular filters under flow loading cannot be assumed to be valid for sloped, closed granular filters under wave loading, even though in practice, they are often used for this purpose. The simpler criteria by Terzaghi (1939) and The Rock manual errata (CIRIA, CUR, CETMEF, 2017), $D_{15,a}/D_{85_u} < 5$ and $D_{15,a}/D_{85,u} < 3.3$ respectively, turned out to be too lenient for this purpose. Combining the test results

of this research with the results from earlier research by Thompson & Shuttler (1975) and van Gent & Wolters (2016), an interface stability criterion of this form can be proposed, namely:

$$\frac{D_{15,a}}{D_{85,u}} < 2.5 \tag{5.1}$$

When applying this interface stability criterion, it would correctly predict if a filter structure would be geometrically closed or not for all tests considered in this chapter, of which the result was not unknown. This criterion is more strict than the criteria proposed by Terzaghi (1939, see equation 2.4) and The Rock Manual errata (2017, see equation 2.13), but still significantly more lenient than the current interface stability criterion for sloped, closed granular filters under wave attack as prescribed in The Rock Manual ($D_{50,a}/D_{50,u} < 2.2$ to 2.5, which is roughly equivalent to $D_{15,a}/D_{85,u} < 1.0$ to 1.3). In figure 5.9, this value of $D_{15,a}/D_{85,u} = 2.5$ is plotted in the Giroud (2003) diagram as a blue line.

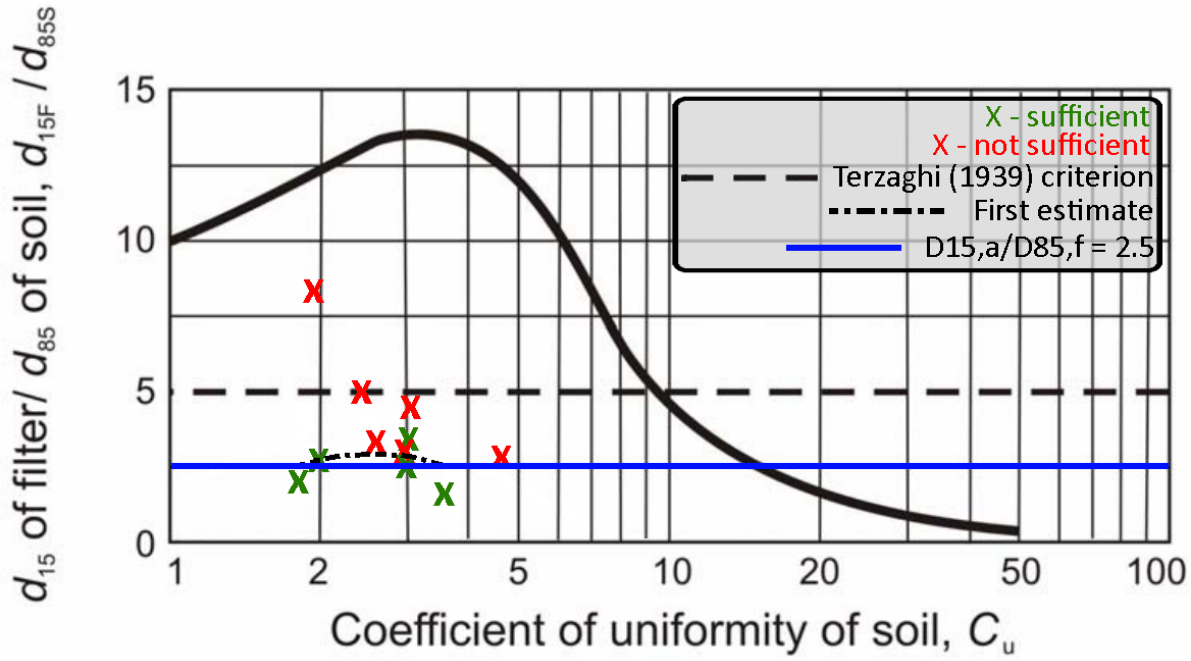

Figure 5.9: Giroud (2003) with data of this research program, Thompson & Shuttler (1975) and van Gent & Wolters (2016).

While a criterion such as presented in equation 5.1 would suffice for the test results considered in this chapter, from figure 5.8 it is evident that in reality, the uniformity coefficient of the under-layer also plays a role. This can, for instance, be seen when comparing under-layer mixes 4 ($D_{15,a}/D_{85,f} = 3.27$, $D_{50,a}/D_{50,f} = 6.56$, $C_{u,u} = 3.04$) and 5 ($D_{15,a}/D_{85,f} = 2.75$, $D_{50,a}/D_{50,f} = 6.34$, $C_{u,u} = 4.56$) used in this research. Even though the material of mix 4 is smaller than that of mix 5, when using mix 4 as the under-layer material a geometrically closed filter was achieved, which was not the case for mix 5. Therefore, to fully encapsulate the stability limit for sloped, closed granular filters under wave loading, an interface stability criterion which incorporates the influence of $C_{u,u}$ is desired.

Though it is not exactly known what such a criterion would look like, an approximation is made with the dash-dotted line in figure 5.9. However, with the amount of data points available, this approximation can only be made for a limited amount of $C_{u,u}$ values. For a more accurate representation of this interface stability criterion, more tests will have to be performed using a wide range of values for $C_{u,u}$.

6

Discussion

In this chapter, the findings of this study are discussed. This is done by evaluating the limitations of the findings, as well as the validity range of the results.

6.1. The interpretation of 'geometrically closed'

Recalling from section 5.1, a number of criteria were established to determine if a filter construction is geometrically closed or not. These criteria were as follows:

A filter structure is geometrically closed if and only if:

For all performed tests using a certain combination of under-layer and armour layer material:

1. No wash-out of under-layer material through the armour layer was observed during any test;

   and

2. No under-layer grains were found inside the armour layer when deconstructing the armour layer after any test;

   and

3. At the end of the test, the damage sustained by the armour layer falls into the category 'start of damage' (S = 2-3) or 'no damage' (S < 2).

While it is attempted to abide by the classical definition of a geometrically closed granular filter, there is a limitation that needs to be taken into consideration when applying these criteria. As discussed in section 5.1, in the case where an under-layer grain passes the interface between the under-layer and armour layer, but falls back onto the under-layer, a filter structure is incorrectly classified as geometrically closed. After all, according to the classical definition of a geometrically closed granular filter, an under-layer grain is not allowed to pass the interface between the under-layer and the amour layer.

One could consider adding a criterion to the list above to counteract this limitation, for instance: "No under-layer grains are allowed to pass the interface between the under-layer and the armour layer." However, if such a criterion was applied, it would be impossible to determine if the filter structure was geometrically closed for any tests performed in this research, as well as the earlier research projects by Thompson & Shuttler (1975) and van Gent & Wolters (2016). This is because, except for a very small portion near the glass sidewalls of a wave flume, the view of the under-layer is obscured by the armour layer, making it impossible to track the exact movements of under-layer grains during a test. Therefore, it was decided that for the purpose of this research, a filter structure was still considered geometrically closed if an under-layer grain passed the interface between the under-layer and armour layer, but fell back onto the under-layer.

During the tests performed for this research, close to the glass sidewall of the wave flume, no under-layer material was observed passing the interface between the under-layer and the armour layer in the tests where under-layer mixes 1 and 4 were used. In the cases where these under-layer mixes were used, the resulting filter structures were ultimately classified as geometrically closed. On the contrary, during the tests where under-layer mixes 2, 3 and 5 were used, under-layer material was observed passing the interface between the under-layer and the armour layer. In the cases where these under-layer mixes were used, the resulting filter structures were ultimately classified as geometrically open. This seems to indicate that the above assumption was safe to use in this case. However, as discussed before, the under-layer material further away from the sidewalls was obscured by the armour layer, which means that the above assumption was still made.

A follow-up study to gain more insight into the exact behaviour of the under-layer material during a test could be performed. In this study a portion of the wooden slope could be replaced with perspex, allowing for the experiments to be filmed from underneath the slope. This would allow for more visibility on the under-layer stones, more so on the stones closest to the slope and less so on the stones closest to the interface of the under-layer and armour layer. To truly observe the under-layer stones closest to the interface between the under-layer and armour layer during a test, purposely made armour layer stones, consisting of a material that is transparent but has a similar density to rubble stone, would have to be used. However, this is a rather unrealistic solution. Not only would it require difficult refractive index matching techniques, which means the fluid temperature would have to be controlled very precisely, different liquids would have to be used, possibly causing problems with Reynolds number scaling.

6.2. Influence of the armour layer damage and thickness

If, at the end of a test, the armour layer damage is higher than 'start of damage' (S = 2-3 (CIRIA, CUR, CETMEF, 2007)), erosion of the armour layer has taken place. This means that parts of the under-layer may have been exposed, which increased the risk of under-layer material wash-out, even if the filter structure was initially constructed as geometrically closed. An example of this can be seen in figure 6.1 (van Gent & Wolters, 2016). It must be noted that this photo was taken during test S02T06 by van Gent & Wolters (2016), where the armour layer damage was S = 8.7. However, van Gent & Wolters observed the formation of holes in the armour layer for damage levels as low as S = 3.6.

Taking the above into consideration, it was established in this report that, if the armour layer damage exceeds S = 3, the filter structure cannot be classified as geometrically closed. For this reason, the third criterion shown in section 6.1 was added. As a result, out of the 13 different filter structures considered in this report (3 by Thompson & Shuttler (1975), 5 by van Gent & Wolters (2016) and 5 from this research), in 2 cases it was unknown if the filter structure was geometrically closed or not. This means that for the analysis, 11 data points were available. Despite this limitation it is assumed that the amount of data points is still significant to support the conclusions drawn in chapter 5.

Figure 6.1: Example of armour layer damage exposing the under-layer. Photo taken during tests by van Gent & Wolters (2016).

For all the filter structures considered in this report, the basis was that the armour layer thickness was $2 * D_{n50,a}$. This is a commonly used armour layer thickness for bank protections and breakwaters. This is why S = 3 was chosen as the upper limit for 'start of damage' in the criteria shown in section 6.1. However, if a larger armour layer thickness than $2 * D_{n50,a}$ is applied, the armour layer damage could exceed S = 3 while the under-layer is still covered by at least two layers of armour layer stone. On the other hand, if a smaller armour layer thickness is applied, for instance $1.5 * D_{n50,a}$, parts of the under-layer could be exposed at lower damage levels than S = 3, increasing the risk of under-layer material wash-out, even if the filter structure was initially constructed as geometrically closed.

In principle, the aim of the experiments performed for this research was to increase the hydraulic load on the under-layer material as much as possible, without causing parts of the under-layer to be exposed. As discussed above, for different armour layer thicknesses this leads to different allowable values for S. This is why, when taking a more critical look at criterion 3 in section 6.1, the use of the armour layer damage S in this criterion is not entirely correct. A better criterion would include a minimum armour layer thickness rather than a maximum armour layer damage level.

A follow-up study to further investigate the influence of armour layer thickness and damage could be performed. In such a study, filter structures with different armour layer thicknesses, for instance $1 * D_{n50,a}$ to $5 * D_{n50,a}$ could be subjected to the same hydraulic conditions. Also, armour layers with pre-made 'damage' (for instance S = 2) could be tested. To keep the the armour layer a constant, the armour layer stones could be held in place by epoxy glue or by a wire mesh (with an opening size of less than one armour stone diameter but more than one under-layer stone diameter). This way, the influence of the armour layer damage and thickness on the amount of wash-out of under-layer material could be quantified.

6.3. Influence of the uniformity coefficient of the under-layer material

In section 5.8 it was shown that a simple interface stability criterion, describing only the ratio between $D_{15,a}$ and $D_{85,b}$, would correctly predict if a filter structure would be geometrically closed or not for all tests considered in this report:

$$\frac{D_{15,a}}{D_{85,u}} < 2.5 \tag{6.1}$$

As discussed in section 5.8, the test results considered in this report seem to indicate that the uniformity coefficient of the under-layer material, $C_{u,u}$, plays a role in the interface stability limit of closed, granular filters under wave loading. Since only 11 data points are available from the tests performed for this research and the research performed by Thompson & Shuttler (1975) and van Gent & Wolters (2016), not enough data is available to fully determine the effect of $C_{u,u}$. However, a first estimate between $C_{u,u} = 1.8$ and $C_{u,u} = 3.5$ was made based on the available data points. This can be seen in section 5.6.

In both the Giroud (2003) and Cistin/Ziems (1974) diagrams there is a peak in the maximum allowable size ratio between the armour layer and under-layer materials at roughly $C_{u,u} = 3$. The exact cause for this peak is unknown, but from the first estimate shown in section 5.6 it looks like this is the case for sloped, closed granular filters under wave loading as well, with a slight peak between $C_{u,u} = 2$ and $C_{u,u} = 3$. In practice, the value of $C_{u,u}$ is commonly between 1.5 and 3.0, therefore it is important to gain a better understanding of the maximum allowable size ratio between the armour layer and under-layer materials within this range of $C_{u,u}$ values.

A follow-up study could be performed in which more combinations of $C_{u,u}$ and $D_{15,a}/D_{85,u}$ are tested, filling in the still existing gaps of the Giroud diagram shown in section 5.6. This way the influence of $C_{u,u}$ on the interface stability of a geometrically closed filter under wave loading can be quantified further.

6.4. Influence of the uniformity coefficient of the armour layer material

In the three test programs considered in this report, the armour layer material was constant throughout each test program. This means that the influence of the uniformity coefficient of the armour layer, $C_{u,a}$, has not yet been determined. Like $C_{u,u}$, $C_{u,a}$ could play a role in the maximum allowable size ratio between the armour layer and under-layer materials. To determine this, a follow-up study could be performed where many different combinations of the values of $D_{15,a}/D_{85,u}$, $C_{u,u}$ and $C_{u,a}$ are tested. The results could then be plotted in a Cistin/Ziems-like plot to determine the influence of $C_{u,a}$.

6.5. Validity range of the test results

The conclusions drawn in chapter 5 are based on 13 data points from three different research projects, including this one. Out of these 13 data points, 11 could be used for the analysis required to answer the research question and sub-questions posed in chapter 1. However, the conclusions drawn in chapter 5 are only valid in a certain range of parameters, determined by the testing parameters used in this study, as well as the studies by Thompson & Shuttler (1975) and van Gent & Wolters (2016).

First of all, tests were performed on two different slopes, 1:2 and 1:3. In practice, slopes of 1:2 are commonly used for breakwaters, while slopes of 1:3 and more gentle are often used for bank protections. However, slopes of 1:1.5 are also commonly used for breakwaters, for which more tests will have to be performed in further research. For slopes more gentle than 1:3 further research could also be performed. However, it is expected that the conclusions drawn in this report are also valid for slopes more gentle than 1:3. This is because, as the slope becomes more gentle, the horizontal component of the gravitational acceleration becomes smaller, causing the under-layer and armour layer stones to be more stable.

For all tests considered in this report, an impermeable core was used. In practice the 'core' of bank protections is always impermeable, since a bank is the interface between a body of water and the land. However, in many breakwaters an permeable core is used. Further research will therefore have to be performed to validate the results from this study for breakwaters with permeable cores.

In all tests considered in this report, the thickness of the armour layer was $2 * D_{n50,a}$. This is a representative armour layer thickness for many breakwaters and bank protections. However, it is expected that the conclusions of this report are also valid for thicker armour layers, as the chance of wash-out of under-layer material decreases as more armour layer material is present. The thickness of the under-layer ranged from $0.5 * D_{n50,a}$ to $1.75 * D_{n50,a}$. Also, in all tests a single under-layer was used between the armour layer and the impermeable core.

Regarding the hydraulic conditions, the breaker parameter ranged from $\xi_{op} = 1.66$ to $\xi_{op} = 3.77$, which means the results are valid for plunging, collapsing and surging breaker types. The wave steepnesses tested ranged from $s_{op} = 0.015$ to $s_{op} = 0.040$.

The tested size ratio between the armour layer and the under-layer material ranged from $D_{15,a}/D_{85,u} = 1.6$ to $D_{15,a}/D_{85,u} = 8.56$. Expressed in terms of the median diameters, the range was $D_{50,a}/D_{85,u} = 4.4$ to $D_{50,a}/D_{50,u} = 15.24$. The relative density of the under-layer material ranged from $\Delta = 1.613$ to $\Delta = 1.637$ and the relative density of the armour-layer material ranged from $\Delta = 1.65$ to $\Delta = 1.984$. The validity range of the coefficient of uniformity of the armour layer is $C_{u,a} = 1.24$ to $C_{u,a} = 1.8$. The validity range of the coefficient of uniformity of the under-layer is $C_{u,u} = 1.78$ to $C_{u,u} = 4.56$.

Finally, assuming an armour layer thickness of $2 * D_{n50,a}$, the conclusions drawn in chapter 5 are only valid for armour layer damage levels up to 'start of damage' (S < 3). For current design practice it is emphasized that in case the design is made for damage levels higher than 'start of damage', conclusions made in this report, as well as the commonly used standard filter rules, cannot be applied. In this case, additional measures should be taken (see van Gent & Wolters (2016)).

7

Conclusions & Recommendations

7.1. Conclusions

In section 1.3 the main research question is formulated, along with the sub-questions. In this section, first the sub-questions will be addressed, followed by the main research question. To answer the posed questions, small scale physical model tests were performed, the results of which were analyzed and combined with results from two earlier research projects regarding closed, granular filters under wave loading.

Taking into account the results from the tests performed for this research, as well as the results from tests performed by Thompson & Shuttler (1975) and van Gent & Wolters (2016), it was found that the interface stability criterion proposed by Terzaghi (1939) ($D_{15,a}/D_{85,u} < 5$) did not correctly predict the stability in the case of sloped, granular filters under wave loading. Therefore, it can be concluded that the interface stability criterion proposed by Terzaghi is not sufficiently safe for sloped, closed granular filters under wave loading.

It was also found that the interface stability criterion according to the Cistin/Ziems diagram (1974) correctly predicted the stability of sloped, granular filters under wave loading for the research by van Gent & Wolters (2016). However, it did not correctly predict the stability of the filter structure for this research and for the research performed by Thompson & Shuttler (1975). Therefore, it can be concluded that the Cistin/Ziems diagram is not safe for sloped, closed granular filters under wave loading.

Finally, it was found that the interface stability criterion according to the Giroud (2003) diagram did not correctly predict the stability in the case of sloped, granular filters under wave loading. According to the diagram, all tested combinations of under-layer and armour layer materials lead to a geometrically closed filter structure. In reality, this was not the case for roughly half of the tested under-layers. Therefore, it can be concluded that the Giroud diagram is not safe for sloped, closed granular filters under wave loading.

Taking into consideration the above, it can be concluded that the most commonly used existing interface stability criteria for closed granular filters under flow loads are not safe for sloped, closed granular filters under wave loading, thereby answering the first research sub-question.

The interface stability criterion for closed granular filters, with a thickness of $2 * D_{n50,a}$, prescribed in The Rock Manual errata (CIRIA, CUR, CETMEF, 2017) ($D_{15,a}/D_{85,u} < 3.3$) is stricter than the criteria proposed by Terzaghi (1939), Cistin/Ziems (1974) and Giroud (2003). However, taking into account the results from the tests performed for this research, as well as the results from tests performed by Thompson & Shuttler (1975) and van Gent & Wolters (2016), it was found that this interface stability criterion did not correctly predict the stability in the case of sloped, granular filters under wave loading. Therefore, it can be concluded that the interface stability criterion for closed filters under flow loading prescribed in The Rock Manual errata is not sufficiently conservative for sloped, closed granular filters

under wave loading, thereby answering the second research sub-question.

Taking into account the results from the tests performed for this research, as well as the results from tests performed by Thompson & Shuttler (1975) and van Gent & Wolters (2016), it was found that a sloped granular filter structure can be classified as 'geometrically closed' if $D_{85,u}$ is larger than 2.5 times $D_{15,a}$. This value was sufficiently safe for all considered tests and for all considered values of $C_{u,u}$, thereby answering research sub-question 3.

From the findings from sub-question 3, a new interface stability criterion for sloped, closed granular filters under wave loading can be proposed, relating the maximum ratio of size of the armour layer material to the size of the under-layer material.

$$\frac{D_{15,a}}{D_{85,u}} < 2.5 \tag{7.1}$$

For all tests considered in this report, applying this interface stability criterion correctly determined whether the filter structure is geometrically closed or not. Therefore, it can be concluded that the interface stability criterion proposed in equation 7.1 is sufficiently safe for sloped, closed granular filters under wave loading, provided that the filter structure falls within the range of parameters discussed in section 6.5.

This criterion is more strict than the criteria proposed by Terzaghi (1939) and The Rock Manual errata (CIRIA, CUR, CETMEF, 2017), but still significantly more lenient than the current interface stability criterion for sloped, closed granular filters under wave attack as prescribed in The Rock Manual ($D_{50,a}/D_{50,u} < 2.2$ to 2.5, which is roughly equivalent to $D_{15,a}/D_{85,u} < 1.0$ to 1.3).

While the interface stability criterion proposed in equation 7.1 is valid for sloped, closed granular filters under wave loading, within the range of parameters discussed in section 6.5, it can also be concluded that the uniformity coefficient of the under-layer also plays a role. However, due to the amount of data points available, the exact influence of the uniformity coefficient of the under-layer is yet to be determined.

7.2. Recommendations

Based on the discussion from chapter 6, a number of recommendations for future research can be made. These recommendations are as follows:

- To perform a follow-up study to gain more insight into the exact behaviour of under-layer grains subject to wave loading. In such a study a portion of the wooden slope could be replaced with perspex, allowing for the experiments to be filmed from underneath the slope. This would allow for more visibility on the under-layer stones.
- To perform a follow-up study to determine the influence of armour layer damage and thickness on the degree of wash-out of under-layer material. In such a study, filter structures with different armour layer thicknesses, for instance $1 * D_{n50,a}$ to $5 * D_{n50,a}$ could be subjected to the same hydraulic conditions. Also, armour layers with pre-made 'damage' (for instance S = 2) could be tested. To ensure that the armour layer damage stays constant though-out a test, the armour layer stones could be held in place by epoxy glue or by a wire mesh (with an opening size of less than one armour stone diameter but more than one under-layer stone diameter).
- To perform a follow-up study to determine the influence of the uniformity coefficient of the armour layer, $C_{u,a}$. In such a study, many different combinations of the values of $D_{15,a}/D_{85,u}$, $C_{u,u}$ and $C_{u,a}$ are tested. The results could then be plotted in a Cistin/Ziems-like plot to determine the influence of $C_{u,a}$.
- To perform more tests to extend the validity range of the parameters discussed in section 6.5. It is mainly recommended to perform future tests:
  - On a slope angle of 1:1.5, as it is a commonly used slope for breakwaters;
  - Using a model with a permeable core;

- Using different, untested combinations of $D_{15,a}/D_{85,u}$ and $C_{u,u}$ to gain a better understanding in the influence of $C_{u,u}$ and to redefine the Giroud (2003) for sloped, closed filters under wave loading;
- Using thicker armour layers ($> 2 * D_{n50,a}$).

References

Bertram, G. E. (1940). *An experimental investigation of protective filters.* Cambridge, Massachusetts: Harvard University.

Busch, K. F., & Luckner, L. (1974). *Geohydraulik für studium und praxis.* Stuttgart: Ferdinand Enke.

Carver, R. D. (1980). *Effects of first underlayer weight on the stability of stone-armored, rubble-mound breakwater trunks subjected to nonbreaking waves with no overtopping; hydraulic model investigation.* (Technical Report No. HL-80-1). U.S. Army Engineer Waterways Experiment Station. Vicksburg, Mississippi.

CIRIA, CUR, & CETMEF. (2007). *The rock manual. the use of rock in hydraulic engineering (2nd edition).* (2nd ed.). London: C683, CIRIA.

CIRIA, CUR, & CETMEF. (2017). *The rock manual errata list. december 5th, 2017.* London.

Cistin, J. (1968). *Konstrukce a stavba filtru syspanych hrazi.* VVHU, Brno.

CUR. (1993). *Rapport 161, filters in de waterbouw.* Gouda: CUR.

CUR. (2000). *Maak- en meetnauwkeurigheden bij de uitvoering van baggerwerken en steenbestortingen*. Leidschendam.

Dai, Y. B., & Kamel, A. M. (1969). *Scale effect tests for rubble mound breakwaters*. Vicksburg, Mississippi.

Douglas, P. A. (1968). *Filter design criteria and their application.* Department of Civil Engineering, Auburn university. Auburn, Alabama.

Giroud, J. P. (2003). Filter criteria. *Jubilee Volume, 75th Anniversary of K. Terzaghi's "Erdbaumechanik" ("Soil Mechanics")*, 221–259.

Giroud, J. P. (2006). *Geosynthetics engineering: Successes, failures and lessons learned.* Technical University of Vienna, Vienna.

Heibaum, M. H. (2004). *Geotechnical filters - the important link in scour protection.* Federal Waterways Engineering & Research Institute. Karlsruhe, Germany.

Kenney, T. C., & Lau, D. (1985). Internal stability of granular filters. *Canadian Geotechnical Journal*, *22*, 215–255.

Kirkegaard, J., Wolters, G., Sutherland, J., Soulsby, R., Frostick, L., McLelland, S., … Gerritsen, H. (2011). *Geohydraulik für studium und praxis.* Leiden, The Netherlands: CRC Press/Balkema.

Laan, G. (1981). *De relatie tussen vorm en gewicht van breuksteen.* (Rapport No. MAW-R-81079). Rijkswaterstaat, Wegbouwkundige Dienst. Delft.

Le Méhauté, B. (1976). Similitude in coastal engineering. *Journal of the Waterways, Harbors and Coastal Engineering Division*, *102(WW3)*, 317–335.

Mansard, E. P. D., & Funke, E. R. (1980). The measurement of incident and reflected spectra using a least squares method. In *Proceedings of 17th conference on coastal engineering* (pp. 154–172). Sydney, Australia.

Montalvo-Bartolomei, A., & Robbins, A. (2015). A historical review of embankment seepage design. 28th ASCE central pennsylvania geotechnical conference, Hershey, PA.

Pilarczyk, K. W. (1998). *Dikes and revetments: Design, maintenance and safety assessment.* Rotterdam: A.A. Balkema.

SBRCURnet. (2017). *Design guideline for underlayers beneath rock armoured slopes under wave loading*. Delft.

Schiereck, G. J., & Verhagen, H. J. (2012). *Introduction to bed, bank and shore protection: Engineering the interface of soil and water.* Delft: VSSD.

Terzaghi, K. (1939). 45th james forrest lecture, 1939. soil mechanics - a new chapter in engineering science. *Journal of the Institution of Civil Engineers*, *12*(7), 106–142.

Terzaghi, K., & Peck, R.B. (1948). *Soil mechanics in engineering practice (1st edition).* New York: John Wiley and Sons, Inc.

Thompson, D. M., & Shuttler, R. M. (1975). Riprap design for wind-wave attack, a laboratory study in random waves. *Wallingford report EX707 for CIRIA*.

U.S. Army Corps of Engineers. (1941). *Investigation of filter requirements for underdrains.* (Technical memorandum No. 183-1). Vicksburg, Mississippi.

U.S. Army Corps of Engineers. (1948). *Laboratory investigation of filters for enid and grenada dams.* (Technical memorandum No. 3-245). Vicksburg, Mississippi.

U.S. Coastal Engineering Research Center. (1984). *Shore protection manual.* Department of the Army, Waterways Experiment Station, Corps of Engineers, Coastal Engineering Research Center.

van der Meer, J. W. (1988). *Rock slopes and gravel beaches under wave attack*. PhD. thesis, Delft University of Technology, Delft.

van Gent, M. R. A., Jacobsen, N. G., & Wolters, G. (2017). *Modelling of open filters under wave loading.* Deltares. Delft.

van Gent, M. R. A., & Wolters, G. (2016). *Onderzoek naar onderlagen. fysiek modelonderzoek naar de stabiliteit van onderlagen onder golfaanval en de invloed daarvan op afdeklagen van breuksteen.* Deltares. Delft.

Verhagen, H. J., & Jansen, L. (2014). *Ratio between stone diameter and nominal diameter.* (Communications on Hydraulic and Geotechnical Engineering No. 2014-01). Faculty of Civil Engineering and Geosciences, TU Delft. Delft.

Verheij, H., Hoffmans, G., Dorst, K., & Vandesande, S. (2012). Interface stability of granular filter structures under currents. ICSE6, Paris, France.

Zelt, J. A., & Skjelbreia, J. E. (1992). Estimating incident and reflected wave fields using an arbitrary number of wave gauges. In *Proceedings of 23rd conference on coastal engineering* (pp. 777–790). Venice, Italy.

Ziems, J. (1968). *Ein beitrag zur kontakterosion nichtbindiger erdstoffe.* TU Dresden, Dresden.

A Material properties

A.1. Armour layer material

The armour layer consists of basalt rubble stone. A sample of this material can be seen in figure A.2. The density of the basalt was determined using Archimedes' principle. First, a sample was taken out of the big bag of basalt stones. After cleaning and drying the sample, the sample was weighed. Then, the volume of the sample was determined by placing the sample under water and measuring the displacement. Using the dry weight and the volume, the density was calculated. After repeating this process 4 times, the average density was found to be 2984 kg/m^3.

Next, another random sample, consisting of 100 stones, was taken from the big bag, cleaned and dried. The individual stones were then weighed and the diameters were determined using equations 2.2 and 2.3, with $F_s = 0.84$. After ordering the stone diameters in a list from the smallest to largest diameter, the grading curve was obtained by plotting the cumulative mass fraction against the diameters. This can be seen in table A.1.

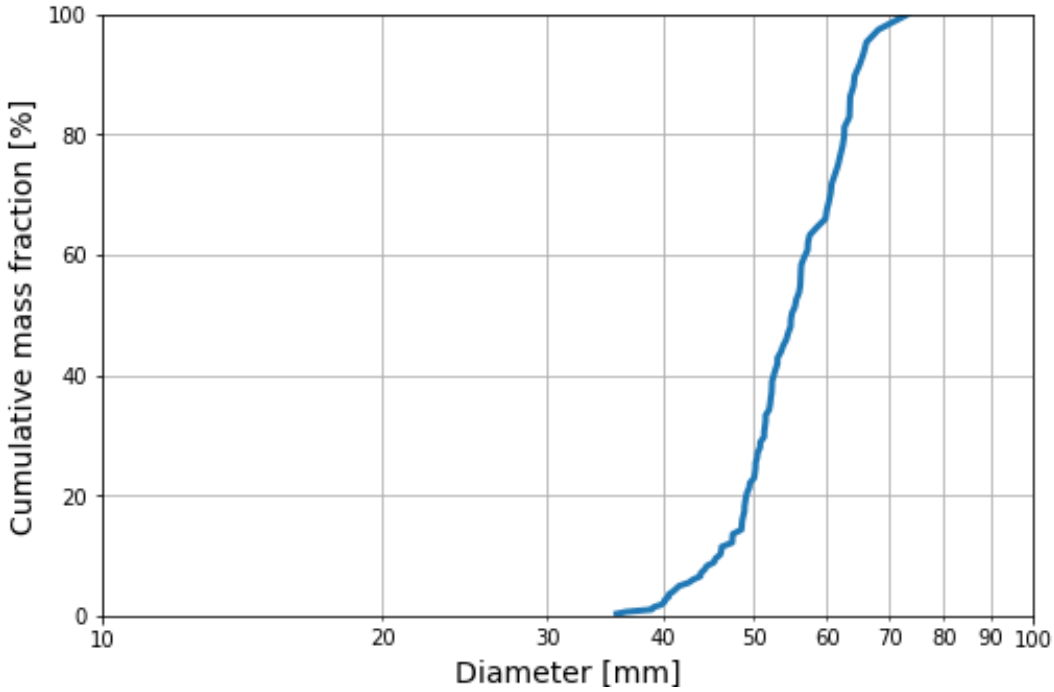

Figure A.1: Grading curve of the armour layer material

Figure A.2: A sample of armour layer material

Using the determined grading curve of the armour layer material, multiple characteristic diameter values and other properties were determined. This can be seen in table A.1. As $D_{85,a}/D_{15,a} = 63.5/48.6 = 1.31$, the armour layer material is classified as a narrowly graded material (See also section 2.1).

Table A.1: Overview of armour layer material properties

Material	D_{10} [mm]	D_{15} [mm]	D_{50} [mm]	D_{n50} [mm]	D_{60} [mm]	D_{85} [mm]	C_u [-]	ρ_s [kg/m^3]
Armour layer	46.0	48.6	55.0	46.2	57.2	63.5	1.24	2984

A.2. Under-layer material

A.2.1. Individual stone sizes

As described in section 3.3.2, the five under-layer materials used are mixes of six different sizes of gravel, namely ”Nederlandse steenslag 1-3mm”, ”Japanese split 2-4mm”, ”Japanese split 4-8mm”, ”Japanese split 8-11mm”, ”Japanese split 11-16mm” and ”Japanese split 16-22mm”. First, the densities and grading curves of these individual stone sizes were determined. This was done using the same method described in section A.1. The resulting grading curves can be seen in figure A.3. Samples of the individual stone sizes can be seen in figures A.4 through A.9. The material properties of the individual stone sizes can be found in table A.2.

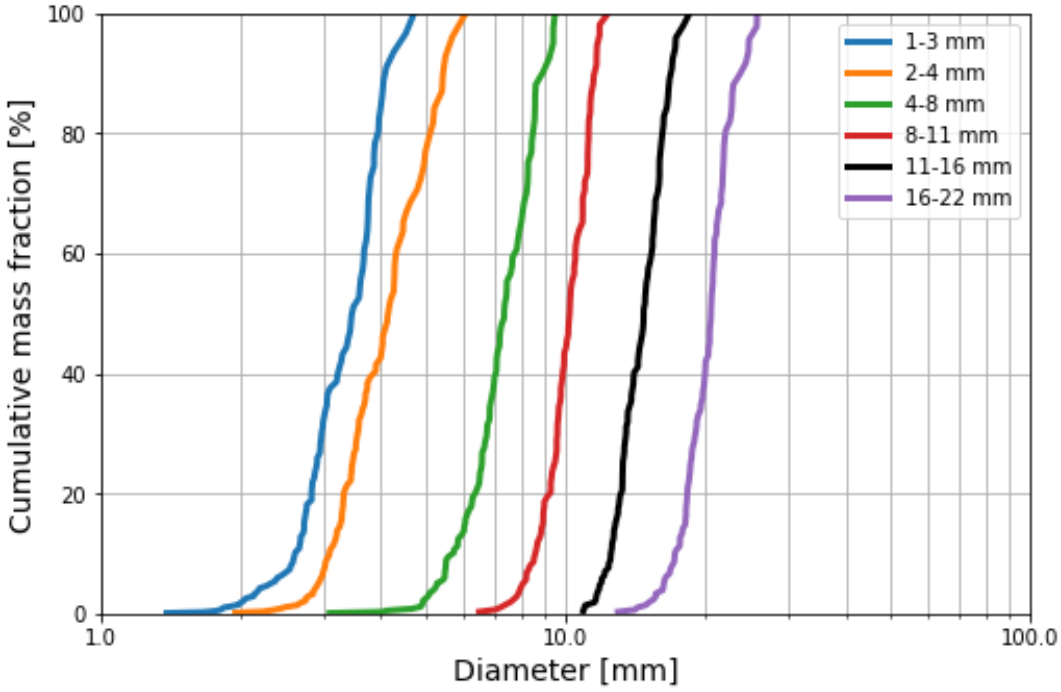

Figure A.3: Grading curves of the individual stone sizes used to create the under-layer mixes.

Figure A.4: A sample of ”Nederlandse Steenslag 1-3 mm”

Figure A.5: A sample of ”Japanese Split 2-4 mm”

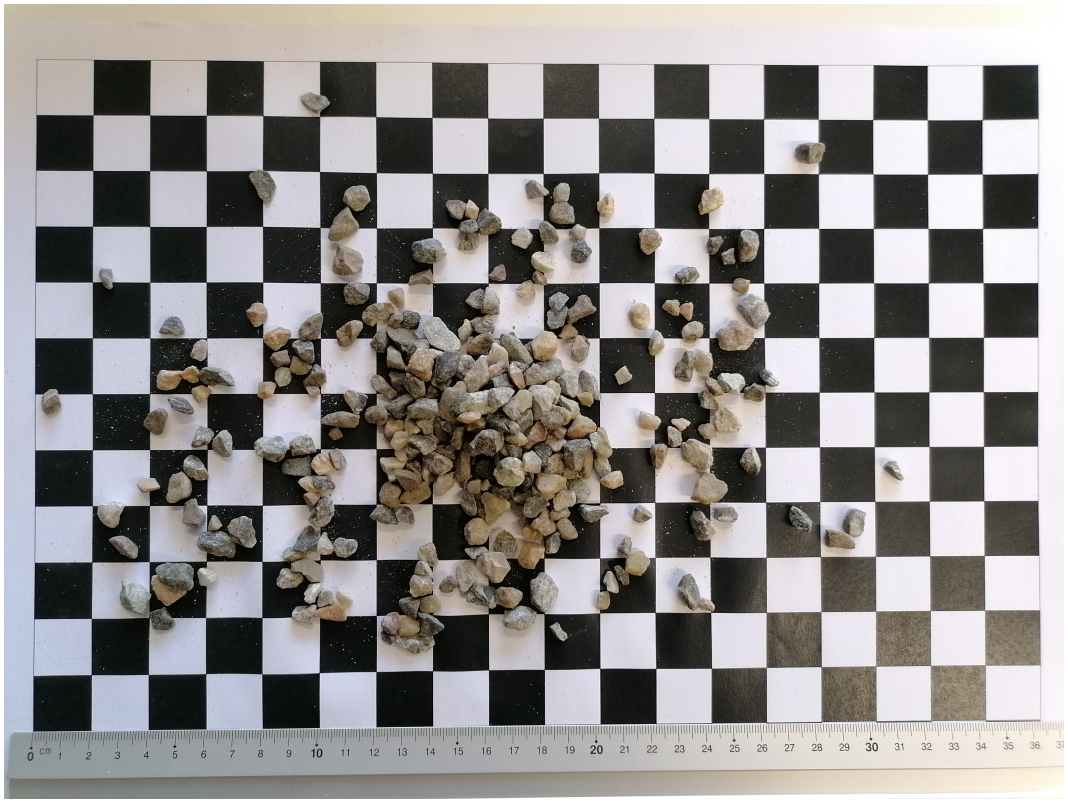

Figure A.6: A sample of ”Japanese Split 4-8 mm”

Figure A.7: A sample of ”Japanese Split 8-11 mm”

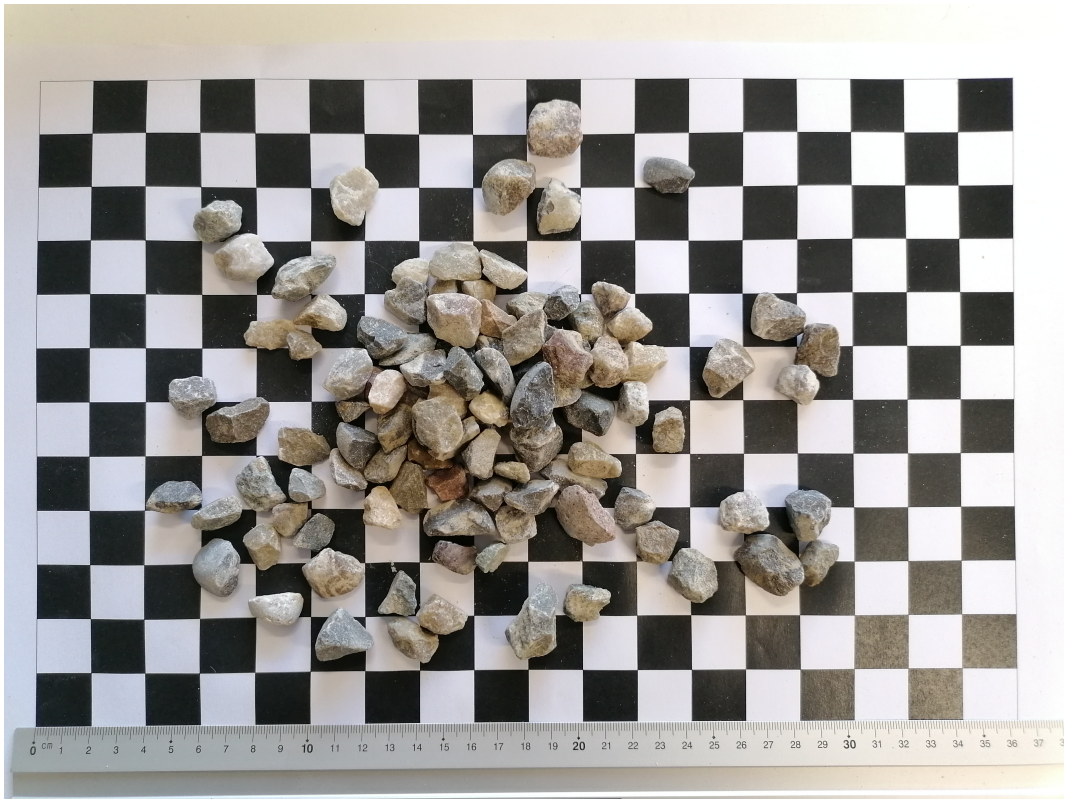

Figure A.8: A sample of ”Japanese Split 11-16 mm”

Figure A.9: A sample of ”Japanese Split 16-22 mm”

Table A.2: Material properties of the individual stone sizes used to create the under-layer mixes.

Material	D_{10} [mm]	D_{15} [mm]	D_{50} [mm]	D_{n50} [mm]	D_{60} [mm]	d_{85} [mm]	C_u [-]	ρ_s [kg/m^3]
1-3 mm	2.6	2.7	3.5	2.9	3.7	4.0	1.40	2613
2-4 mm	3.1	3.3	4.2	3.9	4.3	5.4	1.39	2620
4-8 mm	5.7	6.1	7.4	6.2	7.8	8.6	1.37	2618
8-11 mm	8.6	8.9	10.2	8.6	10.5	11.3	1.21	2626
11-16 mm	12.5	12.8	14.7	12.3	15.3	16.6	1.23	2627
16-22 mm	17.2	18.1	20.5	17.2	20.9	22.8	1.21	2637

A.2.2. Under-layer mixes

As discussed before, the five different under-layer materials consist of mixes of the individual stone sizes described in section A.2.1. Before physically mixing the stones, first, for each mix, desired values of $D_{15,a}/D_{85,u}$ and $C_{u,u}$ were determined. The reasoning behind the different values chosen is discussed in section 3.4. After these values were determined, the theoretical grading curves of the five under-layer mixes were constructed by varying the percentage-by-mass used of each of the six individual stone sizes and taking the resulting weighted average of the grading curves, until the values of $D_{15,a}/D_{85,u}$ and $C_{u,u}$ were as close as possible to the desired values.

After creating the five different under-layer mixes by mixing the six different individual stone sizes with the pre-determined ratios, a sieving curve was made for all five mixes. This was done to check if the realized values of $D_{15,a}/D_{85,u}$ and $C_{u,u}$ were representative of the desired values. An overview of the desired and realized values, as well as the values obtained from the theoretical grading curves, is shown in table A.3. Comparisons between the theoretical and the realized grading curves can be seen in the sub-sections below.

Table A.3: Desired, theoretical and realized values of $D_{15,a}/D_{85,u}$ and $C_{u,u}$ for all under-layer mixes

Mix name	Desired $D_{15,a}/D_{85,u}$	Theoretical $D_{15,a}/D_{85,u}$	Realized $D_{15,a}/D_{85,u}$	Desired $C_{u,u}$	Theoretical $C_{u,u}$	Realized $C_{u,u}$
1	2.00	2.34	2.55	3.00	3.00	2.94
2	4.00	4.43	4.48	3.00	2.82	3.10
3	8.00	7.49	8.56	2.00	1.84	1.96
4	3.00	3.16	3.27	3.00	2.90	3.04
5	3.00	2.75	2.75	4.50	4.51	4.56

Mix 1

A Comparison between the theoretical grading curve and the realized grading curve for under-layer mix 1 can be seen in figure A.10. When sieving mix 1, the largest available sieve size was 16 mm. Therefore, all stones from the sieving sample that were retained by the 16 mm sieve were weighed individually, after which their diameters were calculated based on their masses and densities. As can be seen in figure A.10, the realized grading curve of mix 1 was close to the theoretical grading curve. However, along the entire curve, the realized size of this under-layer mix was slightly smaller than the theoretical size.

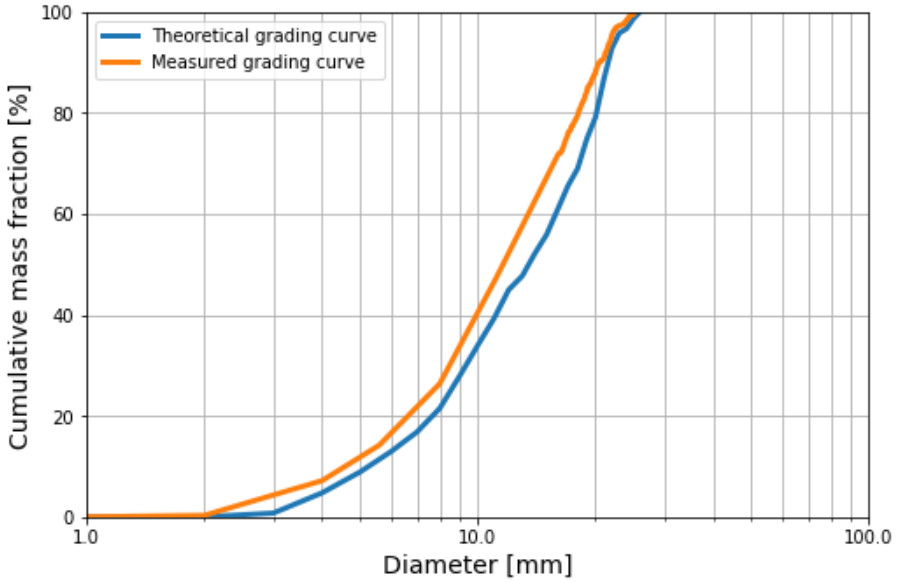

Figure A.10: Comparison between the theoretical grading curve and the realized grading curve for under-layer mix 1.

Mix 2

A Comparison between the theoretical grading curve and the realized grading curve for under-layer mix 2 can be seen in figure A.11. As can be seen in the figure, the realized grading curve of mix 2 was very close to the theoretical grading curve. However, the smallest 20% (by mass) of the realized mix was slightly smaller than the smallest 20% of the theoretical mix.

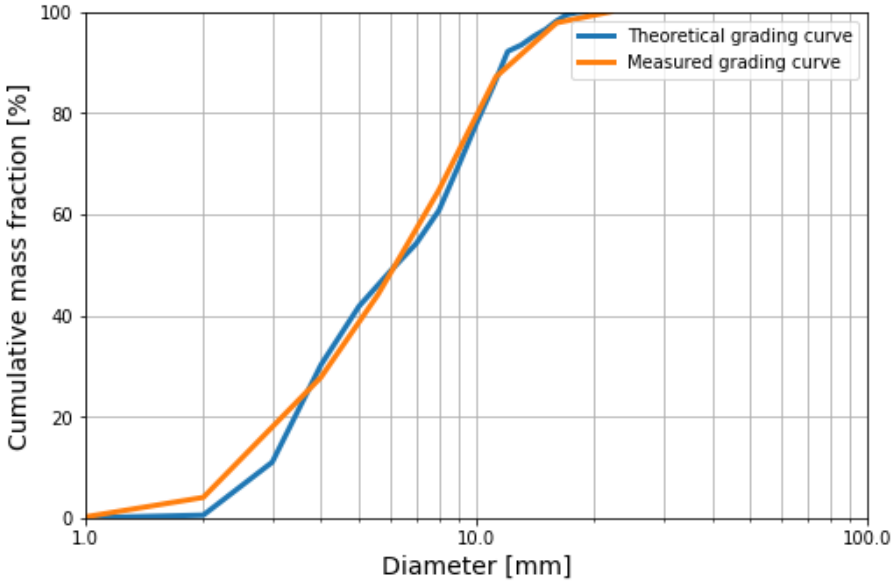

Figure A.11: Comparison between the theoretical grading curve and the realized grading curve for under-layer mix 2.

Mix 3

A Comparison between the theoretical grading curve and the realized grading curve for under-layer mix 3 can be seen in figure A.12. As was the case for mix 1, the realized size of this under-layer mix was slightly smaller than the theoretical size.

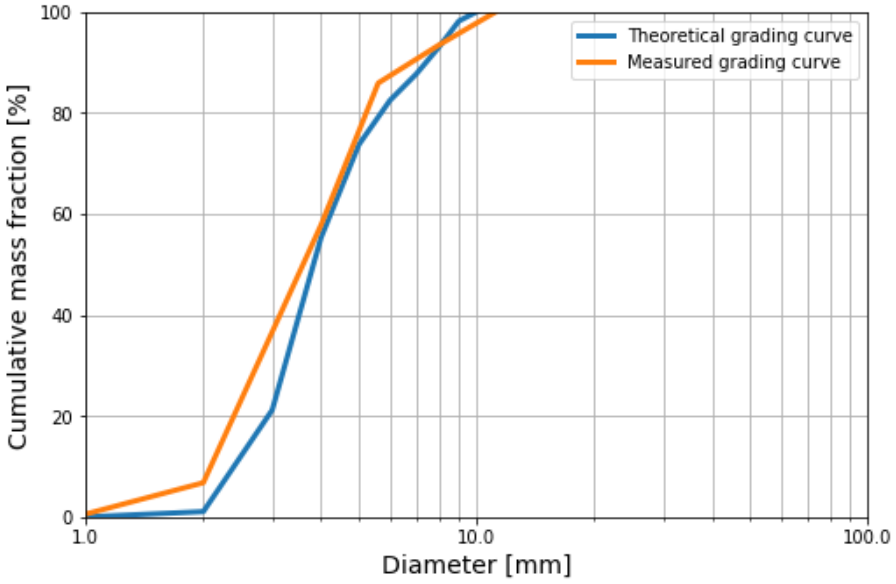

Figure A.12: Comparison between the theoretical grading curve and the realized grading curve for under-layer mix 3.

Mix 4

A Comparison between the theoretical grading curve and the realized grading curve for under-layer mix 4 can be seen in figure A.13. Out of all five under-layer mixes, the realized grading curve was the closest to the theoretical grading curve for this under-layer mix.

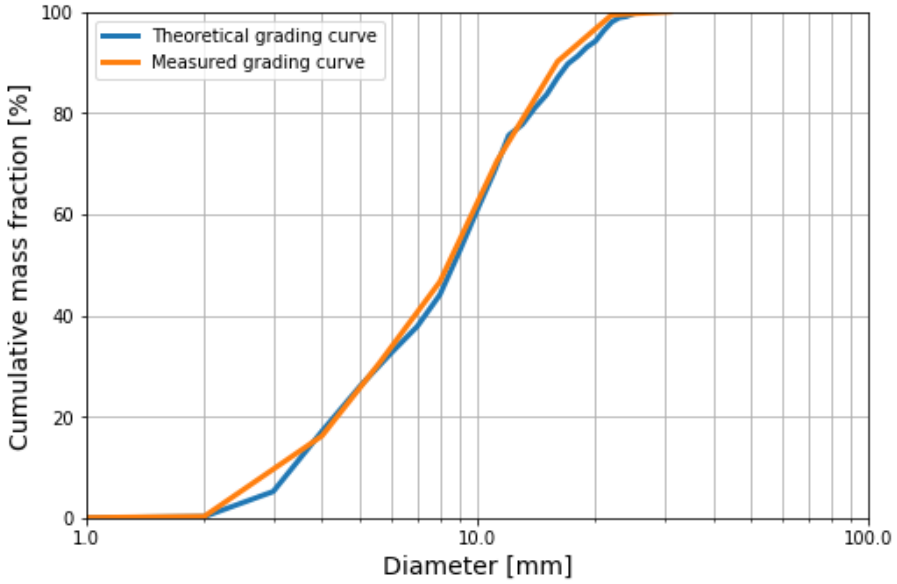

Figure A.13: Comparison between the theoretical grading curve and the realized grading curve for under-layer mix 4.

Mix 5

A Comparison between the theoretical grading curve and the realized grading curve for under-layer mix 5 can be seen in figure A.14. Again, the realized grading curve was very close to the theoretical grading curve, with the realized grading curve being slightly smaller than the theoretical grading curve between D_35 and D_80.

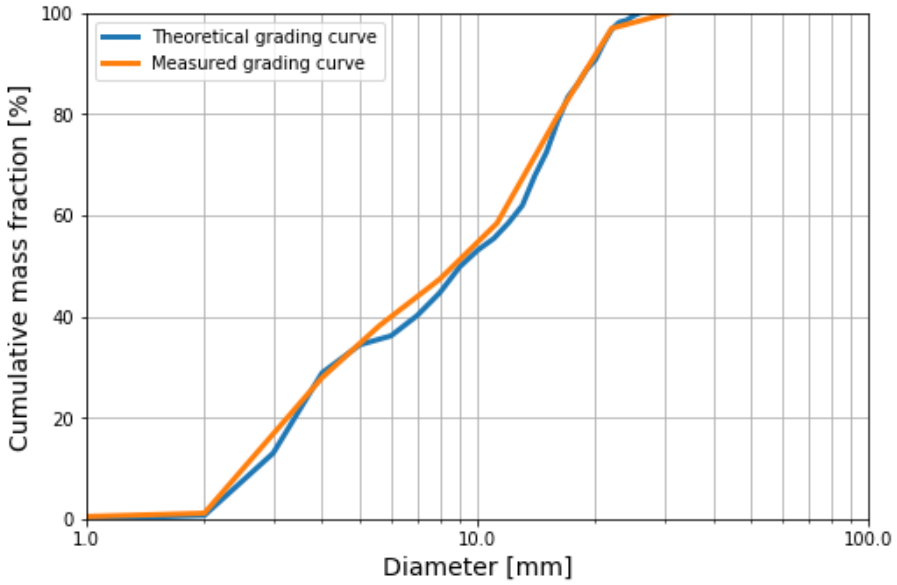

Figure A.14: Comparison between the theoretical grading curve and the realized grading curve for under-layer mix 5.

B

B technical drawing of model setup

A technical drawing of the physical model setup, including a detail of the physical model without rocks, is shown in figure B.1. For a more detailed description of the model setup, the reader is referred to chapter 3.

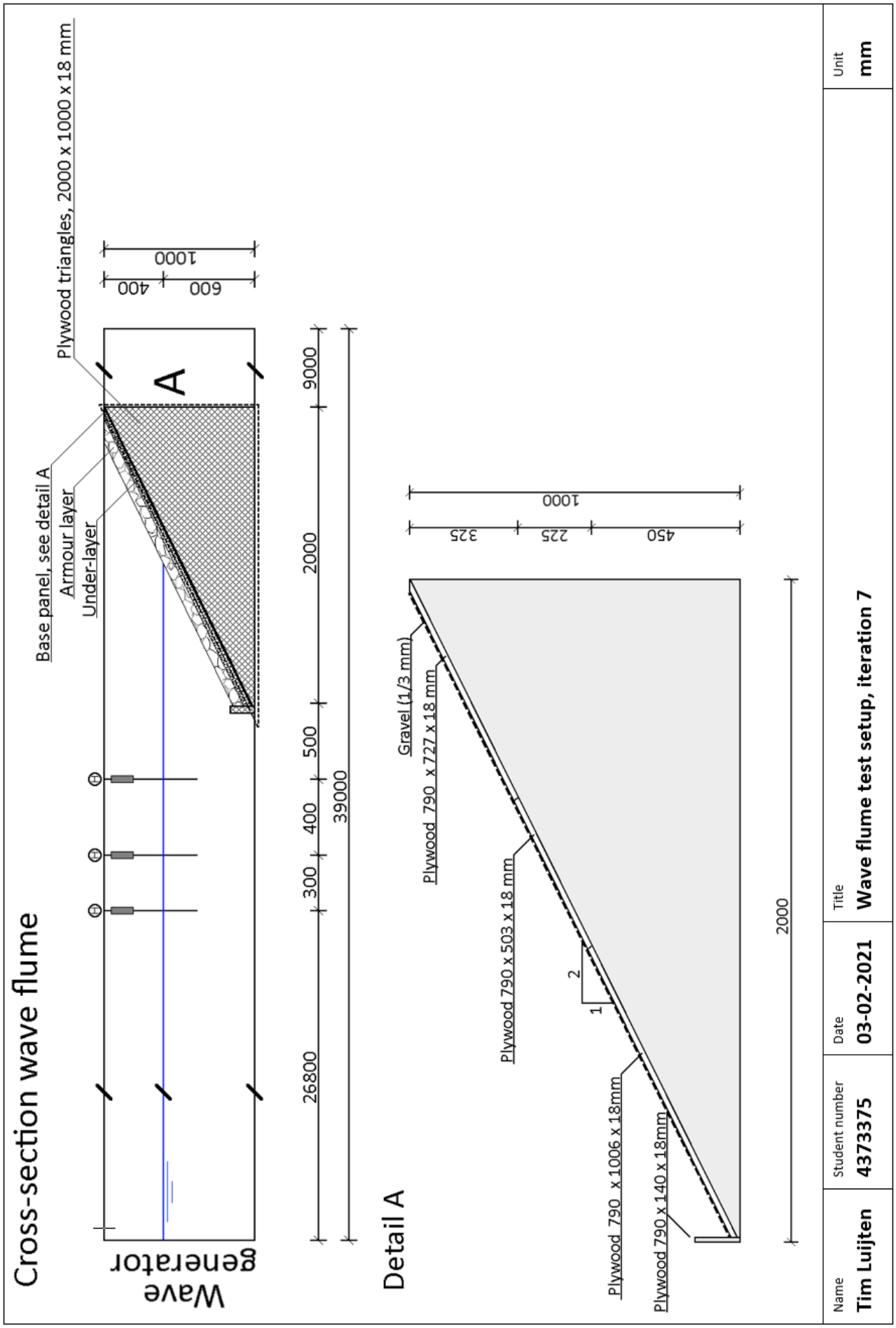

Figure B.1: Wave flume setup, technical drawing

C

C Test results

C.1. Unexpected observations during tests

C.1.1. Small plastic balls in the wave flume

The wave flume at the TU Delft Hydraulic Engineering Laboratory is part of a closed system. When filling the wave flume the water is pumped in from a large tank below the laboratory and when emptying the flume the water is deposited into the same tank. During an earlier experiment small plastic balls with a diameter of roughly 3 mm were used. A significant amount of these plastic balls ended up in the water tank, causing some of these balls to enter the wave flume when it was being filled. During test 1.1.1 it was observed that, due to the wave forcing, these plastic balls would make their way into the armour- and under-layer of the model.Since the size of the plastic balls was in the size range of the smaller under-layer material used for the tests, they could clog up the interface between the armour layer and the under-layer, possibly restricting the movement of under-layer material and thus influencing the test results.

To mitigate this, test 1.1.1 was re-run after emptying the wave flume and re-filling it at a slower rate, causing less plastic balls to enter the flume. Most of the balls that did still enter the flume were collected with a fishnet. This strategy was also used before all subsequent tests. During the re-run of test 1.1.1, as well as during all subsequent tests, no more plastic balls were observed entering the armour- or under-layer. Therefore it is assumed that, even though a few plastic balls remained inside the wave flume, they had no significant influence on the test results.

C.1.2. Breaking waves on the foreshore

During all tests, some breaking waves were observed between the wave paddle and the model location. Naturally, more breaking waves were observed during tests where a higher wave steepness of $s_{op} = 0.04$ was imposed than during tests where a lower steepness of $s_{op} = 0.02$ was imposed. This caused the final value of s_{op} to be lower than expected, resulting in values of ξ_{op} of higher than expected, for all tests (see also table 3.4). Especially for the tests with shorter waves, the measured wave steepness was significantly lower than the imposed steepness.

As discussed in section 3.4, one of the goals is to test the most typical breaker types at bank protections and breakwaters, namely plunging, collapsing and surging breakers. During the tests, all of these breaker types were still observed, with plunging and collapsing breakers mainly occurring during tests with shorter waves and with collapsing and surging breakers mainly occurring during tests with longer waves. This means that the goal set in section 3.4 was still met, despite the unexpected decrease in overall wave steepness.

C.2. Overview of test results

An overview of the model test results is shown in table C.1. In this table a summary of the observations made during each test is shown, as well as the measured armour layer damage.

Table C.1: Small overview of test results

	Test	Armour layer S (SWL +/- 2*H_s)	Under-layer Displacement of under-layer stones (>$D_{50,a}$)	Under-layer Intrusion of under-layer stones into armour layer	Under-layer Washout of under-layer material
Test series 1 $D_{15,a}/D_{85,u} = 2.55$ $D_{50,a}/D_{50,u} = 4.74$ $C_{u,u} = 2.94$	**1.1.1**	0.6	No	No	No
	1.1.2	0.8	No	No	No
	1.1.3	2.4	No	No	No
	1.2.1	0.9	No	No	No
	1.2.2	1.5	No	No	No
	1.2.3	2.3	No	No	No
Test series 2 $D_{15,a}/D_{85,u} = 4.48$ $D_{50,a}/D_{50,u} = 8.89$ $C_{u,u} = 3.10$	**2.1.1**	0.7	No	No	No
	2.1.2	0.9	Yes	No	No
	2.1.3	1.2	Yes	Yes	No
	2.2.1	0.6	No	No	No
	2.2.2	0.8	Yes	No	No
	2.2.3	2.0	Yes	Yes	No
Test series 3 $D_{15,a}/D_{85,u} = 8.56$ $D_{50,a}/D_{50,u} = 15.24$ $C_{u,u} = 1.96$	**3.1.1**	0.9	Yes	Yes	No
	3.1.2	1.8	Yes	Yes	Yes
	3.1.3	3.1	Yes	Yes	Yes
	3.2.1	1.1	Yes	Yes	No
	3.2.2	1.9	Yes	Yes	Yes
	3.2.3	4.3	Yes	Yes	Yes
Test series 4 $D_{15,a}/D_{85,u} = 3.27$ $D_{50,a}/D_{50,u} = 6.56$ $C_{u,u} = 3.04$	**4.1.1**	0.6	No	No	No
	4.1.2	1.1	No	No	No
	4.1.3	2.8	No	No	No
	4.2.1	0.8	No	No	No
	4.2.2	1.3	No	No	No
	4.2.3	2.4	No	No	No
Test series 5 $D_{15,a}/D_{85,u} = 2.75$ $D_{50,a}/D_{50,u} = 6.34$ $C_{u,u} = 4.56$	**5.1.1**	0.4	No	No	No
	5.1.2	1.2	No	No	No
	5.1.3	2.1	No	No	No
	5.2.1	0.4	No	No	No
	5.2.2	1.5	No	No	No
	5.2.3	2.9	Yes	Yes	No

C.3. Realized hydraulic conditions

An overview of the realized hydraulic conditions is shown in table C.2.

Table C.2: Overview of the realized hydraulic conditions

Test	h [m]	H_{m0} [m]	H_s [m]	T_p [s]	T_m [s]	s_{op} [-]	s_{om} [-]	ξ_{op} [-]	ξ_m [-]
1.1.1	0.6	0.089	0.085	1.26	1.13	0.034	0.042	2.71	2.43
1.1.2	0.6	0.115	0.109	1.44	1.24	0.034	0.046	2.72	2.34
1.1.3	0.6	0.142	0.135	1.57	1.38	0.035	0.045	2.67	2.35
1.2.1	0.6	0.074	0.070	1.52	1.34	0.019	0.025	3.58	3.16
1.2.2	0.6	0.105	0.100	1.84	1.56	0.019	0.026	3.64	3.09
1.2.3	0.6	0.130	0.124	2.00	1.70	0.020	0.027	3.56	3.02
2.1.1	0.6	0.090	0.086	1.28	1.14	0.033	0.042	2.73	2.44
2.1.2	0.6	0.114	0.108	1.43	1.24	0.034	0.045	2.71	2.35
2.1.3	0.6	0.141	0.134	1.57	1.38	0.035	0.045	2.68	2.36
2.2.1	0.6	0.078	0.074	1.58	1.39	0.019	0.025	3.63	3.19
2.2.2	0.6	0.104	0.099	1.89	1.57	0.018	0.026	3.76	3.12
2.2.3	0.6	0.134	0.127	2.06	1.73	0.019	0.027	3.61	3.03
3.1.1	0.6	0.090	0.086	1.27	1.15	0.034	0.041	2.71	2.46
3.1.2	0.6	0.116	0.110	1.41	1.24	0.036	0.046	2.65	2.33
3.1.3	0.6	0.142	0.135	1.53	1.36	0.037	0.047	2.60	2.31
3.2.1	0.6	0.078	0.074	1.56	1.39	0.020	0.025	3.58	3.19
3.2.2	0.6	0.105	0.100	1.84	1.56	0.019	0.026	3.64	3.09
3.2.3	0.6	0.136	0.129	2.06	1.74	0.020	0.027	3.58	3.02
4.1.1	0.6	0.091	0.086	1.24	1.14	0.036	0.043	2.63	2.42
4.1.2	0.6	0.116	0.110	1.42	1.25	0.035	0.045	2.67	2.35
4.1.3	0.6	0.139	0.132	1.61	1.34	0.033	0.047	2.77	2.30
4.2.1	0.6	0.078	0.074	1.58	1.41	0.019	0.024	3.63	3.24
4.2.2	0.6	0.103	0.098	1.79	1.56	0.020	0.026	3.58	3.12
4.2.3	0.6	0.134	0.127	2.06	1.74	0.019	0.027	3.61	3.05
5.1.1	0.6	0.091	0.086	1.26	1.14	0.035	0.043	2.68	2.42
5.1.2	0.6	0.117	0.111	1.43	1.25	0.035	0.046	2.68	2.34
5.1.3	0.6	0.141	0.134	1.63	1.35	0.032	0.047	2.78	2.30
5.2.1	0.6	0.078	0.074	1.62	1.39	0.018	0.025	3.72	3.19
5.2.2	0.6	0.103	0.098	1.84	1.56	0.019	0.026	3.67	3.12
5.2.3	0.6	0.133	0.126	2.05	1.74	0.019	0.027	3.60	3.06

C.4. Average armour layer profiles after every test

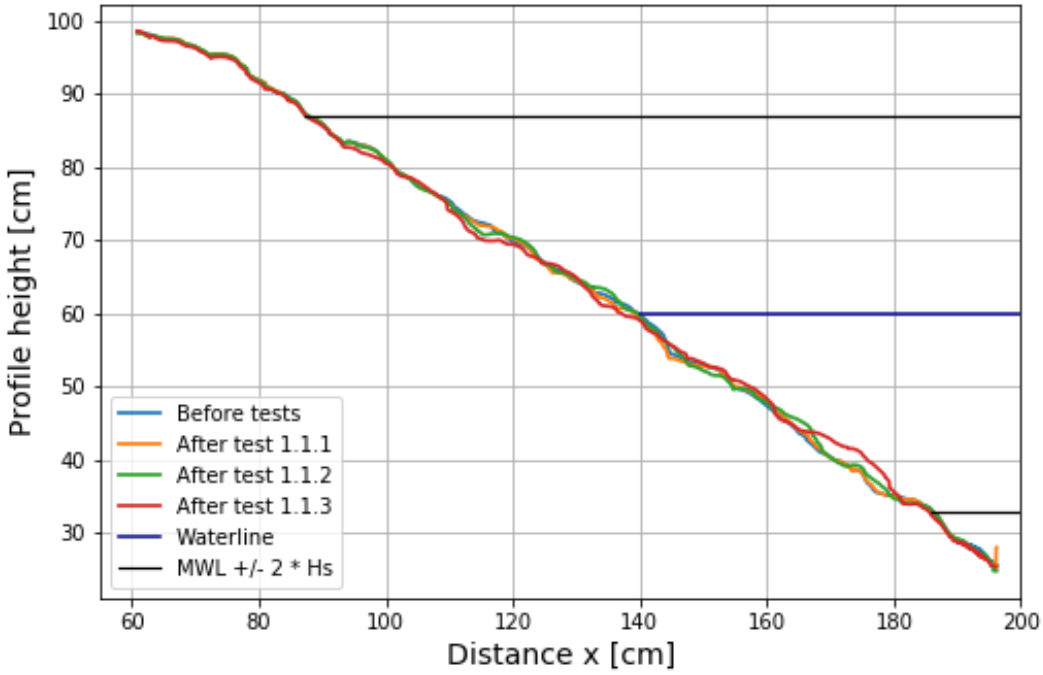

Figure C.1: Average armour layer profiles for all tests in test sub-series TS1.1

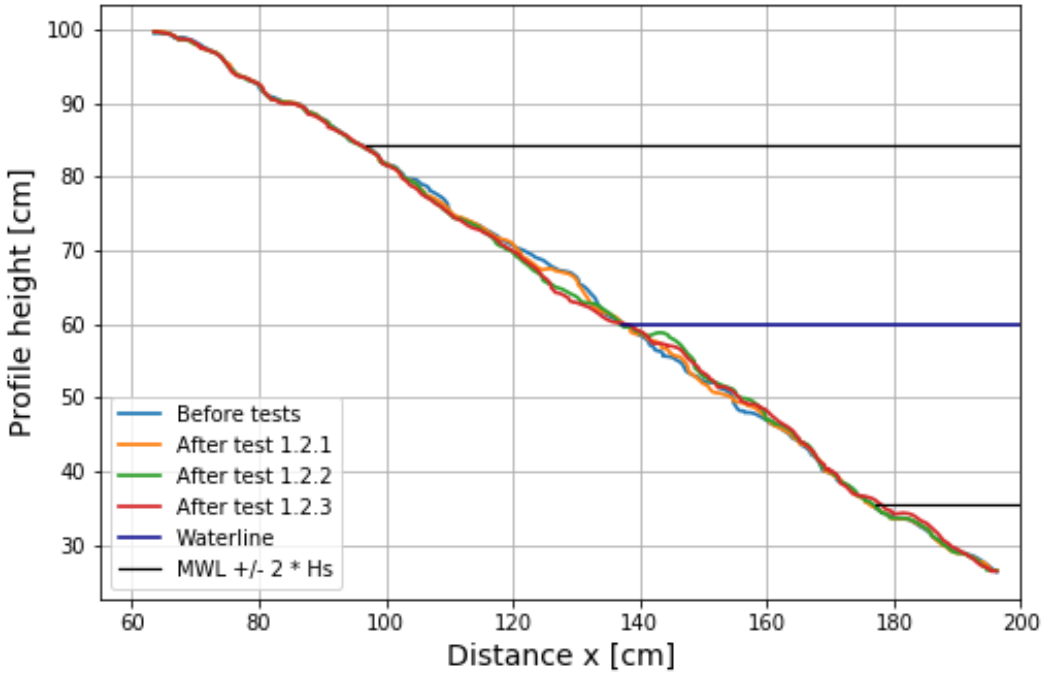

Figure C.2: Average armour layer profiles for all tests in test sub-series TS1.2

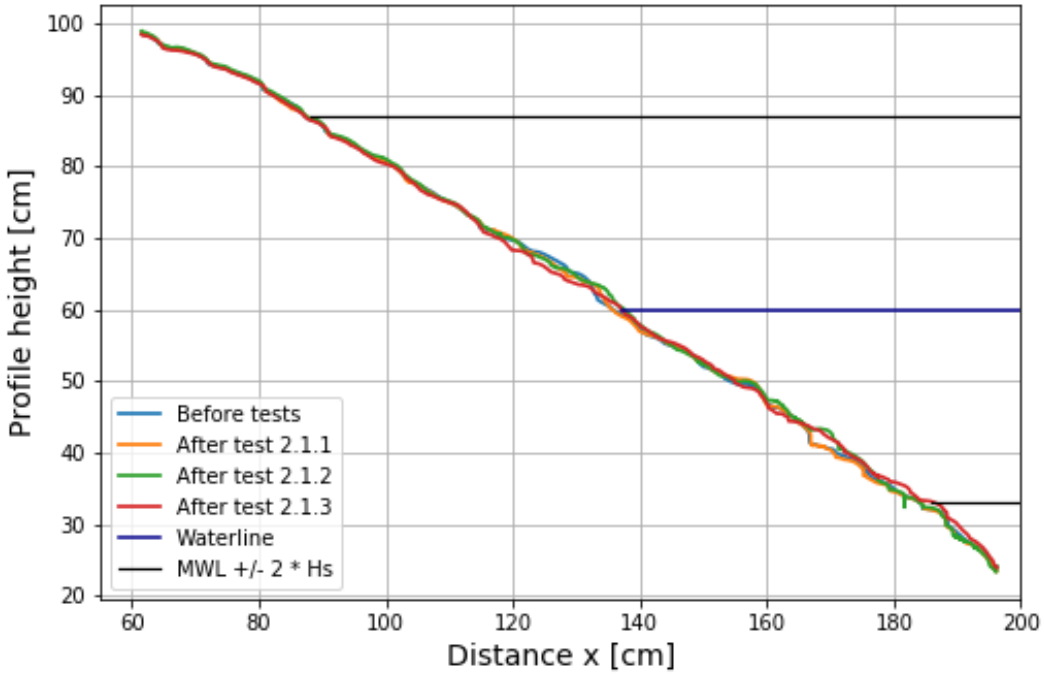

Figure C.3: Average armour layer profiles for all tests in test sub-series TS2.1

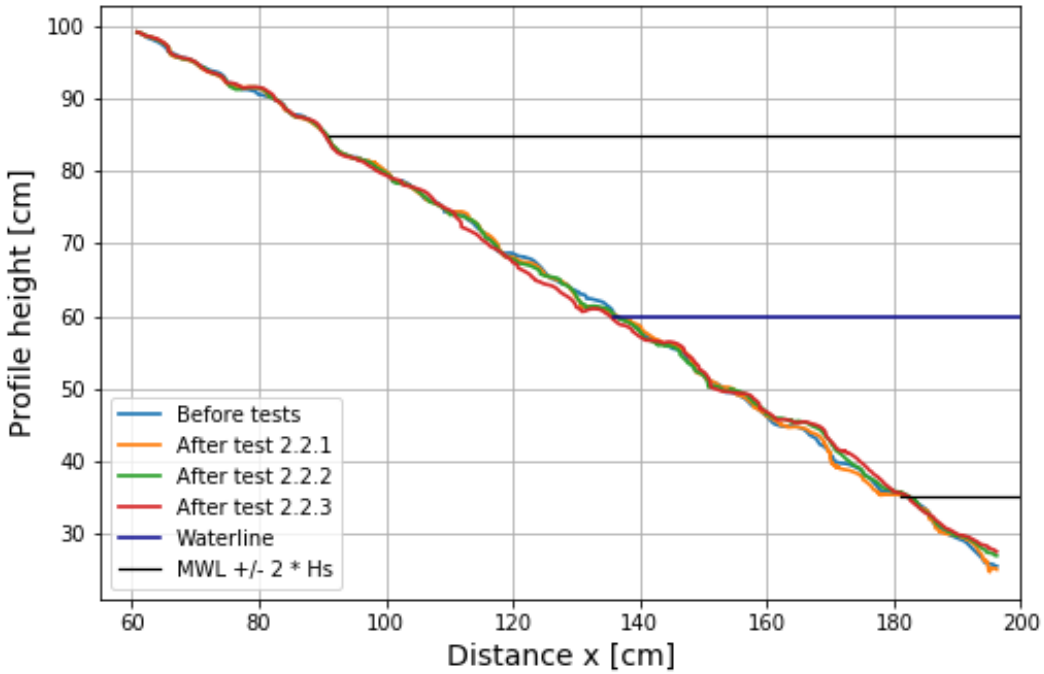

Figure C.4: Average armour layer profiles for all tests in test sub-series TS2.2

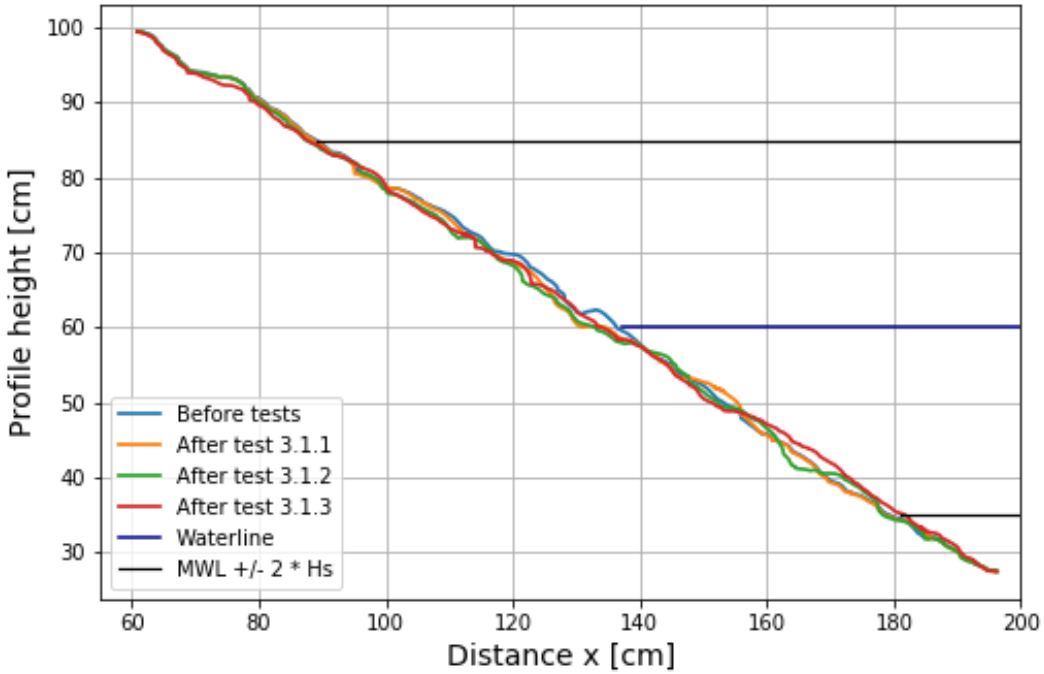

Figure C.5: Average armour layer profiles for all tests in test sub-series TS3.1

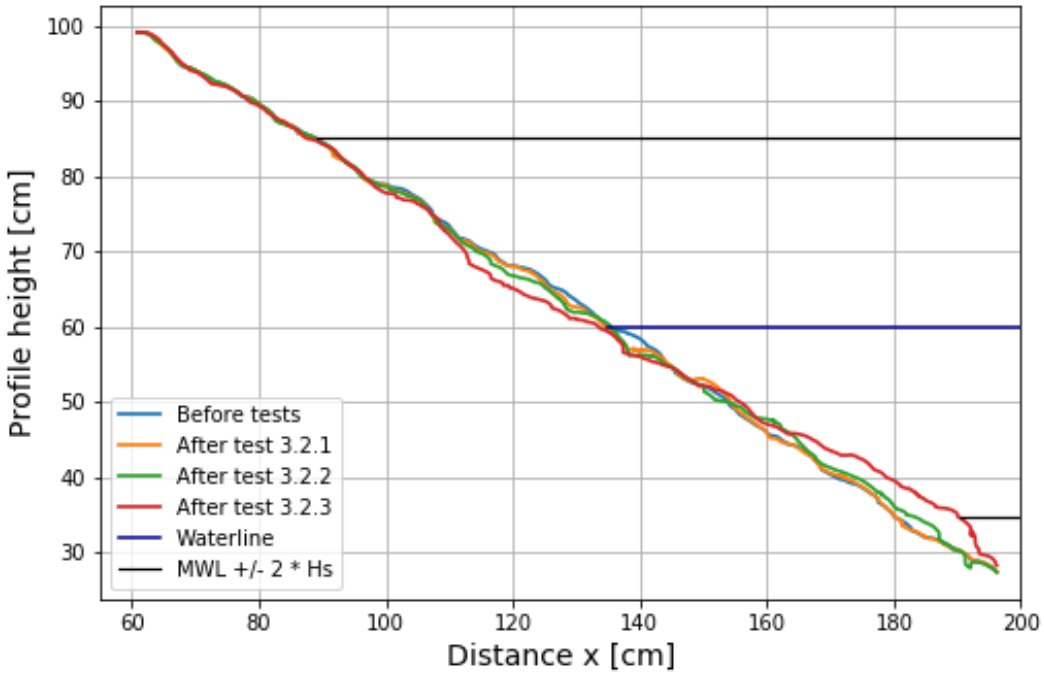

Figure C.6: Average armour layer profiles for all tests in test sub-series TS3.2

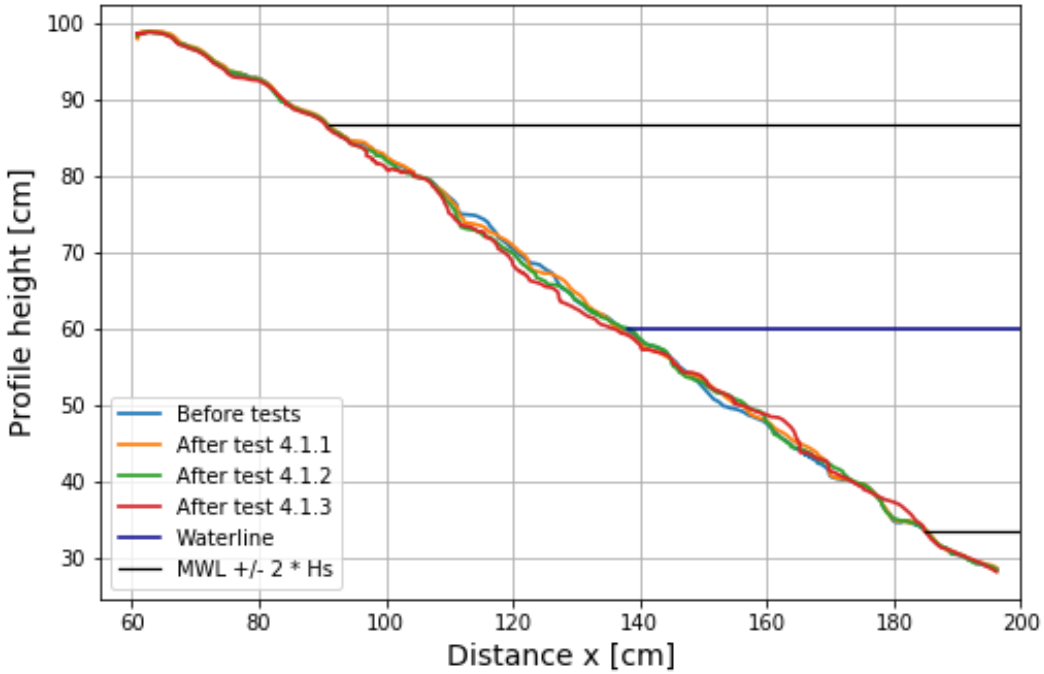

Figure C.7: Average armour layer profiles for all tests in test sub-series TS4.1

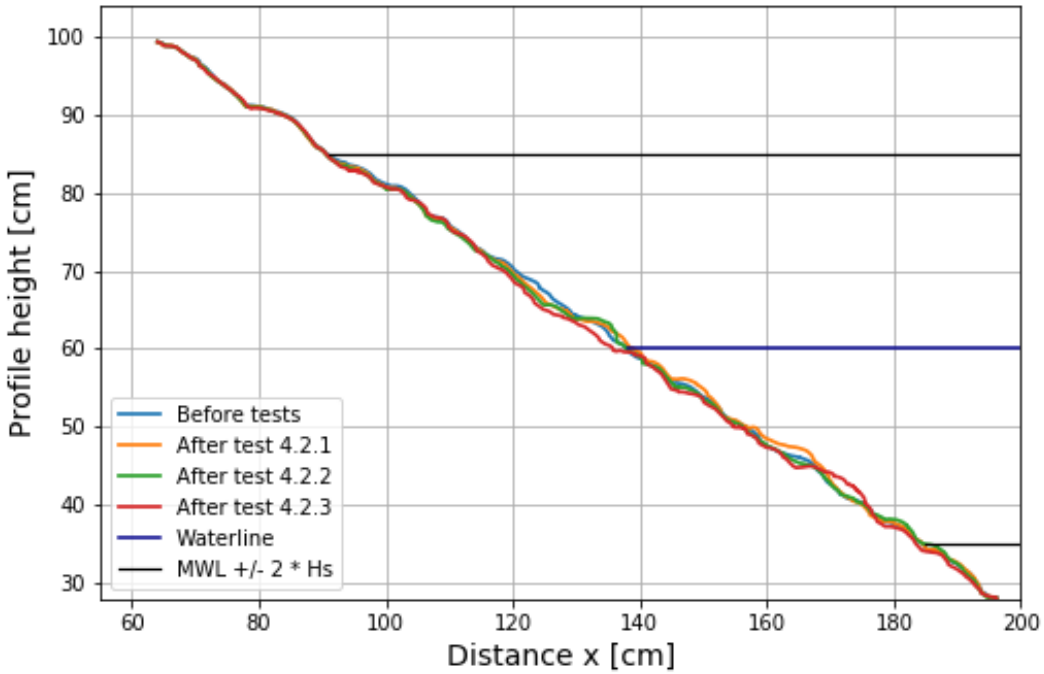

Figure C.8: Average armour layer profiles for all tests in test sub-series TS4.2

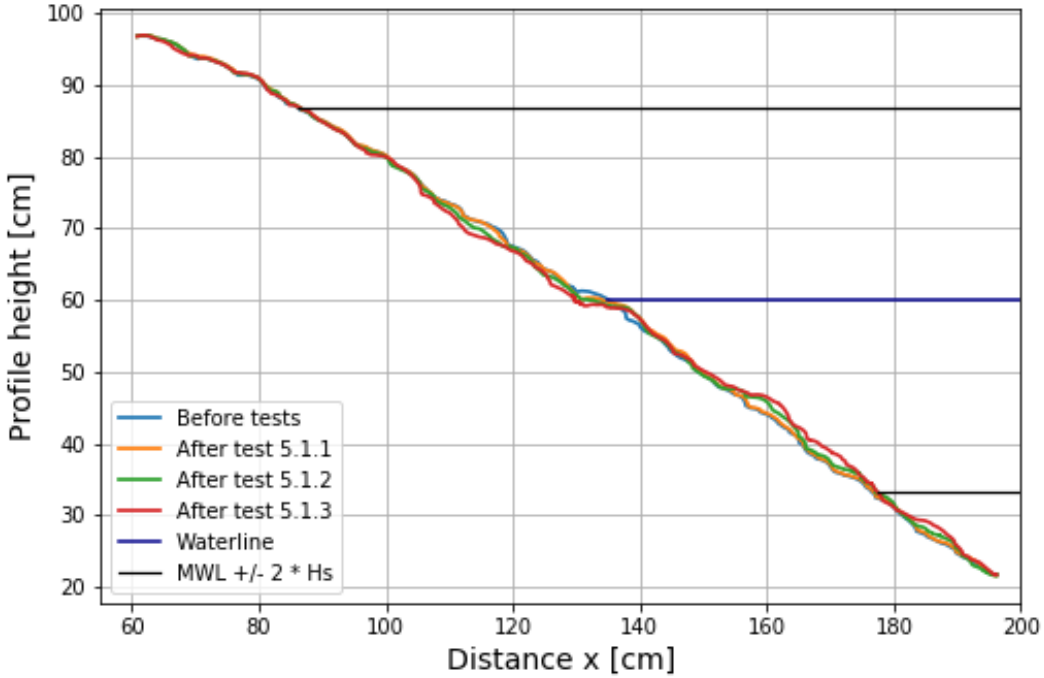

Figure C.9: Average armour layer profiles for all tests in test sub-series TS5.1

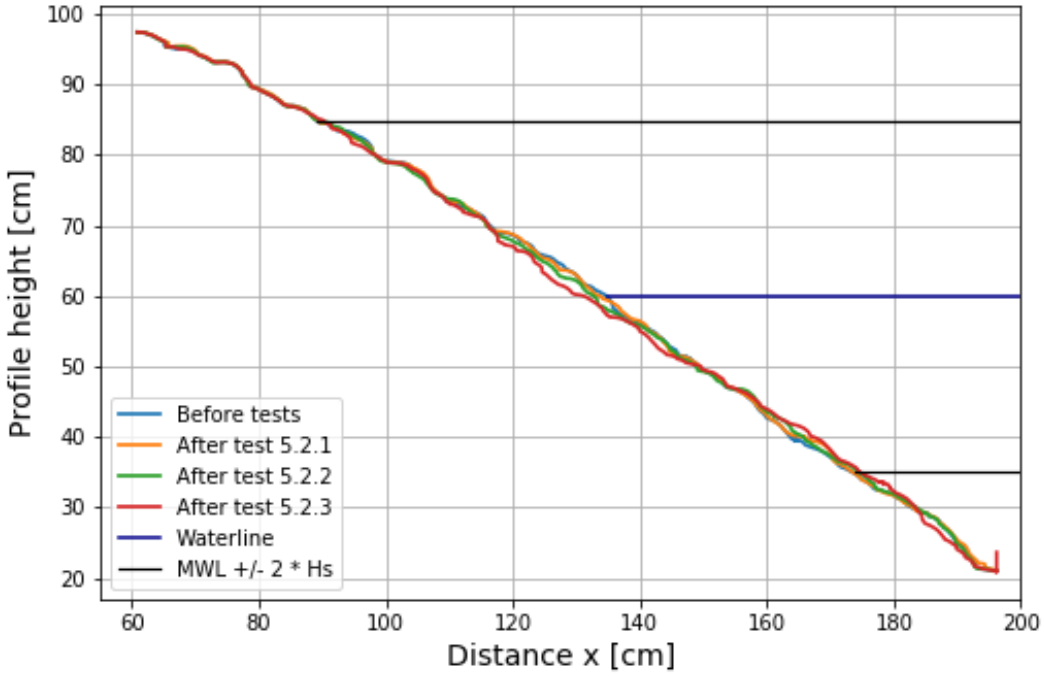

Figure C.10: Average armour layer profiles for all tests in test sub-series TS5.2